Novel barrier coatings based on nanoclay-polymer composites

by
Douglas Murima

Thesis presented in partial fulfilment of the requirements for the degree of Master of Science in the Faculty of Science at Stellenbosch University

Supervisor: Professor Harald Pasch
Co-supervisor: Dr Patrice Hartmann

March 2015

Declaration

By submitting this thesis electronically, I declare that the entirety of the work contained therein is my own, original work, that I am the sole author thereof (save to the extent explicitly otherwise stated), that reproduction and publication thereof by Stellenbosch University will not infringe any third party rights and that I have not previously in its entirety or in part submitted it for obtaining any qualification.

Douglas Murima December 2014

Abstract

The investigation of the barrier properties of highly filled polymer-clay hybrid latex films is described. Montmorillonite (MMT) clay contents ranging from 10–30 wt.% were effectively incorporated into polystyrene-butyl acrylate (PSBA) random copolymers, via miniemulsion polymerization. The optical properties of the films were evaluated using UV-Vis spectroscopy. Compared to the neat films, the PSBA nanocomposites retained remarkable visual properties. The light transmittance for PSBA films with styrene/n-butyl acrylate (S/BA) comonomer contents of 40:60 and 50:50 (mol.%) only decreased from 70% in the neat films to 50% in the nanocomposite films containing 30 wt.% clay. The best optical properties were observed in the films with S/BA comonomer contents of 30:70 (mol.%), the light transmittance only decreased from 85% (neat film) to 60% in the nanocomposite films containing 30 wt.% clay. The improved optical properties for the PSBA-30:70 films (compared to the PSBA-40:60 and PSBA-50:50 counterparts) were attributed to an increase in the low UV-absorbing butyl acrylate component of the copolymer, which at the same time has a low T_g that probably facilitated dispersion of the rigid MMT platelets in the matrix. In this study, the overall water vapour transport behaviour was governed by the MMT clay presence and less affected by the copolymer composition variation. The lower diffusion coefficients in the polymer clay nanocomposites (PCNs) were a result of the impermeable clay platelets which forced the water vapour molecules to follow longer and more tortuous paths to diffuse through the nanocomposite films. The irregular shape in the PSBA-40:60 and PSBA-30:70 neat latex particles was lost in the hybrid particles and well defined, dumb-bell shaped particles were observed. This was because of the faceting effect of the rigid MMT clay platelets. The MMT clay platelets were predominantly adhered to the surface of the PSBA latex particles because MMT clay particles have a larger size than the effective size of the copolymer particles. The stable overall transport coefficients in the PSBA-30:70-MMT films were attributed to the morphological organization of clay platelets in the matrix. The storage modulus of the materials decreased with an increase in clay content. This was attributed to the dual role played by the organoclay, firstly as nanofiller and reinforcing agent leading to the increase in storage modulus, and secondly as a plasticizer leading to a decrease of storage modulus.

Opsomming

Die versperringseienskappe van hoogsgevulde polimeer-klei saamgestelde latekslae is beskryf. ‘n 10–30 wt % Montmorilloniet (MMT) klei inhoud is inkorporeer in polistireenbutielakrilaat (PSBA) onreëlmatige kopolimere, via miniemulsie polimerisasie. Die optiese eienskappe van die lae is bepaal m.b.v. UV-Vis spektroskopie. In vergelyking met die lae sonder klei (sogenaamde ‘neat films’), het die PSBA nanosamestellings interressante visuele eienskappe getoon. Die ligtransmissie van die PSBA lae met ‘n stireeen/n-butielakrilaat (S/BA) komonomeerinhoud van 40:60 en 50:50 (mol %) het slegs afgeneem vanaf 70% in die ‘neat films’ tot 50% in the nanosaamgestelde lae wat 30% klei bevat het. Die beste optiese eienskappe is waargeneem vir die lae wat ‘n 30:70 (mol %) S/BA komonomeerinhoud bevat het; die transmissie het slegs afgeneem vanaf 85% in die ‘neat films’ to 60% in the nanosaamgestelde lae wat 30% klei bevat het. Die verbeterde optiese eienskappe van die PSBA-30:70 films (in vergelyking met die -40:60 and -50:50 films) is toegeskryf aan ‘n toename in die lae UV-absorberende butielakrilaat komponent van die kopolimeer. Terselfdetyd het laasgenoemde ‘n lae T_g-waarde, wat dispersie van die onbuigbare MMT kleiplaatjies in die matriks gefasiliteer het.

In hierdie studie is die algehele waterdampvervoer deur die teenwoordigheid van die MMT klei beheer; dit is minder geaffekteer deur variasie in die samestelling van die kopolimeer. Die lae diffusiekoëffisiënte in die polimeer-klei nanosamestellings is as gevolg van die ondeurdringbare kleiplaatjies, wat die waterdampmolekules dwing om langs langer en meer gekronkelde paaie te diffundeer deur die nanosaamgestelde lae. Die onreëlmatige vorm wat gesien is in die PSBA-40:60 and PSBA-30:70 latekspartikels (sonder klei) het geleidelik verdwyn in die saamgestelde partikels, en goed-gedefineerde partikels met die vorm van handgewigte is waargeneem (in TEM beelde). Die rede hiervoor is die sogenaamde ‘faceting’ effek, wat deur die onbuigbare MMT kleiplaatjies veroorsaak is. Die MMT kleiplaatjies sit hoofsaaklik aan die oppervlaktes van die PSBA latekspartikels. Die rede hiervoor is dat die MMT kleipartikels groter is as die effektiewe grootte van die kopolimeerpartikels. Die stabiele vervoerkoëffisiënte in die PSBA-30:70-MMT films is aan die unieke morfologiese eienskappe toegeskryf.

Die bergingsmodulus van die materiale het monotonies afgeneem met ‘n toename in klei-inhoud. Dit is toegeskryf aan die tweedelige rol wat die organoklei speel – eerstens as ‘n

nanovuller en versterkingsmiddel, wat ‘n toename in bergingsmodulus tot gevolg het, en tweedens as ‘n plastiseerder, wat ‘n afname in bergingsmodulus tot gevolg het.

.

Acknowledgements

First and foremost, I would like to thank God for the gift of life and making this study possible.

Secondly, I would like to express my special gratitude and immeasurable appreciation to my promoters, Professor Harald Pasch, for the enthusiastic encouragement, and Dr. P. C. Hartmann for all the guidance and support. My sincere thanks also go to my mentor, Dr. Helen Pfukwa, for her patience, motivation and immense knowledge. Furthermore, I would like to thank my colleagues in the research group of Professor Pasch.

Besides my supervisor, I would like to extend my appreciation to all members of the Polymer Science Division especially Mrs Erinda Cooper, Mrs Aneli Fourie, Mr. Deon Koen, Mr. Calvin Maart and Mr. Jim Motshweni. Furthermore I would like to thank the whole Department of Chemistry and Polymer Science.

I would like to thank Ineke Tiggleman for IGA analysis, Mahommed Jaffer for TEM, Elsa Malherbe for NMR analysis, Illana Bergh for TGA, Dr Nadine Pretorius for SEC and Pauline Skillington for DMA.

I would like to thank Mpact for the financial support of this research.

Last but not least, I would like to thank my beloved family for the moral support, and all my friends who stood by me during all the good and hard times.

Table of Contents

List of Figures

List of Tables

List of Abbreviations

PSBA	poly(styrene-co-butyl acrylate)
MMT	montmorillonite clay
VBDAC	vinylbenzyldodecyldimethylammonium chloride
PSBA-MMT	poly(styrene-co-butyl acrylate)/montmorillonite nanocomposite
MMT-VBDA	montmorillonite modified with vinylbenzyldodecyldimethylammonium chloride
PCN	polymer clay nanocomposite
AIBN	azobisisobutyronitrile
SDS	sodium dodecyl sulphate
HD	hexadecane
MEHQ	monomethyl-ether hydroquinone
KOH	potassium hydroxide
THF	tetrahydrofuran
TMS	tetramethylsilane
T_g	glass transition temperature
T_{onset}	onset temperature of decomposition
CEC	cation exchange capacity
NMR	nuclear magnetic resonance
FTIR	fourier transform infrared
SEC	size exclusion chromatography
TEM	transmission electron microscopy
DSC	differential scanning calorimetry
DMA	dynamic mechanical analysis
TGA	thermogravimetric analysis
IGA	intelligent gravimetric sorption analyser

Chapter 1

1 Introduction

1.1 General Introduction

Incorporation of plate-like fillers such as nanoclays into polymers to yield with hybrid materials is now known as an economical way to improve the properties of the polymers and has thus become an area of intensive research activity. These hybrid materials, normally termed Polymer Clay Nanocomposites (PCNs), are potential alternatives to conventional polymer composites. At nano-scale levels they have shown improvements in mechanical properties, heat distortion temperature, flame retardancy and enhanced barrier properties. [1-3]

Buoyed by their configuration, plate-like fillers (layered silicates) are impermeable; hence force a tortuous pathway for a permeant traversing through a nanocomposite. Although it has been proven and reported that gas/vapour and liquid permeability through polymeric films can be reduced with small nanoclay loadings[3,4], the need to determine and optimise the performance of these materials with regard to high nanoclay loadings still remains a focus for extensive research.

Over the past years, methods employed in the packaging and coating industries to design and prepare materials that regulate mass transport of permeates have shifted from conventional solvent-based to water-based coatings.[5-7]. This has largely been due to the environmental, health and safety concerns associated with using solvent-based coatings. Conventional polymerization methods such as emulsion polymerization are related to a number of challenges such as filler dispersion (especially at high loadings) and not being suitable for all monomers. These, among other challenges, prompted the development of miniemulsion polymerization methods which facilitate the preparation of water-based hybrid materials, overcome limitations associated with polymerizing monomers with low water solubility and migration of monomer droplets from micelles. [8-11]

The development of the miniemulsion approach as a polymerization technique paved way for preparation of hybrid polymer-clay materials. [12] Although effective encapsulation of nanoclay platelets within polymer particles has been reported using the miniemulsion polymerization method, the encapsulation of high loadings of nanoclay platelets (above 10 wt.%) with a broad size distribution still remains a challenge. However, the use of semi-

exfoliated to exfoliated layered silicates and reactive surfactants (relative to conventional surfactants) which maximize polymer-clay interactions has brought about significant changes in the properties of the final composite. [13-16]

The work discussed in this thesis involves the investigation of the water vapour sorption behaviour of highly filled water-based polymeric films prepared via the miniemulsion polymerization method.

1.2 Goals and Objectives

The main aim of this study was to investigate the water vapour sorption behaviour of highly filled polymer latex films (≥10 wt.% of clay), and to correlate it with their molecular properties. The clay used in this study was sodium montmorillonite and poly(styrene-co-butyl acrylate), abbreviated PSBA, was the copolymer of choice.

The objectives of this study were to:

a) Synthesize water based PSBA latexes of compositions S/BA: 50/50, 40/60 and 30/70 mol.%.

   - Prepare PSBA-MMT latexes with the respective copolymer compositions of S/BA with the following PSBA/MMT ratios: PSBA-MMT-10%, PSBA-MMT-20% and PSBA-MMT-30%

   - Determine the chemical and morphological properties of the latexes
   - Prepare films from the latexes and analyse the thermomechanical properties of the materials

   - Examine how the incorporation of high MMT contents and the variation of the copolymer composition affect the chemical and thermo-mechanical properties of the materials.

b) Measure the water vapour sorption properties of the PSBA and PSBA-MMT latex films and correlate the findings with their molecular properties

1.3 Thesis Layout

A short introduction together with the goals and objectives of this study are given in Chapter 1.

The broad theoretical base of this work is presented in Chapter 2. It includes a brief overview of PCNs, outlining their preparation and characterization. The first part of this chapter also gives a historical background to the miniemulsion polymerization method as well as what has been reported in literature on the incorporation of plate-like fillers such as clays.

The last part focuses on the transport coefficients and the principles of permeation and sorption in polymers. Here, the theoretical sorption models together with the specific methods of evaluating permeation properties with regard to their thermodynamic and kinetic behaviour are looked at. This chapter also outlines the factors affecting penetrant sorption through polymer matrices, which entails the specific penetrant in review and the physicochemical properties of the polymer.

Chapter 3 describes the preparation of poly (styrene-co-butyl acrylate) /montmorillonite clay (PSBA-MMT) latexes and films with varying MMT contents up to 30 wt.%, and different copolymer compositions of the PSBA matrix, via the miniemulsion polymerization method. The characterization methods of the latexes and films are also given.

Chapter 4 investigates the effect of MMT content on the water vapour sorption properties of the PSBA latex films. Here, the measurements of the sorption properties using the intelligent gravimetric sorption analyser (IGA) are given. This chapter also presents the correlation between the impact of copolymer compositions and water vapour sorption properties of the PSBA-MMT latex films. This chapter mainly focuses on the correlation of the water vapour sorption behaviour of the PSBA-MMT latex films with molecular properties.

Chapter 5 gives the summary and conclusions of this study as well as recommendations for future work.

1.4 References

[1] Zengeni, E.; Hartmann, P. C.; Pasch, H. *ACS Appl. Mater. Interfaces* **2012**, *4*, 6957.

[2] Valandro, S. R.; Lombardo, P. C.; Poli, A. L.; Horn Jr, M. A.; Neumann, M. G.; Cavalheiro, C. C. S. *Mater. Res.* **2014**, *17*, 265.

[3] Cloete, V. PhD, Stellenbosch University**, 2011.**

[4] Zengeni, E. MSc, University of Stellenbosch, **2009**.

[5] Landfester, K. *Macromol. Rapid Commun.* **2001**, *22*, 896.

[6] van Herk, A. M. *Adv. Polym. Tech.* **2010**, *233*, 18.

[7] Sun, Q.; Schork, F.; Deng, Y. *Compos. Sci. Technol.* **2007**, *67*, 1823.

[8] Faucheu, J.; Gauthier, C.; Chazeau, L.; Cavaillé, J.; Mellon, V.; Lami, E. B. *Polym. J.* **2010**, *51*, 6.

[9] Pham, B. T. T.; Zondanos, H.; Such, C. H.; Warr, G. G.; Hawkett, B. S. *Macromolecules* **2010**, *43*, 7950.

[10] Chern, C. S. *Prog. Polym. Sci.* **2006**, *31*, 443.

[11] Zgheib, N.; Putaux, J.; Thill, A.; D'Agosto, F.; Lansalot, M.; Bourgeat-Lami, E. *Langmuir : ACS Appl. Mater. Interfaces* **2012**, *28*, 6163.

[12] Landfester, K.; Weiss, C. K. *Adv. Polym. Sci.* **2010**, *229*, 1.

[13] Vazquez, A. *Appl. Clay Sci.* **2008**, *41*, 24.

[14] van den Dungen, E. T. A.; Galineau, J.; Hartmann, P. C. *Macromol. Symp.* **2012**, *313-314*, 128.

[15] Bonnefond, A.; Paulis, M.; Bon, S. A.; Leiza, J. R. *Langmuir : ACS Appl. Mater. Interfaces* **2013**, *29*, 2397.

[16] Bonnefond, A.; Mičušík, M.; Paulis, M.; Leiza, J. R.; Teixeira, R. F. A.; Bon, S. A. F. *Colloid. Polym. Sci.* **2012**, *291*, 167.

Chapter 2

2 Overview of organic-inorganic hybrid materials

2.1 Hybrid organic-inorganic nanocomposites

Hybrid organic-inorganic nanocomposites represent a new class of materials that bear improved performance properties compared to microcomposites. [1,2] This is due to the fact that polymer matrices supported by virgin or modified inorganic nanoparticles combine the functionalities of the polymer itself with those of the inorganic nanoparticles. [3] The unique properties of the hybrid nanocomposite materials have resulted in improvements in areas such as optical, [4] thermomechanical, [5] and barrier properties [6] of the materials. As such, this has opened doors for further research in a wide range of industrial applications that include drug delivery, [7,8] electronics, [9] coating and packaging of materials, [10,11] as presented in Figure 2.1.

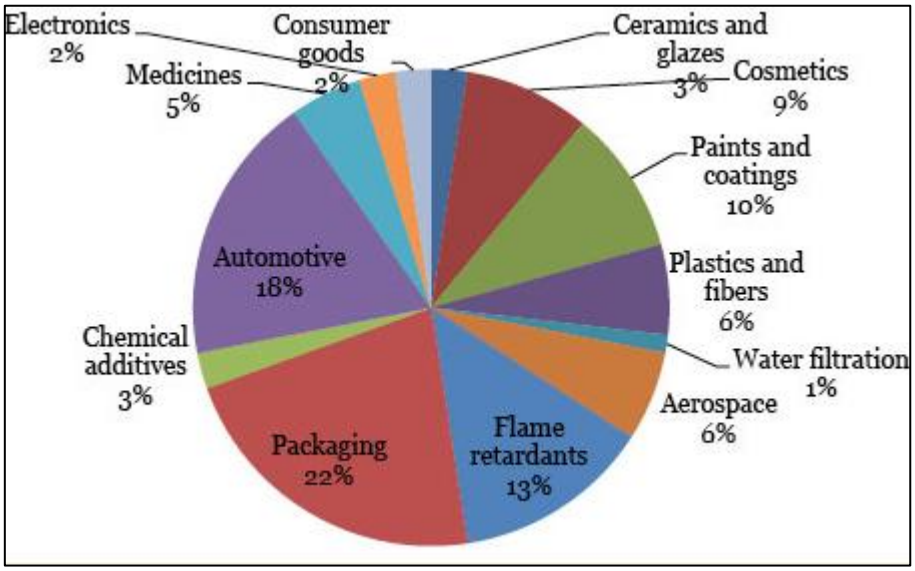

Figure 2.1: Industrial applications of organic-inorganic hybrid nanocomposites. [12]

Preparation of organic-inorganic nanocomposites is often achieved by incorporating inorganic nanoparticles into selected polymer matrices. A range of inorganic nanoparticles such as cerium oxide, [13] magnetite, [14] titanium dioxide, [15] silica, [16-18] and clay [19-22] have been successfully incorporated into polymer materials for targeted end-use applications. The most common inorganic nanoparticles belong to the layered silicates. Materials obtained from incorporating clay platelets in polymer matrices are usually termed polymer-clay nanocomposites (PCNs).

2.1.1 Polymer-clay nanocomposites

Polymer-clay nanocomposites are materials in which the dispersed clay particles have one of their dimensions in the nanometre scale. [23] The increased research on clay layered-silicates as inorganic fillers is due to the availability, low cost and high surface area-to-volume ratio of the individual clay layers. [24] The simple mixing of polymer and layered silicates doesn't usually lead to the generation of a nanocomposite material but a poor dispersion of stacked sheets, whose dimensions are in the micrometre scale. Separation into discrete phases usually takes place, generating microcomposites in most instances. This is because clay minerals are naturally hydrophilic and the polymer phase is hydrophobic hence they are incompatible. [25] To generate PCNs, the polymer chains must penetrate into the interlayer spaces within the clay tactoids which forces the individual platelets to separate and disperse in the polymer matrix. [26] However, the stacked clay layers may not fully separate into individual platelets leading to different structures such as phase separated (microcomposites), intercalated (microcomposites) and exfoliated (nanocomposites) as illustrated in Figure 2.2. Exfoliated clay platelets are almost impermeable to small molecules such as water vapour and have been reported to provide excellent barrier properties in nanocomposites. [27,28]

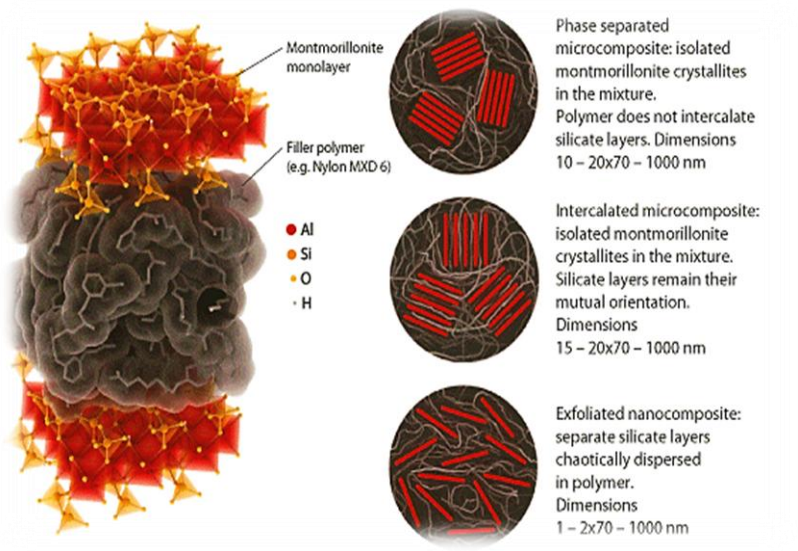

Figure 2.2: Schematic illustration of the terminology used to describe PCNs structures. [29]

2.1.2 Structure and chemistry of clay

2.1.2.1 Types of clay nanofillers

Clay minerals that are mostly employed in preparing polymer-clay nanocomposites fall into two families, the 1:1 phyllosilicates (non-swelling clays) and the 2:1 phyllosilicates (swelling clays).

1:1 Phyllosilicates: Also known as the kaolinite group. The structural sheets composed of one silicate layer (tetrahedral) tightly bonded to one aluminium oxide/hydroxide layer (octahedral) are held together by hydrogen bonds. However because of the numerous bonds, the sheets are held rather tightly together and are thus not expandable (non-swellable).

2:1 Phyllosilicates: The layer of minerals is composed of a magnesium layer octahedrally coordinated to oxygen atoms and hydroxyl molecules. This central layer is sandwiched between two tetrahedral silicate layers in a 2:1 fashion that dictates the family name. The most common smectite in this family is montmorillonite (MMT) clay and the reason for an expandable interlayer is the presence of large and low-valent hydrated ions. [30]

2.1.2.2 Chemistry of clay

The layer thickness of the 2:1 phyllosilicates is about 1 nm and the lateral dimension of the layers may vary from 30 nm to several micrometres (or even larger), depending on the particular silicate. A van der Waals gap exists between the layers usually called a gallery or interlayer. Isomorphic substitution within the crystal structure of the gallery (i.e. Al^{+3} replaced by Mg^{+2}) generates negative charges that are counterbalanced by alkali and alkaline earth ions present in the gallery. MMT clay is a very popular choice for making nanocomposites because of its small particle size (less than 2 micrometres) amongst the naturally occurring clays, and a high surface area in the range 600-800 m^2/g. The high swelling capacity is essential for efficient intercalation of polymer chains. MMT clay is characterized by a moderate surface charge known as the cation exchange capacity (CEC) which is usually expressed in Meq/100g. However, because the moderate surface charge for each layer varies, the CEC is considered an average value. [31] The architecture of MMT is presented in Figure 2.3.

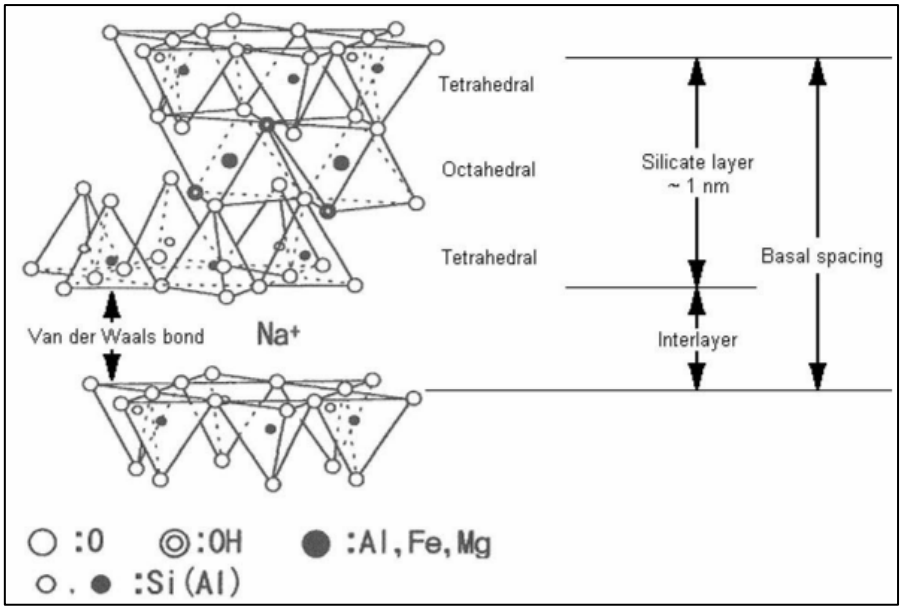

Figure 2.3. General structure of MMT clay. [32]

Pristine clay usually contains hydrated K^+ (or Na^+) ions. MMT clay is hydrophilic, hence immiscible with the hydrophobic polymer matrix. To make the MMT clay miscible with the hydrophobic polymer matrix, the hydrophilic clay surface must be modified to permit the intercalation of polymer chains into the inter-layer galleries. Clay modification can be accomplished by methods such as physical treatment via ultrasound and plasma, [33] binding of organic and inorganic ions at the edges of the clay, [34] and ion exchange reactions within the interlayer galleries using alkylphosphonium and alkylammonium cations. [33] The modification processes decrease the surface energy of the inorganic clay platelets and improve the wetting characteristics of the polymer matrix resulting in a larger interlayer spacing. The resulting product will be the organically modified clay, which is more compatible with the organic polymer matrix. [26,35]

2.1.3 Surface modification of clay

An easier way to modify the clay surface is the traditional ion exchange method. This is because the inorganic cations present in the interlayer galleries are not strongly bonded to the clay surface hence small organic cationic surfactant molecules can replace them during the cation exchange reactions, enlarging the interlayer spacing in the process as presented in Figure 2.4. [23,36] However, the basal spacing of the resultant organoclay depends on the degree of cation exchange. [37] MMT modified via cation exchange has been studied extensively and in practical applications in the area of polymer-clay nanocomposites. The molecular architecture and chain length of the alkylammonium modifiers have been reported to exert

significant effects on the exfoliation of clay platelets, morphology and thermal properties of the PCN [38]. It was found that in order for the clay modification to be effective, the alkyl chains of the modifier should bear at least eight carbon atoms and longer. In addition to the molecular structure of the alkylammonium surfactant, the loading of the surfactant into the organoclay galleries influences the clay dispersion in the polymer matrix. [39] Another advantage of the organic cations is the provision of groups that may react with the polymer matrix or copolymerize with the present monomers to improve the strength of the interface between the clay sheets and the polymer matrix. [19,40]

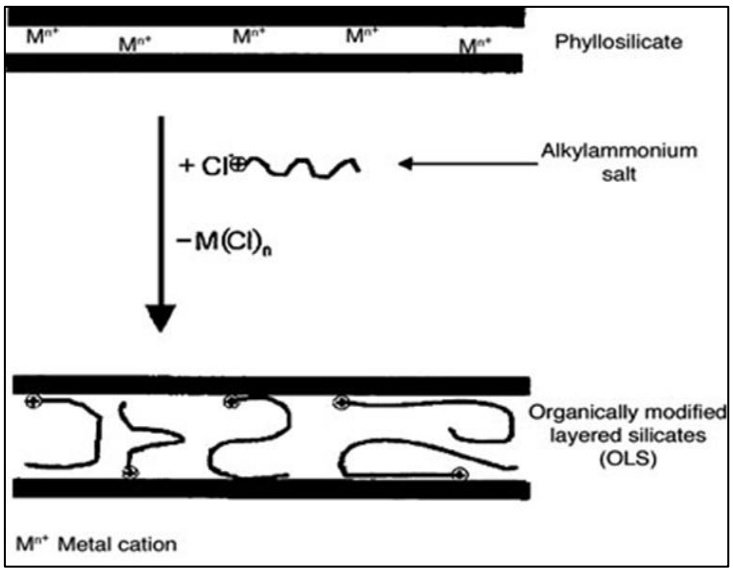

Figure 2.4: Schematic picture of an ion exchange reaction. [23,41]

2.1.4 Preparation approaches and characterization of PCNs

The primary goal in the preparation of PCNs is to break up the primary nanoparticle agglomerates and facilitate their dispersion in the polymer matrix. To achieve this, the experimental conditions must be tailored in such a way that they are compatible with the chemistry of the polymer. There are three main techniques for polymer-clay nanocomposite synthesis that include melt-compounding, solvent-based blending and in situ polymerization.

2.1.4.1 Melt-compounding

Melt compounding is regarded as one of the oldest techniques in the preparation of PCNs. The method involves mixing clay by annealing it (statically or under shear) with polymer, above the softening point of the polymer. Melt compounding is popular as it was found to be compatible with processes that include extrusion, blow moulding and injection; hence it is utilised industrially more than any other method. [42] This technique is usually limited to

thermoplastics but its concepts can be used for thermoset processes, especially if one considers reactive injection moulding or resin transfer moulding. However, the method rather yields microcomposites than the desired nanocomposites as it is difficult for polymer chains to penetrate the confined clay galleries and that if modified clay is used, the clay modifier may decompose due to the heat applied causing the clay interlayer distance to decrease significantly. [43]

2.1.4.2 Solvent-based blending

Also known as solution blending, it is a solvent-assisted process by which a polymer or prepolymer is filled with nanosized clay particles, either individual clay platelets or intercalated layer stacks. Generally the basic principle of the procedure is that a solvent capable of dissolving the polymer and swelling the clay is selected. The polymer solution and the clay suspension are mixed under high shear or ultrasonic stirring, and then the solvent is removed by evaporation (film casting or freeze drying) or by precipitation in a non-solvent. The polymer-clay mixture is then subjected to thermal treatment for drying [44].

2.1.4.3 In situ polymerization

The method was first reported by Toyota researchers for the synthesis of polyamide nanocomposites, which led to rapid growth in the nanocomposites research. [45] For generations of PCNs, the clay is swollen in monomer. Polymerization is initiated from inside the clay galleries. The growth of polymer chains expands the inter layer galleries facilitating the exfoliation of the clay tactoids. [46] In situ polymerization has been reported to be compatible with heterogeneous polymerization methods such as suspension, emulsion and mini-emulsion polymerization. [47] Although semi-exfoliated and exfoliated structured PCNs can be obtained by other methods such as solution blending and melt compounding, control of clay dispersion remains a great challenge. However, using in situ polymerization methods it is possible to manipulate filler dispersion and latex morphologies due to improved polymer-clay interactions which leads to highly organized structures that include encapsulated nanoparticles, [19] cellularly arranged and armoured polymer-clay nanocomposites. [48]

There are several heterophase processes that allow for the fabrication of nanoparticles in aqueous media. As compared to step-growth polymerizations, free-radical polymerizations, in particular in the heterophase, present several advantages. In addition to providing the ability to conduct the reaction in water which is a non-toxic medium, heterophase polymerization

allows the easy removal of the product from the reactor. The most common heterophase polymerization method is emulsion polymerization, which is used in various industrial applications. [46] This technique is however not well suited to the polymerization of highly hydrophobic monomers and the encapsulation of preformed or inorganic nanoparticles. [1,49-51] In this work, miniemulsion polymerization was employed as the *in-situ* polymerization method to prepare PCNs.

2.1.4.4 Miniemulsion polymerization

The miniemulsion polymerization method has been reported to be a versatile technique in the preparation of a wide range of polymers and structured materials in confined geometries., [52-54] The great versatility of this method arises from the usage of the droplet as a template, meaning the droplet composition stays constant during polymerization and can therefore be adjusted before or during the emulsification process. This allows for the conduction of co-polymerizations and encapsulation of solid or liquid particles.

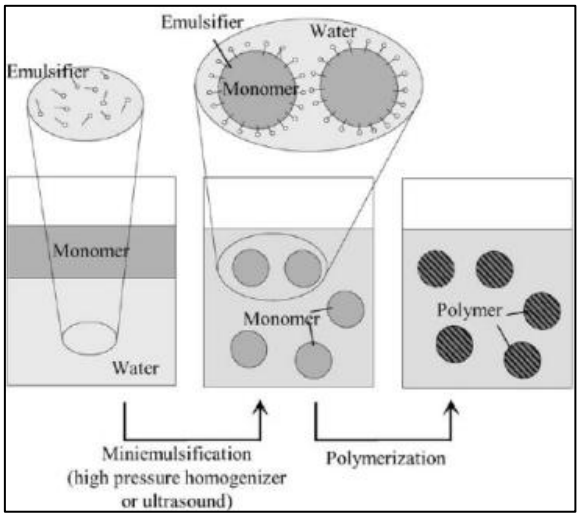

Figure 2.5. The principle of miniemulsion polymerization. [1,53]

Generally, miniemulsions consist of small and stable, but narrowly distributed droplets in a continuous phase. The system is usually obtained by high shear methods such as ultra-sonication or high pressure homogenizers which break down the monomer droplets to a size range of 50-500 nm. The stability of the droplets is ensured by the combination of the amphiphilic component, the surfactant and the osmotic pressure agent also known as the co-stabilizer (soluble and homogeneously distributed in the droplet phase), as illustrated in Figure 2.5. Surfactants (ionic or non-ionic) in adequate amounts are used to provide the mini-emulsion droplets with colloidal stability against coalescence. The co-stabilizer has a lower

solubility than the rest of the droplet phase and hence builds up an osmotic pressure which counteracts the Laplace pressure (difference between the pressure inside the monomer droplet/polymer particle and the pressure in the continuous phase). [55] The instability of a miniemulsion has been reported to have an influence on the number of monomer droplets and therefore on the rate of polymerization, particle size and average molecular weight of the final product. [56] In miniemulsion, because most of the prepared monomer droplets are small and reside on the droplet surfaces, relatively little monomer is available in the aqueous phase. This means the free surfactant concentration will be below the critical micelle concentration (CMC) therefore nucleation occurs primarily within the monomer droplets.

Preparation of polystyrene and poly(styrene-co-butyl acrylate) latexes has been reported. [57-59] In a series of studies, Zengeni et al [19] investigated the encapsulation of Laponite clay in polystyrene and poly(styrene-co-butyl acrylate) and as much as 20 wt.% was effectively encapsulated. However, up to 50 wt.% clay content was incorporated in the different polymer matrices, without necessarily being encapsulated, but attached on the polymer particle surfaces. Stable highly filled latexes, (> 10 wt.% clay), could only be obtained with total solids contents not exceeding 10 %.

The current study focuses on manipulating the robustness of miniemulsification to: (a) incorporate as much as 30 wt.% MMT clay in poly(styrene-co-butyl acrylate); (b) vary the copolymer composition of poly(styrene-co-butyl acrylate) latexes, and investigate the barrier properties of the resultant films cast from the latexes, regarding the water vapour sorption behaviour of the films.

2.1.5 Characterization of PCNs

2.1.5.1 PCN latex particle size

The incorporation of clay platelets in polymer matrices significantly influences the particle size and particle size distribution of the latex. The determination of these parameters is important as they play a significant role in the final product applications. The most common methods used for particle size analysis are transmission electron microscopy (TEM) and dynamic light scattering (DLS). [60,61] However, quantification of the clay with these techniques still remains a challenge since clay platelets, encapsulated or bound on the polymer particle surface, are not evenly distributed throughout the polymer matrix.

2.1.5.2 Molecular weight of polymer

Size Exclusion Chromatography (SEC) remains the most versatile route for determining the molecular weight of PCN materials. Molecular weight characteristics of polymers play a vital role on their overall physical properties. The presence of clay in PCNs affects the molecular weight and molecular weight distribution of the polymer chains but often complicates the determination of molecular weights using the SEC method. This is because the clay and polymer have to be separated via reverse ion exchange processes prior to SEC analysis and the constraint in achieving this is determined by the type and degree of interactions between the clay platelets and the polymer.

2.1.5.3 Morphology of PCNs

Scanning electron microscopy (SEM), TEM and x-ray diffraction (XRD) are the common techniques employed in analysing the morphological properties of PCNs which are generally described by the way in which clay platelets are dispersed in the polymer matrix. [32] XRD is used to investigate the degree of exfoliation of the clay tactoids by measuring the distance between the basal layers of layered silicates (d-spacing) using Bragg's law (Equation 2,1):

$$n\lambda = 2d\,\mathrm{Sin}\theta \qquad (2.1)$$

where λ is the wavelength of the X-ray radiation, n is the order of interference, d is the interlayer distance and θ is the measured diffraction angle. Intercalation and exfoliation alters the dimensions of gaps between the silicate layers and so an increase in the interlayer distance indicates that a nanocomposite has formed.[37] Although XRD is a versatile technique for measuring the d-spacing, it may be insufficient for measurement in disordered and exfoliated materials that give no XRD peaks. This technique also does not give any information about the location of clay platelets in the polymer matrix. [62] Like TEM, SEM is usually employed to investigate the morphology. However, the information given is limited to the nanoparticles located on the surface of the polymer particles. Using TEM, the contrast between the clay platelets and the particles provides a visual clue that the material has an intercalated, semi-exfoliated or fully exfoliated structure. However, the major drawback is obtaining a sample that is a true representation of the whole PCN film or latex. [63]

2.1.5.4 Thermo-mechanical properties

Thermo-mechanical properties of PCNs are obtained from the material's response to cyclic deformation as a function of temperature. These properties, measured by dynamic mechanical analysis (DMA), are closely related to the material's processing and end-use applications.

Molecular motions and relaxations that take place during the measurements give results such as storage modulus (G') and glass transition temperature (T_g). The presence of clay platelets in the polymer matrix can supress the mobility of polymer chains due to the interactions between the clay platelets and the polymer matrix, a factor which often leads to improved thermo-mechanical properties. [5,64] However, for the interactions to be effective, the clay platelets must be fully exfoliated and evenly dispersed within the polymer matrix. The material's melting temperature, crystallisation behaviour and glass transition temperature can also be effectively measured by differential scanning calorimetry (DSC).

2.1.5.5 Thermal stability

The most widely used technique employed in determining the material's ability to resist thermal degradation is thermogravimetric analysis. This method is based on continuous measurements of the material's weight change as a function of temperature on a sensitive balance in air or inert atmosphere. This is referred to as non-isothermal TGA and the decomposition profile is monitored typically from room temperature to around 600-800 °C. Improvement in thermal stability is related to the effect of the clay char which acts as an insulator and barrier to mass transport at the decomposition site. [65-67]

2.2 Mass transport in polymers

2.2.1 Introduction

The uptake and transport of molecules through polymer systems can be of great importance to the end use applications of materials. Permeability is a critical performance parameter in many industrial applications such as petrochemical, [68] water purification, [69] electronics, [70] medical, [71] and packaging, [72] where the rate of permeation of molecules from the environment to the product (or vice versa) must be controlled. This is usually done to counteract consequences that include:

- Reduced shelf life of beverages, pharmaceuticals and foodstuffs;
- Decreased reliability of electronic systems leading to high repair costs;
- Enhanced moisture degradation/corrosion rates in poorly protected systems leading to high maintenance costs.

Mass transport of small molecules such as oxygen and water vapour through polymers is a function of both the polymer and the diffusing species i.e. (a) the morphology of the polymer matrix, (b) molecular size and physical state of the diffusing species, (c) surface or interfacial

energies of the monolayer films, and (d) solubility limit of the solute within the polymer matrix. [73,74] It is reported that films made from polymer systems containing polar functional groups such as poly(ethylene-co-vinyl alcohol) are excellent gas barriers in the anhydrous state, but poor to water and water vapour permeation. [75] On the other hand, films derived from hydrophobic polymer systems such as polystyrene, polyethylene and poly(styrene-co-butyl acrylate) are poor gas barriers but provide good barriers to water and water vapour. [76,77] Besides the polymer, coating additives and fillers such as silica and clay affect the moisture sorption behaviour of the polymeric film. [78] Polymeric films are the common materials employed as coatings to protect sensitive materials from the environment. As such, the product requirements of polymeric coatings and films can be challenging, usually requiring mechanical performance, optical transparency and barrier performance at minimum thickness and cost. A direct exploitation of the good barrier properties of a PCN is in ceramic tiles and surface coating, [79-81] drug delivery, [82] and food packaging industries. [11]

The effectiveness of the filler to improve the barrier properties of a coating is mostly governed by the morphology (filler content, exfoliation and dispersion in the polymer matrix). [83] However, little has been reported on the effect of varying the copolymer composition on the morphology of the final coating, and the correlation thereof, on the moisture sorption behaviour of the polymeric films.

2.2.2 Nanoclay-based barrier coatings

One of the major advantages of the nanocomposites is their enhanced barrier properties. [22,27,84] This is largely due to the fact that clay platelets have a large surface area-to-volume ratio and are impermeable, therefore forcing an alternative pathway for a permeate traversing the nanocomposite structure. [85] One intuitively understandable idea is that molecules diffusing in the polymer will be slowed by increasing tortuosity as they meet essentially impermeable clay platelets in their path and have to find a way around them as illustrated in Figure 2.6. It is reported that gas and vapour permeability through polymeric structures can be reduced even with small nanoclay loadings (< 10 wt.%). [28]

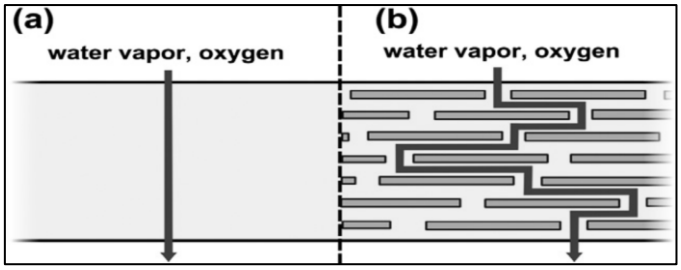

Figure 2.6: Illustration of clay platelets acting as obstacles to molecules' diffusion. [81]

2.2.3 Transport principles

Permeation is a complex mass transport process describing the movement of gases and vapours through a polymeric film. The transport behaviour is generally classified into three different categories. [86]

a) When the diffusion rate is less than the sorption rate and the sorption-equilibrium is rapidly reached, the permeation is then called "Fickian" and the gas transport follows the solution-diffusion model.

b) When the diffusion rate is very high relative to the sorption rate, the permeation is "Anomalous" and is sorption controlled.

c) When the sorption and diffusion rates are comparable, the permeation process is "Non-Fickian". This is the most complicated of the three and usually occurs in the case of liquid penetrants through glassy polymer membranes. [87]

The rate of gas/vapour sorption in a polymeric film can be used to estimate the diffusion coefficient. The diffusion coefficient values can be used to investigate the relative mobility rates of a penetrant and a polymer chain during the sorption process. [88]

In 1855, by analogy to Fourier's law of heat conduction, Fick proposed the law of mass diffusion, which states that "the rate of transfer of diffusing substances through a unit area of a section is proportional to the concentration gradient measured normal to the section. [89] The permeate flux through a polymeric membrane, *J*, is driven by the concentration gradient of the absorbed molecules in the polymer matrix and mathematically expressed as:

$$J = -D\frac{\partial C}{\partial x} \qquad (2.2)$$

where D is the diffusivity, C is the concentration of the diffusing species and x is the space co-ordinate measured normal to the section. [90] Equation 2.2 allows us to calculate the passage of flux in a steady-state system, where the concentration gradient of the permeating species is invariant with time. In most applications, diffusion of small molecules through a polymeric

system is restricted to one direction, where a gradient of concentration is present and transport only occurs along the x-axis. [91] In these cases, the transport is described by a change in concentration with time and is expressed in the form of a second order differential equation by Fick's second law (see Equation 2.3). [92]

$$\frac{\partial C}{\partial t} = \mathbf{D}\frac{\partial^2 C}{\partial x^2} \qquad \textbf{(2.3)}$$

Thomas Graham first formulated the solution-diffusion model which describes the mechanism whereby gases and vapours move through a polymeric film from a region of high partial pressure on one side of the film/membrane, to a region of lower partial pressure on the other side. [93] A quantitative solution to Graham's solution-diffusion model was then constructed based on Henry's law of solubility, where the concentration of gas in the membrane was directly proportional to the applied partial pressure as illustrated in Figure 2.7. [94]

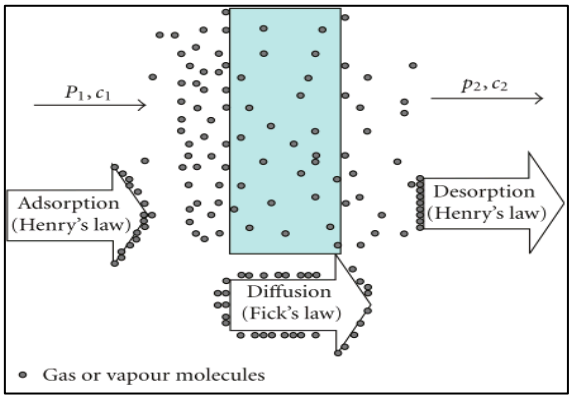

Figure 2.7: General mechanism of gas permeation through a polymeric film. [11]

The sorption and diffusion steps in the solution-diffusion model are governed by the chemical and physical properties of the polymer film, external conditions such as temperature and penetrant concentration, as well as interactions between the polymer matrix and the diffusing species. [28,95] The rate of permeation is generally expressed by the permeability rather than by a diffusion coefficient. Permeability (P) [$mol.cm^2.Pa^{-1}.cm^{-3}.s^{-1}$] of small molecules through a polymer film therefore depends on two coefficients; solubility and diffusion. It is mathematically expressed as the product of the solubility coefficient (S) [$mol.Pa^{-1}.cm^{-3}$] and the diffusion coefficient (D) [$cm^2.s^{-1}$] as illustrated in Equation 2.4. [96]

$$\boldsymbol{P = S \times D} \qquad \textbf{(2.4)}$$

When specific interactions between penetrant and polymer such as hydrogen bonding become important, the relationship in Equation 2.4 is more complicated. In the presence of swelling

vapours such as water in ethyl cellulose, solubility and diffusivity show concentration dependence. [97,98] The polymeric system may progressively lose its compactness. As such, at higher concentrations, the polymeric film may dissolve in the water vapour. [99]

2.2.4 Equilibrium sorption models

The sorption of a penetrant in a polymer matrix is described by the sorption isotherm which correlates, at constant temperature, with the amount of sorbed penetrant to the relative pressure of the phase outside the polymer. Depending on the particular polymer-penetrant interactions, sorption isotherms may display significant differences in shape which can be theoretically explained by various models as presented in Figure 2.8. [74]

It is reported that the micro-voids in a glassy polymeric system can immobilize a portion of the penetrant molecules (by entrapment or binding at high energy sites) at their molecular peripheries. This system typically shows a concave shaped sorption isotherm termed the Langmuir type. [100]. On the contrary, for high penetrant concentrations in rubbery polymers, the sorption isotherm displays a convex shaped curve. This can be explained by the preference for the formation of penetrant-penetrant interactions and is known as the Flory-Huggins isotherm type. [101] However, because polymeric systems are usually complex, the Dual sorption mode (Brunauer, Emmett and Teller mode) which is a combination of the Langmuir and Flory-Huggins sorption mode is often observed. [102]

At low penetrant activity there is preferential sorption of the penetrant on specific sites while, at high activity, strong interactions with the penetrating species leads to increased polymer chain mobility which may induce structural transformations or clustering of the permeate molecules. Linear isotherms imply that Henry's law (ideal dissolution) is valid over the entire range of penetrant activities. However, non-linear isotherms consequently indicate that the sorption process deviates from ideality, i.e. they reflect interaction between permeant molecules and the polymer structure.

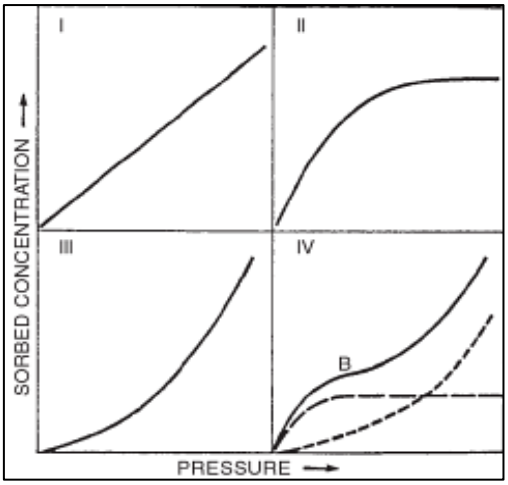

Figure 2.8: Sorption isotherm models. (I) Henry's law model; (II) Langmuir type; (III) Flory-Huggins type; (IV) BET (dual sorption mode) model type. B represents the site saturation point [103]

2.2.5 Experimental method

Sorption kinetics is one of the most common experimental techniques to investigate the diffusion of small molecules in polymer systems. In the simplest experiment, the polymeric film remains initially under vacuum, and the gas or vapour is introduced and maintained at constant pressure. The vapour or gas then dissolves and diffuses into the membrane. The weight gain is measured with a balance and the relative mass uptake is reported as a function of time over a range of partial pressures. The investigation of the water vapour sorption in polymers can easily be performed gravimetrically. A well-known solution was developed by Crank et al, [104] which is more suitable to moderate and long-time approximation. Assuming an ideal Fickian transport process, the sorption data for a membrane with plane sheet geometry can be represented by Equation 2.5. [105,106]

$$\frac{Mt}{Meq} = 1 - \frac{8}{\pi^2} \sum_{n=0}^{\infty} \frac{1}{(2n+1)^2} \exp\left(-\frac{(2n+1)^2 D \pi^2 t}{l^2}\right) \qquad (2.5)$$

where ***Mt*** (mg) is the amount of sorbed water at time t, ***Meq*** (mg) is the amount of water vapour sorbed at equilibrium, ***l*** (cm) is the thickness of the film, ***D*** is the diffusion coefficient and ***n*** are values from 0 to infinity. At sufficiently short times where $0.1 < \frac{Mt}{Meq} < 0.5$, the water vapour uptake is proportional to the square root of time as shown in Equation 2.6.

$$\frac{Mt}{Meq} = \frac{4\sqrt{D}}{l\sqrt{\pi}}\sqrt{t} \qquad (2.6)$$

Applying these methods, the diffusion coefficient can be determined in isothermal sorption experiments. By plotting $\frac{Mt}{Meq}$ against $\frac{\sqrt{t}}{l}$, we obtain a straight line until $t_{\frac{1}{2}}$, the half-life time

where $\frac{Mt}{Meq} = \frac{1}{2}$. The diffusion coefficient value is then estimated from the slope of this curve. The solubility coefficient (***S***) is calculated from the equilibrium penetrant in the kinetic curve and is expressed as the ratio between the penetrant concentration at equilibrium ***C***, and the vapour pressure ***P*** exerted by the penetrant such as water vapour, above the film as shown in Equation 2.7. The equilibrium penetrant concentration ***C*** is calculated from the initial and equilibrium amounts of the sorbed penetrant as illustrated in Equation 2.8. [107]

$$\mathbf{S} = \frac{\boldsymbol{C}}{\boldsymbol{P}} \qquad \textbf{(2.7)}$$

$$\mathbf{C} = \frac{\boldsymbol{Meq - Mo} \times \boldsymbol{Vm}}{\boldsymbol{Vp} \times \boldsymbol{MOH_2}} \qquad \textbf{(2.8)}$$

where ***Meq*** (mg) and ***Mo*** (mg) is the final and initial mass of the film following the uptake of water vapour, ***Vp*** (cm^{-3}) is the volume of the film, $\boldsymbol{M_{H2O}}$ ($gmol^{-1}$) is the molecular weight of water and ***Vm*** (22414 cm^{-3}) is the molar volume of the water at standard conditions of temperature and pressure.

2.2.6 Factors influencing mass transport

2.2.6.1 Concentration

Henry's law for ideal gas sorption explains that solubility is directly proportional to the external gas pressure. Although Henry's law does not always apply, the equilibrium concentration of sorbed molecules will increase with external concentration. [108] However, large deviations are observed between theoretical predictions and the experimental parameter values for non-ideal conditions particularly at elevated penetrant pressures. Diffusion coefficients may depend on concentration if there are significant interactions between polymer and the diffusing species. Since diffusion is driven by concentration gradients, the initial high external concentrations will promote rapid diffusion. As time progresses, the system will reach an equilibrium concentration determined by solubility and external concentration. Increasing the equilibrium concentrations may then have negative or positive effects on permeation rates through the material.

2.2.6.2 Polymer chemistry

Chemical composition of the polymer matrix will have a strong influence on the diffusion and solubility properties of small molecules in the polymer system. Polymer matrices with polar backbones will have a strong affinity on polar molecules such as water. As such,

diffusion coefficients can increase with the absorbed concentration of molecules due to strong interactions that induce structural transformations such as swelling of the polymer matrix. [109]

2.2.6.3 Free volume

Free volume describes an intrinsic property of the polymer matrix arising from gaps left between entangled polymer chains. Free volume pores are dynamic and transient in nature since the size and existence of any individual free volume depends on the vibrations and motions of the surrounding polymer chains. [110] The absorption and diffusion of small molecules in polymeric systems will depend to a significant extent on the available free volume within the polymer matrix. The greater the free volume, the higher the mobility of the molecules. However, free volume depends on other factors such as temperature, crystallinity and molecular orientation of the polymer system. [111]

2.2.6.4 Filler particles

Most common inorganic fillers such as clay and silica are usually considered as impermeable relative to the polymer matrix. Diffusing molecules would need to work their way around the impermeable clay particles, increasing path lengths and reducing mass transport rates. Improved barrier properties from the nano-sized fillers would therefore be expected from the increased lengths of diffusion paths. [112] If the diffusing species have an affinity for the surfaces of the filler particles then the interface between the polymer matrix and the filler may provide absorptive sites for the molecules, thereby increasing the solubility and reducing the permeation rates. [113]

The main factor, then, is expected to be the tortuosity, which is directly connected to the shape of the clay platelets and degree of dispersion within the polymer matrix. As such, the focus of this work is to incorporate as much as 30 wt. % MMT clay loadings in PSBA matrix with varying copolymer compositions. A correlation on the effect of copolymer composition variation and MMT clay loadings shall then be drawn regarding water vapour sorption behaviour of the PSBA-MMT films.

2.3 References

[1] van Herk, A. M. *Adv. Polym. Tech.* **2010**, *233*, 18.

[2] Jeon, I.; Baek, J. *Materials* **2010**, *3*, 3654.

[3] Paul, D. R.; Robeson, L. M. *Polym. J.* **2008**, *49*, 3187.

[4] Priolo, M. A.; Gamboa, D.; Holder, K. M.; Grunlan, J. C. *Nano Lett.* **2010**, *10*, 4970.

[5] Nair, T. M.; Kumaran, M. G.; Unnikrishnan, G.; Pillai, V. B. *J. Appl. Polym. Sci.* **2009**, *112*, 72.

[6] Ebina, T.; Mizukami, F. *Adv. Mater.* **2007**, *19*, 2450.

[7] Arun, R. *Sci. Pharm.* **2008**, *76*, 567.

[8] Del Valle, E. M. M. *Process Biochem.* **2004**, *39*, 1033.

[9] Ray, S. S. *Macromol. Chem. Phys.* **2014**, *215*, 1162.

[10] Mathiazhagan, A.; Rani, J. *Int. J. Chem. Reactor Eng.* **2011**, *Vol. 2*, 11.

[11] Siracusa, V. *Int. J. Polym. Mater.* **2012**, *2012*, 1.

[12] Bitinis, N.; Hernandez, M.; Verdejo, R.; Kenny, J. M.; Lopez-Manchado, M. A. *Adv. Mater.* **2011**, *23*, 5229.

[13] Zgheib, N.; Putaux, J.; Thill, A.; D'Agosto, F.; Lansalot, M.; Bourgeat-Lami, E. *Langmuir : ACS Appl. Mater. Interfaces* **2012**, *28*, 6163.

[14] Ramirez, L. P.; Landfester, K. *Macromol. Chem. Phys.* **2003**, *204*, 10.

[15] Chaichana, E.; Pathomsap, S.; Shiono, T.; Jongsomjit, B. *Chem. Eng. J.* **2013**, *17*, 33.

[16] Vlasveld, D. P. N.; Groenewold, J.; Bersee, H. E. N.; Picken, S. J. *Polym. J.* **2005**, *46*, 12567.

[17] Sanchez, C.; Julian, B.; Belleville, P.; Popall, M. *J. Mater. Chem.* **2005**, *15*, 3559.

[18] Saito, R.; Hosoya, T. *Polym. J* **2008**, *49*, 4546.

[19] Zengeni, E.; Hartmann, P. C.; Pasch, H. *ACS Appl. Mater. Interfaces* **2012**, *4*, 6957.

[20] Yoon, D. H.; Jang, J. W.; Seo, S. S.; Jeong, S.; Cheong, I. *Adv. Polym. Tech.* **2013**, *32*, 9.

[21] Yilmaz, O.; Cheaburu, C. N.; Durraccio, D.; Gulumser, G.; Vasile, C. *Appl. Clay Sci.* **2010**, *49*, 288.

[22] Somwangthanaroj, A.; Tantiviwattanawongsa, M.; Tanthapanichakoon, W. *Chem. Eng. J.* **2012**, *16*, 13.

[23] Gacitua, W.; Ballerini, A.; Zhang, J. *J. Mater. Chem.* **2005**, *7*, 159.

[24] Greesh, N.; Sinha Ray, S.; Bandyopadhyay, J. *Ind. Eng. Chem. Res.* **2013**, *52*, 16220.

[25] Theng; Benny, K. G. *Formation and properties of clay-polymer complexes*; Elsevier, **2012**; Vol. 4

[26] Nguyen, Q. T.; Baird, D. G. *Adv. Polym. Tech.* **2006**, *25*, 270.

[27] Sun, L.; Boo, W. J.; Clearfield, A.; Sue, H. J.; Pham, H. Q. *J. Membr. Sci.* **2008**, *318*, 129.

[28] Cloete, V. PhD, Stellenbosch University, **2011**.

[29] Anoukou, K.; Zaïri, F.; Naït-Abdelaziz, M.; Zaoui, A.; Messager, T.; Gloaguen, J. *Compos. Sci. Technol.* **2011**, *71*, 197.

[30] Utracki, L. A.; Broughton, B.; González, N.; de Carvalho, L. H.; Achete, C. A. *Polym. Eng. Sci.* **2011**, *51*, 559.

[31] Golubeva, O. Y.; Gusarov, V. V. *Glass Phys. Chem* **2007**, *33*, 237.

[32] Fu, X.; Qutubuddin, S. *Polym. J.* **2001**, *42*, 807.

[33] Bergaya, F.; Lagaly, G. *Appl. Clay Sci.* **2001**, *19*, 1.

[34] Voorn, D. J.; Ming, W.; Van Herk, A. M. *Macromolecules* **2006**, *39*, 4654.

[35] Kiliaris, P.; Papaspyrides, C. D. *Prog. Polym. Sci.* **2010**, *35*, 902.

[36] Tombácz, E.; Szekeres, M.; Baranyi, L.; Micheli, E. *Colloids Surf., A* **1998**, *141*, 379.

[37] Greesh, N.; Hartmann, P. C.; Cloete, V.; Sanderson, R. D. *J. Polym. Sci., Part B: Polym. Phys.* **2008**, *46*, 3619.

[38] Akelah, A.; Moet, A. *J. Membr. Sci.* **1996**, *31*, 3589.

[39] Krishnamoorti, R.; Vaia, R. A.; Giannelis, E. P. *Chem. Mater.* **1996**, *8*, 1728.

[40] Xi, Y.; Frost, R. L.; He, H.; Kloprogge, T.; Bostrom, T. *Langmuir : ACS Appl. Mater. Interfaces* **2005**, *21*, 8675.

[41] Fischer, H. *Mater. Sci. Eng., C.* **2003**, *23*, 763.

[42] Sinha Ray, S.; Okamoto, M. *Prog. Polym. Sci.* **2003**, *28*, 1539.

[43] Ogawa, M.; Kuroda, K. *Bull. Chem. Soc. Jpn.* **1997**, *70*, 2593.

[44] Mittal, V. *Advances in polyolefin nanocomposites*; CRC Press, **2011**

[45] Huang, X.; Brittain, W. J. *Macromolecules* **2001**, *34*, 3255.

[46] Mittal, V. *In-situ synthesis of polymer nanocomposites*; John Wiley & Sons, **2011**

[47] Peruzzo, P. J.; Bonnefond, A.; Reyes, Y.; Fernández, M.; Fare, J.; Ronne, E.; Paulis, M.; Leiza, J. R. *Int. J. Adhes. Adhes.* **2014**, *48*, 295.

[48] Negrete-Herrera, N.; Putaux, J.; David, L.; Haas, F.; Bourgeat-Lami, E. *Macromol. Rapid Commun.* **2007**, *28*, 1567.

[49] Van Herk, A. M. *Adv. Polym. Tech.* **2010**, *233*, 1.

[50] Landfester, K.; Weiss, C. K. *Adv. Polym. Sci.* **2010**, *229*, 1.

[51] Zhang, Y.; Landfester, K.; Taden, A. *Macromolecules* **2014**, *47*, 1030.

[52] Xu, Z. Z.; Wang, C. C.; Yang, W. L.; Deng, Y. H.; Fu, S. K. *J. Magn. Magn. Mater.* **2004**, *277*, 136.

[53] Schork, F. J.; Luo, Y.; Smulders, W.; Russum, J. P.; Butté, A.; Fontenot, K. In *Polymer Particles*; Okubo, M., Ed.; Springer Berlin Heidelberg: **2005**; Vol. 175, p 129.

[54] Landfester, K. *Macromol. Rapid Commun.* **2001**, *22*, 896.

[55] Zetterlund, P. B.; Okubo, M. *Macromol. Theory Simul.* **2006**, *15*, 40.

[56] Mirzataheri, M.; A., R. M.; Atai, M. *Polymer Int.* **2011**, *60*, 613.

[57] Zengeni, E. MSc, University of Stellenbosch, **2009**.

[58] Tong, Z.; Deng, Y. *Ind. Eng. Chem. Res.* **2006**, *45*, 2641.

[59] Bonnefond, A.; Paulis, M.; Bon, S. A.; Leiza, J. R. *Langmuir : ACS Appl. Mater. Interfacess* **2013**, *29*, 2397.

[60] Morgan, A. B.; Gilman, J. W. *J. Appl. Polym. Sci.* **2003**, *87*, 1329.

[61] Wang, Y.; Zhang, L.; Tang, C.; Yu, D. *J. Appl. Polym. Sci.* **2000**, *78*, 1879.

[62] Zengeni, E.; Hartmann, P. C.; Pasch, H. *Macromol. Chem. Phys.* **2013**, *214*, 62.

[63] Cavaill, J. Y.; Vassoille, R.; Tholletl, G.; Rios, L.; Pichot, C. *Colloid. Polym. Sci.* **1991**, *269*, 11.

[64] Sadeghi, F.; Fereydoon, M.; Ajji, A. *Adv. Polym. Tech.* **2013**, *32*, E53.

[65] Agag1, T.; Koga, T.; Takeichi, T. *Polym. J.* **2001**, *42*, 10.

[66] Bo, X.; Zheng, Q.; Song, Y.; Shangguan, Y. *Polym. J.* **2006**, *47*, 2904.

[67] Bourbigot, S.; Gilman, J. W.; Wilkie, C. A. *Polym. Degrad. Stab.* **2004**, *84*, 483.

[68] Favre, E.; Svendsen, H. *J. Membr. Sci.* **2012**, *407*, 1.

[69] Broderick, A. H.; Manna, U.; Lynn, D. M. *Chem. Mater.* **2012**, *24*, 1786.

[70] Aluicio-Sarduy, E.; Baidak, A.; Vougioukalakis, G. C.; Keivanidis, P. E. *J. Phys. Chem. C.* **2014**, *118*, 2361.

[71] Lehner, R.; Wang, X.; Marsch, S.; Hunziker, P. *Nanomed. Nanotechnol. Biol. Med.* **2013**, *9*, 742.

[72] Rhim, J.; Park, H.; Ha, C. *Prog. Polym. Sci.* **2013**, *38*, 1629.

[73] George, S. C.; Thomas, S. *Prog. Polym. Sci.* **2001**, *26*, 985.

[74] Nielsen, L. E. *J. Macromol. Sci., Pure Appl. Chem.* **1967**, *1*, 929.

[75] Kit, K. M.; Schultz, J. M.; Gohil, R. M. *Polym. Eng. Sci.* **1995**, *35*, 680.

[76] Sun, Q.; Schork, F.; Deng, Y. *Compos. Sci. Technol.* **2007**, *67*, 1823.

[77] Greesh, N.; Hartmann, P. C.; Sanderson, R. D. *Macromol. Mater. Eng.* **2009**, *294*, 206.

[78] Picard, E.; Gérard, J. F.; Espuche, E. *J. Membr. Sci.* **2008**, *313*, 284.

[79] Cao, X. Q.; Vassen, R.; Stoever, D. *J. Eur. Ceram. Soc.* **2004**, *24*, 1.

[80] Shklover, V.; Braginsky, L.; Witz, G.; Mishrikey, M.; Hafner, C. *J. Comput. Theor. Nanosci.* **2008**, *5*, 862.

[81] Chatham, H. *Surf. Coat. Technol.* **1996**, *78*, 1.

[82] Kumari, A.; Yadav, S. K.; Yadav, S. C. *Colloids Surf., B.* **2010**, *75*, 1.

[83] Alix, S.; Follain, N.; Tenn, N.; Alexandre, B.; Bourbigot, S.; Soulestin, J.; Marais, S. *J. Phys. Chem. C.* **2012**, *116*, 4937.

[84] Merinska, D.; Kalendova, A.; Tesarikova, A. *AIP Conference Proceedings* **2014**, *1599*, 186.

[85] de Paiva, L. B.; Morales, A. R.; Valenzuela Díaz, F. R. *Applied Clay Science* **2008**, *42*, 8.

[86] Choudalakis, G.; Gotsis, A. D. In *Handbook of Polymernanocomposites. Processing, Performance and Application*; Springer: **2014**, p 415.

[87] Paul, D. R. *Berichte der Bunsengesellschaft für physikalische Chemie* **1979**, *83*, 294.

[88] Felder, R. M.; Huvard, G. S. *Curr. Appl Phys.* **1980**, *16*, 315.

[89] Lever, R. F.; Mandel, G. *J. Phys. Chem. Solids* **1962**, *23*, 599.

[90] Bramhall, G. *Wood Sci.* **1976**, *8*, 153.

[91] Treybal, R. E. *Mass-transfer operations*; McGraw-Hill New York, **1968**; Vol. 3

[92] Paul, A.; Laurila, T.; Vuorinen, V.; Divinski, S. V. In *Thermodynamics, Diffusion and the Kirkendall Effect in Solids*; Springer: **2014**, p 115.

[93] Stannett, V. *J. Membr. Sci.* **1978**, *3*, 97.

[94] Favre, E. *J. Membr. Sci.* **2004**, *229*, 241.

[95] Findenig, G.; Leimgruber, S.; Kargl, R.; Spirk, S.; Stana-Kleinschek, K.; Ribitsch, V. *ACS Appl. Mater. Interfaces* **2012**, *4*, 3199.

[96] Follain, N.; Valleton, J.; Lebrun, L.; Alexandre, B.; Schaetzel, P.; Metayer, M.; Marais, S. *J. Membr. Sci.* **2010**, *349*, 195.

[97] Lin, H.; Freeman, B. D. *Macromolecules* **2005**, *38*, 8394.

[98] Nazan , K.; Şahbaz, F. *J. Food Eng.* **2004**, *61*, 459.

[99] Bertuzzi, M. A.; Castro , E. F.; Armada, M.; Gottifredi, J. C. *J. Food Eng.* **2007**, *80*, 972.

[100] Kadam, A. A.; Karbowiak, T.; Voilley, A.; Debeaufort, F. *Food Sci. Technol. Res.* **2014**.

[101] Jeck, S.; Scharfer, P.; Schabel, W.; Kind, M. *Chem. Eng. Process.* **2011**, *50*, 543.

[102] Follain, N.; Belbekhouche, S.; Bras, J.; Siqueira, G.; Marais, S.; Dufresne, A. *J. Membr. Sci.* **2013**, *427*, 218.

[103] Sorrentino, A.; Gorrasi, G.; Tortora, M.; Vittoria, V. *Polym. Compos.* **2006**, 273.

[104] Crank, J. *J. Polym. Sci., Part A: Polym. Chem.* **1953**, *11*, 151.

[105] Nguyen, V. N.; Perrin, F. X.; Vernet, J. L. *Corros. Sci.* **2005**, *47*, 397.

[106] Ritger, P. L.; Peppas, N. A. *J. Controlled Release* **1987**, *5*, 37.

[107] Yasuda, H.; Stannett, V. *J. Polym. Sci., Part A: Polym. Chem.* **1962**, *57*, 907.

[108] Merkel, T. C.; Freeman, B. D.; Spontak, R. J.; He, Z.; Pinnau, I.; Meakin, P.; Hill, A. J. *Chem. Mater.* **2003**, *15*, 109.

[109] Mali, S.; Sakanaka, L. S.; Yamashita, F.; Grossmann, M. V. E. *Carbohydr. Polym.* **2005**, *60*, 283.

[110] Choudalakis, G.; Gotsis, A. D.; Schut, H.; Picken, S. J. *Eur. Polym. J.* **2011**, *47*, 264.

[111] Choudalakis, G.; Gotsis, A. D. *Curr. Opin. Colloid Interface Sci.* **2012**, *17*, 132.

[112] Merkel, T. C.; He, Z.; Pinnau, I.; Freeman, B. D.; Meakin, P.; Hill, A. J. *Macromolecules* **2003**, *36*, 6844.

[113] Gorrasi, G.; Tortora, M.; Vittoria, V.; Pollet, E.; Lepoittevin, B.; Alexandre, M.; Dubois, P. *Polym. J.*

2003, *44*, 2271.

Chapter 3

3 Water-based poly(styrene-co-butyl acrylate)/MMT latexes

3.1 Introduction

Polystyrene is an interesting material for the packaging industry since it presents several advantages such as (a) lightweight and significant mechanical rigidity and (b) being less fragile than glass. [1] Poly(n-butyl acrylate) provides performance characteristics to polymer formulations for copolymer plastics and cross-linkable polymer systems. [2] Montmorillonite (MMT) clay was employed as the reinforcing filler and its modification is described in detail later in this chapter. Vinylbenzyldodecyldimethylammonium chloride (VBDAC) was chosen as the clay modifier due to its compatibility with styrene monomer and the ability to copolymerize with butyl acrylate and styrene monomers. [3,4] In this study, styrene-butyl acrylate copolymers shall be abbreviated as PSBA.

The main focus of this study was to prepare polymer-clay hybrid latexes with varying copolymer compositions of PSBA-50:50, PSBA-40:60 and PSBA-30:70 mol.%. For each copolymer composition, the latexes were prepared with the following PSBA/MMT ratios: 100/0, 90/10, 80/20 and 70/30 wt.%. The experimental section of this chapter is divided into two parts. The first part describes the surface modification of Na^+-MMT by ion exchange using VBDAC. Modification was qualitatively characterized by Fourier transform infrared spectroscopy (FTIR) and quantitatively determined by thermogravimetric analysis (TGA).

The second part describes the preparation of neat PSBA latexes via miniemulsion polymerization. Transmission electron microscopy (TEM) was employed to investigate the latex particle size, distribution and morphology. Nuclear magnetic resonance (NMR) was employed to determine the chemical compositions and component ratios of the synthesized copolymers relative to the theoretical comonomer inputs. Size exclusion chromatography (SEC) was used to determine the molecular weight distributions of the PSBA copolymer materials. UV-Vis spectroscopy was used to investigate the optical properties of the PSBA films. Differential scanning calorimetry (DSC) was used to investigate the glass transition temperature (T_g) of the neat polymers and the PCNs. Dynamic mechanical analysis (DMA) was used to investigate the response of the materials to oscillatory deformation as a function of temperature, providing the storage modulus (G′), the loss modulus (G″), and the damping

factor (tanδ = G″/G′) of the PCNs. The synthetic procedure for the preparation of PSBA/MMT hybrid materials is also described.

3.2 Experimental

3.2.1 Materials

Styrene and n-butyl acrylate were supplied by Sigma-Aldrich. N-butyl acrylate was purified by passing through a basic alumina column to remove hydroquinone and monomethyl ether hydroquinone (MEHQ) inhibitors. Styrene was washed successively with a 0.03M aqueous potassium hydroxide (KOH) solution and distilled water to remove the inhibitor. The washed styrene was then distilled at 40 °C under reduced pressure to remove impurities and possible oligomers which could result from auto-polymerization. Azobisisobutyronitrile (AIBN) was supplied by Sigma-Aldrich and purified by recrystallization from methanol. Montmorillonite (MMT) clay with a CEC of 92.6 meq/100g was supplied by Rockwood Additives Limited, UK. Sodium dodecyl sulphate (SDS, 99%), 4-vinyl benzyl chloride (99%), N,N-dimethyldodecylamine (99%), hexadecane (HD, 99%) and silver nitrate ($AgNO_3$) were supplied by Sigma-Aldrich and used as received. VBDAC was synthesized using a method reported elsewhere [5] and its structure was confirmed by ^{1}H NMR spectroscopy (see Appendix 1).

3.2.2 Surface modification of MMT by ion-exchange

MMT (10 g) was dispersed in 750 mL distilled water. The mixture was stirred for 2 hr. until a clear dispersion was obtained. The organic modifier, VBDAC (4.25g), was dissolved in 250 mL distilled water, and added drop-wise to the MMT clay dispersion. The mixture was stirred for 24 hr. at room temperature. The dispersion was left to stand and excess water was decanted. The obtained precipitate was recovered by successive centrifugation steps at 3500 relative centrifugal force (RCF) for 5 min. Several washings were done on the obtained precipitate with distilled water until no free organic modifier was detectable using the silver nitrate test (a white precipitate was observed upon addition of a few drops of 0.1 mol silver nitrate to the supernatant). The obtained VBDA-MMT paste was put into a sealable container and stored in a fridge. Powder samples used to evaluate the extent of modifier grafting onto the MMT clay platelets were obtained by drying the VBDA-MMT overnight at 45 °C under vacuum. Modification of MMT was qualitatively assessed by FTIR and extent of VBDA grafting quantitatively determined by TGA.

3.2.3 Preparation of PSBA neat latexes with varying copolymer compositions

The styrene-butyl acrylate comonomer ratios were varied as given in Table 3.1. For each composition, the monomer miniemulsion was prepared by dispersing styrene, butyl acrylate, AIBN (0.4 wt.% relative to monomer), HD (4 wt.% relative to monomer in a 10 mM SDS solution (0.2 wt.% relative to water). The miniemulsion was formulated to maintain the total solids content of the latex at 10%. The dispersion was stirred for 30 min in an ice bath and then sonicated for 2 min at 50% amplitude without use of pulse, in an ice bath. The energy exerted on the solution was 4 kJ. The miniemulsion was transferred to a three-necked round bottom flask connected to a condenser and a nitrogen inlet, then purged with nitrogen for 15 min. The temperature of the oil bath was then raised to 70 °C, and the polymerisation reactions carried out for 4 hr. Samples for analysis were air dried, prior to drying in the oven under vacuum overnight. The PSBA component ratios were determined by ^{1}H NMR spectroscopy.

Table 3.1: Amount of Sty and BuA used in the miniemulsion recipe.

Sty/BuA (mol. %)	Amount of Sty (g)	Amount of BuA (g)
50/50	2.24	2.76
40/60	1.76	3.24
30/70	1.29	3.71

3.2.4 Preparation of PSBA-MMT hybrid latexes

3.2.4.1 Aqueous MMT-VBDA dispersions

In a typical procedure, a pre-determined amount of the VBDA-MMT paste was dispersed in 30 mM aqueous solution of SDS and stirred for 2 hr. The resulting dispersion was sonicated for 20 min at 90% amplitude and a pulse rate of 1sec for 5 min, exerting 65 $\pm$ 5kJ of energy, using a Vibra Cell Autotune series 750VCX high intensity ultrasonic processor (Sonics, U.S.A).

3.2.4.2 Styrene-butyl acrylate monomer miniemulsions

The monomer miniemulsion was prepared using the method described in section 3.2.3.

3.2.4.3 Co-sonication and polymerization

The aqueous MMT-VBDA and the styrene-butyl acrylate dispersions were added together and co-sonicated for 4 min, in an ice bath, at 50% amplitude exerting 10 ± 2 kJ of energy

with no pulse. The resultant hybrid miniemulsion was transferred to a three-necked round bottom flask connected to a condenser and a nitrogen inlet, and purged with nitrogen for 30 min. The temperature of the oil bath was then raised to 75 °C, and the polymerisation reactions carried out for 4 hr. The miniemulsion formulations for all materials are tabulated in Appendix 2.

3.2.4.4 Film preparation

Polymer films were prepared by casting 20 mL of latex (10% solids) into glass pans measuring 5 cm in diameter. The samples were allowed to air-dry 24 hr. in order to allow film formation, after which they were dried in an oven at 45 °C for a week. They were then stored in a desiccator to keep them dry.

3.2.5 Analytical Methods

3.2.5.1 Chemical composition and molecular weight determination

3.2.5.1.1 FTIR

FTIR measurements were conducted on the dried powder of VBDA-MMT clay using a 1650 Fourier transform infrared spectrophotometer (Perkin Elmer, USA). Thirty two scans were recorded for each sample with a wavenumber resolution of 4 cm^{-1} using the ATR mode.

Sample preparation

About 5-10 mg of the dried powder was placed on the ZnSe crystal sample holder with no further modification.

3.2.5.1.2 NMR

The dried latex samples were dissolved in $CDCl_3$ (50 mg/mL) and analysed by a Varian Inova 400 MHz NMR spectrometer by averaging 16 scans with a 0.3µsec pulse delay.

3.2.5.1.3 SEC

Sample prep: The dried neat latex samples were dissolved completely in THF (2 mg/mL). For the nanocomposites, a reverse cation exchange reaction was used in an effort to separate clay-attached and free copolymer chains.

Free copolymer chains

200 mg samples of the nanocomposites were each dissolved in 50 mL THF and then the free chains were separated from the anchored ones by high-speed ultracentrifugation (5000 RCF).

The supernatant solution was filtered using a 0.45 µm pore size filter to remove clay particles and the clay-attached copolymer chains. The recovered supernatant and clay-attached copolymers were separately dried in an oven at 45 °C for seven days to remove the solvent. The dried free copolymer samples were dissolved completely in THF (2 mg/mL).

Clay-attached copolymer chains

100 mg of the dried clay-attached copolymer samples were each dispersed in 25 mL THF and subsequently 0.3 g of LiBr was added to the solution. The mixture was stirred at room temperature at 400 rpm for 7 days. However, the clay-attached copolymers progressively swelled in the solution, forming microgels and no separation could be achieved. Further efforts were made using toluene and DMF at elevated temperatures but to no avail.

Experimental set-up

The SEC instrument comprised of a Waters 1515 isocratic HPLC pump, Waters 717 plus autosampler, Waters dual wavelength absorbance detector and Waters 2414 refractive index (RI) detector at 30 °C. Data processing was performed using Breeze Version 3.30 SPA Waters software. Separation was achieved using two PLgel (Polymer Laboratories) 5µm Mixed-C (300 × 7.5 mm) columns connected in series along with a PLgel 5µm guard column (50 × 7.5 mm). The columns were kept at a constant temperature of 30 °C. THF Chromasolv HPLC grade solvent (0.125% BHT stabilised, Sigma-Aldrich) was employed as the mobile phase at a flow rate of 1mL/min and 100 µL injection volumes were used. Each sample contained 2 mg/mL of the crude solution. The system was calibrated using polystyrene standards with a molar mass range $800-2\times10^6$ $g.mol^{-1}$ (Polymer Laboratories).

3.2.5.2 Morphology and particle size distribution

TEM

The obtained latex was diluted with distilled water at a ratio of 5 drops of water per drop of latex. A 3µL aliquot of the diluted latex was transferred by a micropipette onto a 300-mesh copper grid. Bright field TEM images were recorded at 200 kV with a Tecnai $G^2$20 high resolution TEM (FEI, Netherlands) equipped with LaB_6 filament and a Gatan GIF Tridiem post-column energy filter. The image contrast was enhanced by inserting an energy filter of 20 eV in the electron beam path in order to filter out inelastically scattered electrons, which contribute towards background noise in the digitally recorded images.

3.2.5.3 Visual/optical properties

UV-Vis spectroscopy

The optical properties of the films were determined from UV-Vis absorption spectra recorded on a Specord 210 Plus (Analytika Jena) spectrophotometer. The wavelength range of interest was 200–800 nm. The cell path length used was 1 cm.

3.2.5.4 Thermal stability and thermo-mechanical property analysis

3.2.5.4.1 TGA

Thermograms of dry powder VBDA-MMT clay and PCN samples (10mg) were recorded on a Q500 TGA 7 thermogravimetric analyser (Perkin Elmer, U.S.A). The TGA experiments were carried out under nitrogen atmosphere at a gas flow rate of 5mL/min. The temperature was increased from 25 °C to 850 °C at a heating rate of 15 °C/min.

3.2.5.4.2 DSC

The DSC runs were conducted on a Q100 DSC system (TA Instruments, U.S.A) calibrated with indium metal according to standard procedures. Heating and cooling rates were maintained at a standard 10 °C/min. The samples (6mg each) were first subjected to a heating ramp up to 160 °C, after which the temperature was kept isothermal at 160 °C for 5 min to erase the thermal history. The cooling cycle from 160 °C to -40 °C followed the isothermal stage during which data was recorded.

3.2.5.4.3 DMA

DMA measurements were conducted using a Physica MCR 501 rotational rheometer (Anton Paar, Germany) in oscillatory mode. Analyses of PSBA-MMT were performed in the range 10 °C–140 °C. All tests were conducted under 0.1% deformation and a 15 N normal force, with an oscillatory frequency of 1 Hz. Prior to the analysis, the polymer films were sectioned into disk shaped films measuring 3 cm in diameter. The thickness of all samples was in the range 200–400 µm.

3.2.6 Results and Discussion

3.2.6.1 Montmorillonite modification

The modification of Na^+-MMT was investigated using FTIR and TGA. Figure 3.1 shows the IR spectra of MMT, VBDAC and VBDA-MMT.

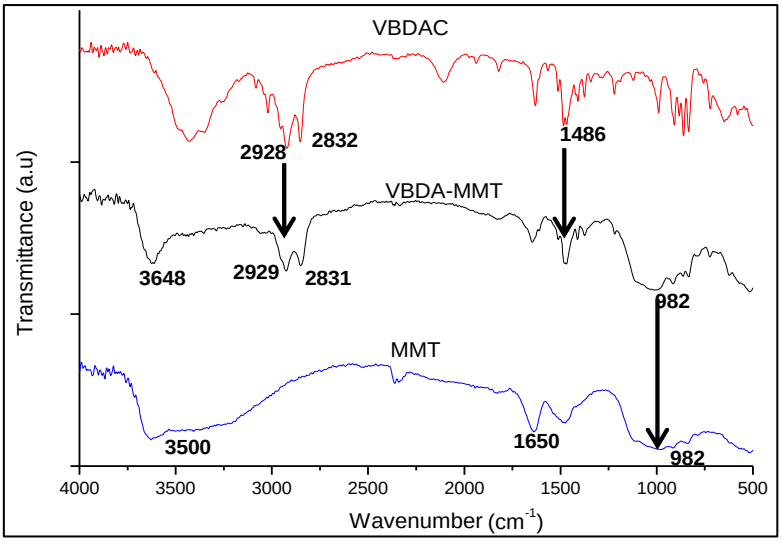

Figure 3.1: IR spectra of pristine MMT, VBDA-MMT and the free organic modifier VBDAC.

The bands at 3500–3600 cm^{-1}, 1650 cm^{-1} and 982–1000 cm^{-1} correspond to bands from MMT. The broad peak centred at 3500 cm^{-1} in the spectrum of MMT was attributed to the adsorbed moisture during MMT modification and that at around 982 cm^{-1} suggested the presence of the Si–O–Si groups in the octahedral sheets of MMT. The symmetrical and asymmetrical vibrations of $–CH_2–$ of the alkyl chains of VBDAC at 2928 cm^{-1} and 2832 cm^{-1} appear in the spectra of both the VBDA-MMT and VBDAC. [6] The shifting of the asymmetric C–H vibrations of the $H_3C–N^+$ from 1486 cm^{-1} in VBDAC to 1479 cm^{-1} in VBDA-MMT was attributed to attachment of the VBDAC onto the MMT surface via its cationic headgroup. [7] Additionally, the intensity of the characteristic peak at 1650 cm^{-1} of the water coupled with octahedral cations and H–O–H bending vibrations, was lowered by incorporation of VBDA molecules.

To complement FTIR results and gain a quantitative insight into the extent of modification, TGA was used (after extensive washing). Figure 3.2 shows the TGA thermograms of neat MMT, VBDAC and VBDA-MMT. The amount of weight loss of unmodified MMT is about 5% by around 100 °C which is attributed to its unbound water molecules. Modified MMT was characterised by one broad weight loss step from 100–500 °C. According to literature, a temperature window of 200–600 °C is usually chosen since it is the thermal decomposition temperature range for most alkylammonium modifiers. [8] As such, the difference in the weight loss between the pristine and modified clay confirms that the surface modification of nanoclay layer has been successful. [7,9,10] The thermal decomposition profile of VBDAC is characterised by two weight loss steps, first between 130−275 °C. This was attributed to the decomposition of VBDAC molecules. However, a second weight loss step is observed

between 275–500 °C. This was attributed to the thermal degradation of products from thermally induced auto-polymerization reactions of VBDAC. [3]

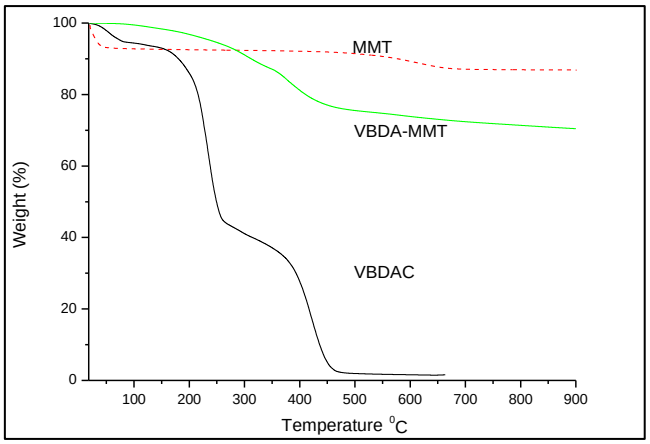

Figure 3.2: Thermal gravimetric thermograms of MMT, VBDA-MMT and VBDAC.

The weight losses in the temperature range 130–600 °C were used to calculate the amount of grafted VBDA on the MMT surface according to Equation 3.1. [11]

$$\text{Amount of grafted VBDA} = \frac{\frac{W_{130-600}}{100-W_{130-600}} \times 100 - W_{MMT}}{M} \qquad \textbf{(3.1)}$$

where $\mathbf{W_{130\text{-}600}}$ is the weight loss between 130 °C and 600 °C, $\mathbf{W_{MMT}}$ is the weight loss of unmodified MMT between 130 and 600 °C, and **M** (g.mol^{-1}) is the molecular weight of VBDAC. The calculated amount of VBDA^{+} molecules in the VBDA-MMT was found to be 0.0757 meq/100g, which translates to 81.8% exchange of the available exchangeable sites.

3.2.6.2 Molecular weight distribution of PSBA and its nanocomposites

The molecular weight distributions are shown in Figures 3.3 and 3.4. Efforts to separate the MMT-grafted copolymer from the clay were not successful. This was attributed to copolymerization of the VBDA modifier which has a styrene moiety, with butyl acrylate and styrene. [6,10] Therefore, the molecular weight distribution and dispersity reported in this study are those of unbound copolymer that grew between MMT clay platelets and did not directly interact with MMT.

The synthesized neat PSBA latexes had a higher molecular weight than the hybrid latex particles. One of the disadvantages related to the conventional free radical polymerization mechanism is the poor control of the molecular weight and molecular weight distribution.

[12,13]. In this study, the molecular weights of the free copolymer fractions from the hybrid latexes gradually decreased with increase in MMT clay loading as shown in Table 3.2. It presents the molecular weights and dispersity (D) of the neat PSBA and the PSBA/MMT hybrid nanocomposites. The neat copolymers and the free copolymer fractions were characterized with broad dispersity index values as expected of polymers prepared by conventional free radical polymerization. [14].

The presence of MMT clay platelets may hinder the growth of polymer chains which leads to a gradual decrease in molecular weight with increase in clay content. [15] Samakande, [16] studied the synthesis and characterization of surfmers for the synthesis of polystyrene-clay nanocomposites and attributed the decreasing trend to the presence of clay platelets which impede the diffusion of monomers and initiator radicals. In another study by Choi et al, [17] a similar trend was observed and the results were attributed to clay platelets acting as "additional micelles" which allow polymerization to take place in more micelles, decreasing molecular weight in the process. It is also thought that the molecular weights of nanocomposites are affected to some extent by the clay type. [18] As such, because of the large surface area-to-volume ratio of MMT clay platelets, most initiator radicals adsorb onto the VBDA-MMT surface thereby increasing the chain termination probability and decreasing the initiator efficiency. [19] The molecular weights for the neat PSBA-40:60 and PSBA-30:70 materials were too high and out of the calibration range, therefore no conclusive information regarding their molar mass, molar mass distribution and dispersity could be gathered.

The dispersity values for PSBA-30:70 hybrid latexes were higher than those of PSBA-40:60 and PSBA-50:50 hybrid latexes. This may be attributed to the presence $VBDA^+$ molecules which competitively copolymerized with styrene due to its high reactivity ratio (~0.8 relative to that of butyl acrylate~0.2) and butyl acrylate due to its high amounts. [20]

Table 3.2: Number average molecular weight (M_n), weight average molecular weight (M_w) and dispersity values of neat PSBA and the free copolymer fractions.

PSBA-Sample	M_n (g.mol^{-1})	M_w (g.mol^{-1})	Dispersity
PSBA-30:70-MMT00%	---	out of range	---
PSBA-30:70-MMT10%	56700	134100	2.4
PSBA-30:70-MMT20%	55700	133600	2.4
PSBA-30:70-MMT30%	54300	128700	2.4
PSBA-40:60-MMT00%	---	out of range	---
PSBA-40:60-MMT10%	65200	123800	1.9
PSBA-40:60-MMT20%	58400	116800	2.0
PSBA-40:60-MMT30%	54100	113600	2.1
PSBA-50:50-MMT00%	615300	1078600	1.7
PSBA-50:50-MMT10%	66200	125700	1.9
PSBA-50:50-MMT20%	57100	108400	1.9
PSBA-50:50-MMT30%	50800	106700	2.1

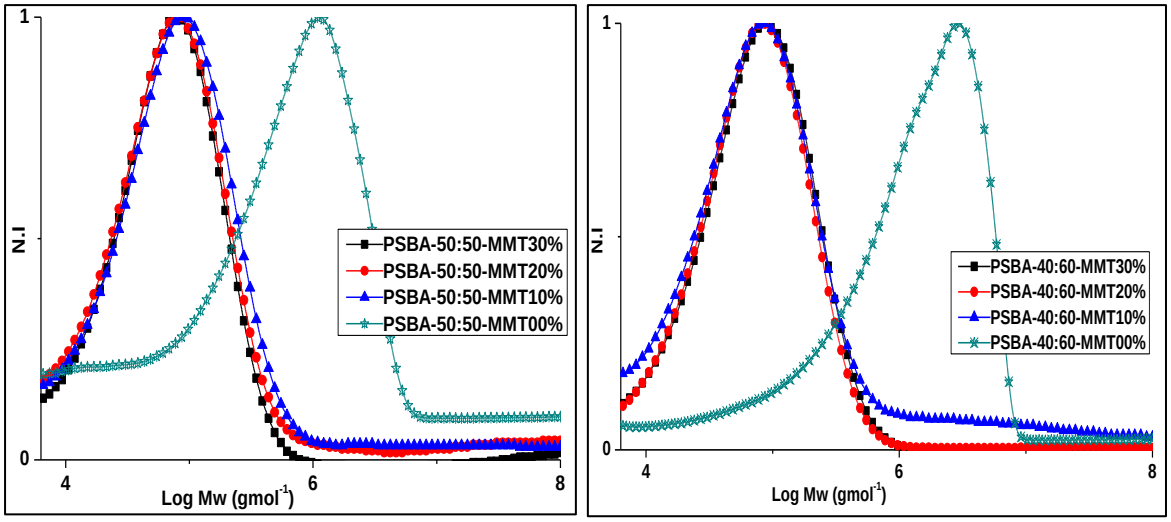

Figure 3.3: Molecular weight distribution profiles for neat PSBA-50:50, PSBA-40:60 samples and the free copolymer fractions.

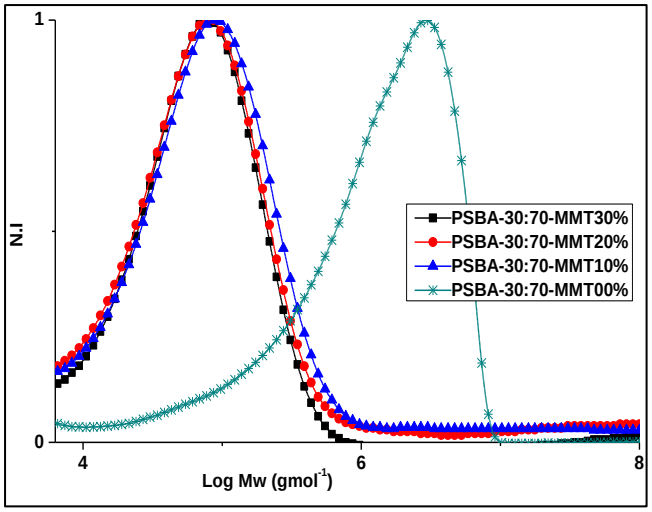

Figure 3.4: Molecular weight distribution profiles for PSBA-30:70 samples and the free copolymer fractions.

3.2.6.3 Chemical composition of PSBA neat latexes

The main purpose of preparing neat PSBA latexes was to use them as references to assess the effect of incorporating MMT on the final properties of the PSBA-MMT materials.

The ^{1}H NMR spectrum of the neat PSBA is presented in Figure 3.5. The signals at ~3.4–4.1 ppm in the copolymers are ascribed to the methylenic protons adjacent to the ester group of the butyl acrylate component (labelled 4). The signal at 0.8-1ppm is ascribed to the methyl group of butyl acrylate (labelled 5), while that around 7.2ppm is ascribed to the phenylic protons of the styrene ring (labelled 1, 2 and 3).The relative amounts of styrene and butyl acrylate units incorporated into the copolymers were calculated using the ^{1}H NMR data, by integration of signals corresponding to styrene (labelled 1, 2, 3) and butyl acrylate (labelled 5) components according to Equation 3.2. [21] The experimental amounts of styrene/butyl acrylate in the copolymers are given in Table 3.3 and the signal integrations are shown in Appendices 3 to 5.

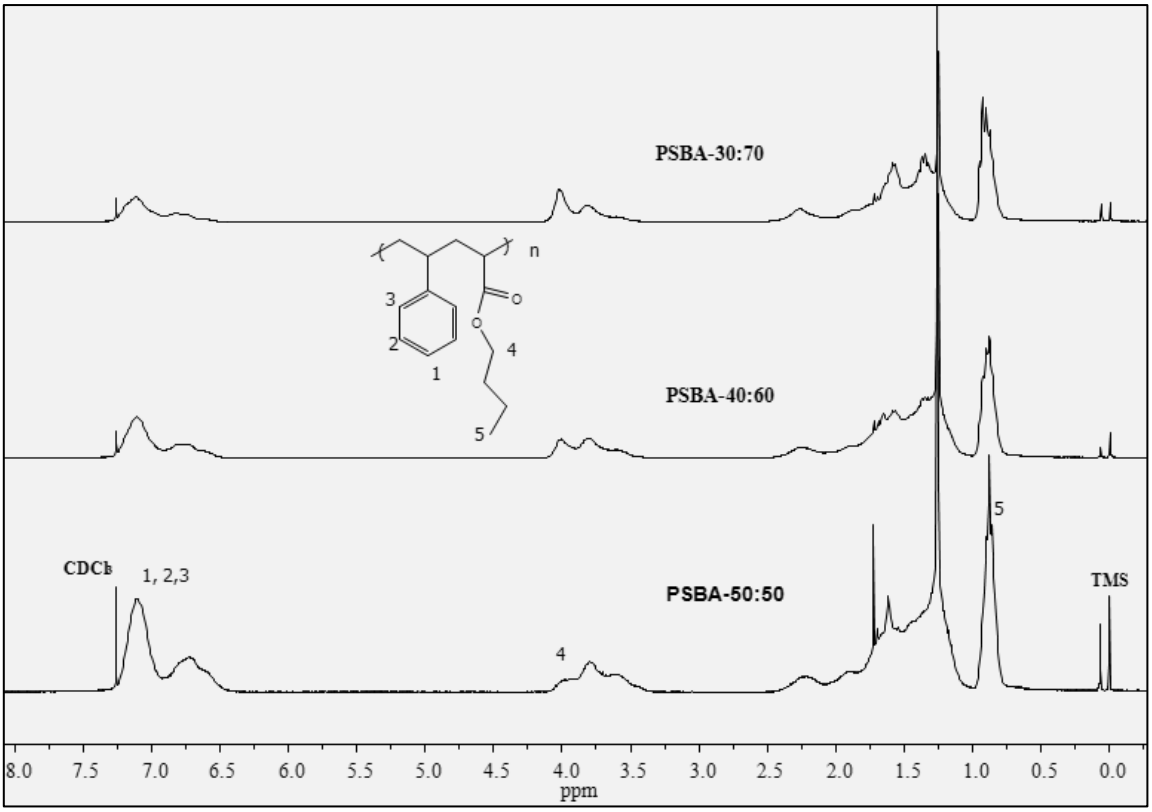

Figure 3.5: ^{1}H NMR spectra of unfilled PSBA samples.

$$S\% = \frac{\frac{S}{5}}{\frac{S}{5}+\frac{B}{2}} \times 100 \qquad (3.2)$$

where **S%** is the amount of styrene in the copolymer, **S** and **B** are peak integrals for styrene (7.2 ppm) and butyl acrylate (3.6 ppm) respectively. The signal at 1.26 ppm was associated with possible impurities from residual water and that around 0.1 ppm due to silicone grease used to seal the joints of the polymerization reactor set-up. The signal around 7.62 ppm was the chloroform ($CDCl_3$) used as the solvent. Tetramethylsilane (TMS) was used as the reference peak.

Table 3.3: Experimental amounts of styrene and butyl acrylate in the copolymers as determined by ^{1}H NMR peak integration

Theoretical mol.%		Experimental mol.%		Integral proton ratio	
Sty	BuA	Sty	BuA	Sty	BuA
30	70	22	78	1	2.1
40	60	40	60	1	0.9
50	50	50	50	1	0.6

3.2.6.4 Morphological properties

PSBA latexes prepared by miniemulsion, through co-sonication, [5] using different concentrations of MMT and varying the copolymer composition were analysed by TEM. The contrast between MMT clay platelets (dark phases) and the copolymer particles assisted in giving an indication on the extent of clay platelet dispersion and location in the copolymer matrix. For better clarity on the latex particles' shape and size distribution, the neat latexes were viewed at low magnification while the hybrid latexes were viewed at higher magnification. The morphologies of the PSBA based latexes are shown in Figure 3.6.

The neat PSBA-50:50 latex particles exhibited predominantly spherical nanoparticles with a narrow size distribution (~80–100 nm) as approximated by TEM studies. The spherical shape of the nanoparticles was gradually lost and a broader size distribution (~15–300 nm and ~20–400 nm) was observed in the PSBA-40:60 and PSBA-30:70 latex nanoparticles, respectively. The observed shape distortion has been attributed to the thermodynamic instability of low T_g copolymer particles prepared by miniemulsion. [22] It is generally understood that macroemulsions are kinetically stable; microemulsions are thermodynamically stable while miniemulsions, are stable against molecular diffusion and coalescence. [22]

The irregular shapes might also have been enhanced during sample preparation of the materials for TEM studies as they were transferred from the bulk solution to the copper grid, causing them to collapse, as the high BA content gives the materials T_gs that are too low for the preparation conditions. All neat PSBA latex particles have a larger size distribution than their respective hybrid latex particles as observed from TEM imaging. This was attributed to stabilization of the latex particles by presence of clay platelets which have a higher SDS concentration (30mM) than the neat copolymer latex particles (10mM). [3,23]

The irregular shape seen in the PSBA-40:60 and PSBA-30:70 neat latexes was gradually lost in the hybrid particles and better defined, dumb-bell shaped particles were observed. However, because of a faceting effect caused by the presence of the rigid MMT clay platelets, the hybrid latexes for all the copolymer compositions were non-spherical. MMT clay platelets were predominantly adhered on the surface of the PSBA latex particles because MMT clay platelets have a larger size than the effective size of the copolymer particles.

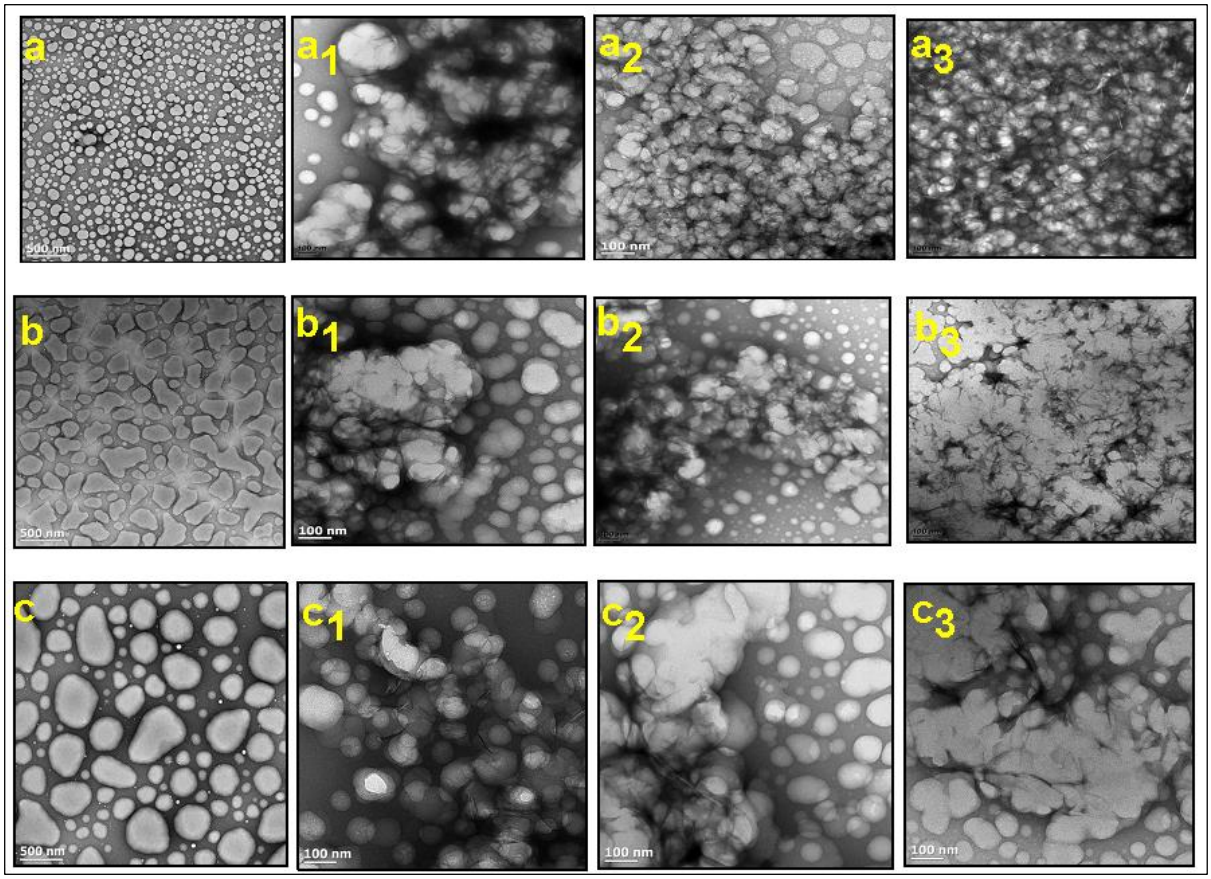

Figure 3.6: Transmission electron microscopy images of (a) neat PSBA-50:50 and its hybrid latexes [(a_1) PSBA-50:50-MMT10%, (a_2) PSBA-50:50-MMT20%, (a_3) PSBA-50:50-MMT30%]; (b) neat PSBA-40:60 and its hybrid latexes [(b_1) PSBA-40:60-MMT10%, (b_2) PSBA-40:60-MMT20% (b_3) PSBA-40:60-MMT30%]; and (c) neat PSBA-30:70 and its hybrid latexes [(c_1) PSBA-30:70-MMT10%, (c_2) PSBA-30:70-MMT20%, (c_3) PSBA-30:70-MMT30%].

Greesh et al, [18] investigated the role of nanoclay shape and surface characteristics on the morphological properties of polystyrene hybrid latex particles and reported aggregated particles, as was found in this study. This may be because VBDA molecules are anchored on both sides of the MMT platelet surface and copolymer particles share the same clay platelet forming a network of assembled, rather than isolated copolymer particles. [18,24,25]

3.2.6.5 Optical properties

The optical clarity of PSBA-MMT films containing 10–30 wt.% clay platelets was investigated by UV-Vis spectroscopy in the region of 200–800nm. There was loss of intensity in the UV-Vis region of 350–800nm with increase in MMT clay content in all the copolymer nanocomposites. This was attributed to scattering of light by the increasing MMT clay platelets content in the copolymer matrix. [26] Comparing the neat films and the PCNs with MMT-30%, the transmittance decreases only from 70% to 50% for PSBA-40:60 and PSBA-50:50 respectively. However, the best optical properties were observed in the PSBA-30:70 films. The transmittance for the PSBA-30:70 films decreased from 85% (neat film) to 60%

(MMT-30% film) but remained higher than the transmittance for PSBA-40:60 and PSBA-50:50 films for all clay loadings.

Figure 3.7 shows the percentage transmittance of light (measured at 500 nm) through the polymeric films plotted as a function of MMT clay content.

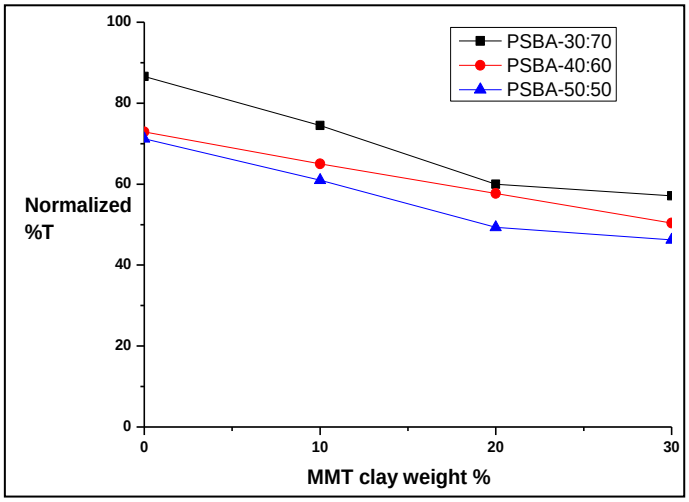

Figure 3.7: Normalised (%) light transmittance, as determined by UV-Vis spectroscopy at 500nm, as a function of MMT clay for neat PSBA-50:50, PSBA-40:60, PSBA-30:70 films and the nanocomposites.

Ahmadi et al, [27] reported that albeit their micro-lateral size, when single clay platelets are dispersed in a polymer matrix the resulting nanocomposite is optically clear in the visible region. The visual clarity properties of the PSBA neat films and the nanocomposites with varying VBDA-MMT clay content are displayed in Figure 3.8.

Figure 3.8: Visual clarity due to nano-dispersed VBDA-MMT platelets in PSBA film matrix.

There is a significant decrease in the visual clarity of the PSBA-MMT nanocomposites compared to the neat (unfilled) copolymer. This is because large clay particles are made of highly organised platelets that scatter light. [28] However, transparency occurs in polymer-clay nanocomposites when individual clay platelets are either fully or semi-exfoliated to such an extent that the degree of disorder allows for isotropic transmission of light. [29]

3.2.6.6 Thermal stability

The thermal stability of neat PSBA and PSBA-MMT nanocomposites was analysed by TGA, where the sample mass loss due to volatilization of degraded by-products was monitored as a function of the temperature ramp. When the heating is operated under an inert atmosphere, a non-oxidative degradation occurs.

Table 3.4 shows the TGA data of the PSBA and PSBA-MMT materials. From Table 3.4, the onset temperature and the temperature at which 50% degradation occurred increased upon incorporation of MMT in the PSBA matrix. This was attributed to a restricted thermal motion of copolymer chains localized within the clay galleries, promoting thermal stability of the PCNs. [30]. The onset temperature for the neat PSBA-40:60 film specimen was found to be higher than that of the respective PCNs. This was attributed to the thermal degradation of the VBDA molecules. [31] However, the extent to which the thermal stability was improved did not correlate linearly with the MMT content since the extraordinary thermal stability in PCNs (as reported previously) is not only due to clay content, but other factors such as degree of nanoclay dispersion in the polymer matrix, morphology and type of interaction at the interface between the clay platelets and the polymer matrix. [18,32,33]

Table 3.4: TGA data for neat PSBA films and PSBA-MMT PCNs.

Poly (sty-co-BuA) sample	T °C $_{Onset}$	T °C $_{50\%\ wt.\ loss}$
PSBA-50:50-MMT00%	353	436
PSBA-50:50-MMT10%	401	452
PSBA-50:50-MMT20%	379	446
PSBA-50:50-MMT30%	385	448
PSBA-40:60-MMT00%	401	446
PSBA-40:60-MMT10%	398	454
PSBA-40:60-MMT20%	397	468
PSBA-40:60-MMT30%	385	448
PSBA-30:70-MMT00%	358	454
PSBA-30:70-MMT10%	387	462
PSBA-30:70-MMT20%	398	476
PSBA-30:70-MMT30%	395	476

Figure 3.9 shows the thermograms of PSBA and PSBA PCNs. The graphs show the decomposition behaviour of the materials as temperature increased from 100–800 °C. The residual weight at 600 °C in all the materials was found to increase with increasing MMT clay content incorporated during preparation of the films. The "dip" in the decomposition of the PSBA-MMT nanocomposites from 200–300 °C was attributed to the thermal degradation of the VBDA molecules grafted on the MMT platelets. Furthermore, all the PCNs were found to be thermally more stable relative to the neat copolymer materials.

The improvement in thermal stability of polymer matrices filled with layered silicates is attributed to the formation of clay char which consequently acts as a mass transport barrier and thermal insulator between the bulk polymer matrix and the site where degradation is taking place. [34-36]

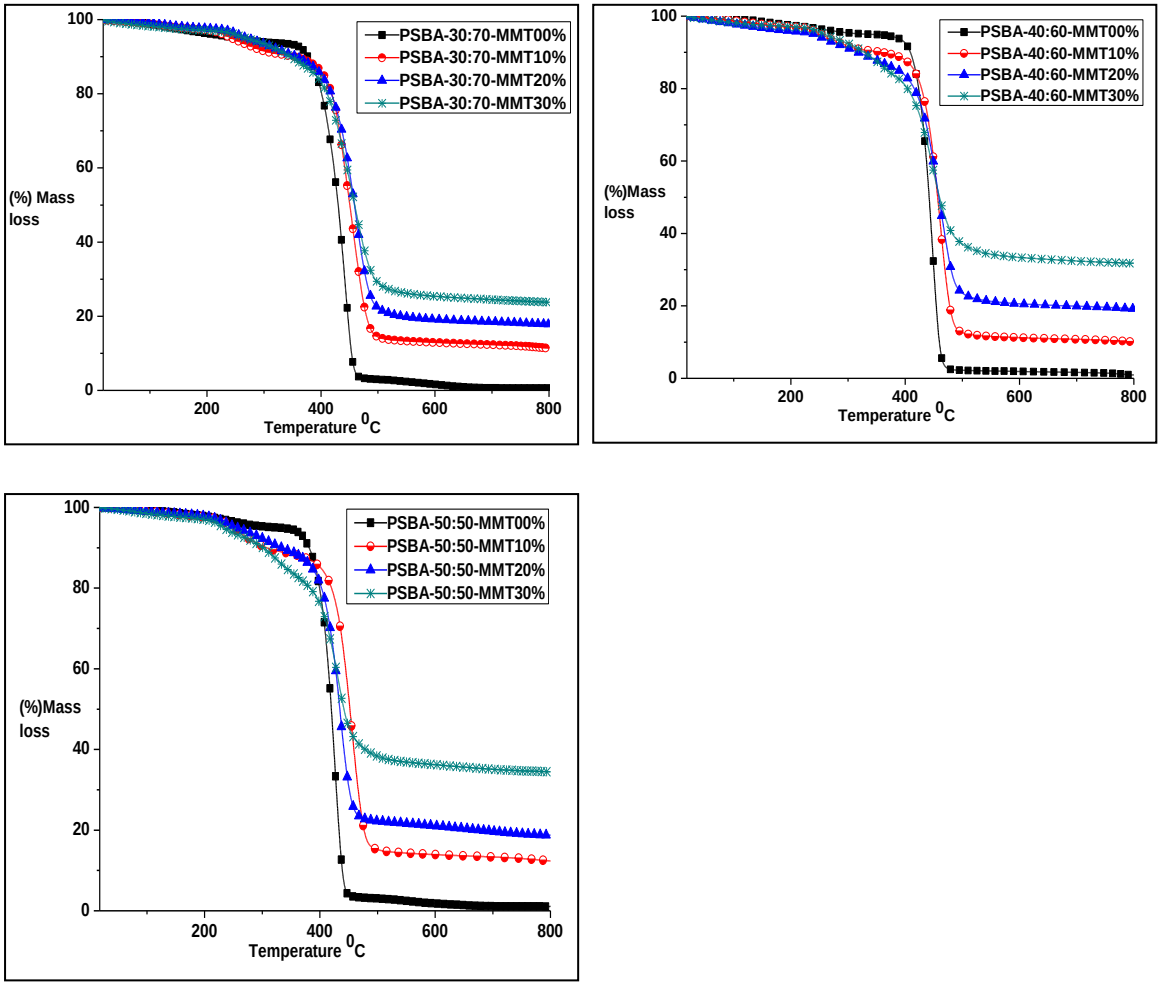

Figure 3.9: Thermal gravimetric curves of neat PSBA-50:50, PSBA-40:60 and PSBA-30:70 films and the nanocomposites.

In literature, the better thermal stability of PCNs is also attributed to hindered out-diffusion of the volatile decomposition products as a direct result of the decrease in permeability, usually observed in exfoliated PCNs. [37]

3.2.6.7 Thermo-mechanical properties

To investigate the effect of VBDA-MMT and the copolymer matrix on the thermomechanical properties and glass transition temperature (T_g) of the materials, differential scanning calorimetry, DSC, and dynamic mechanical analysis, DMA, were used.

3.2.6.7.1 DSC

Literature has reported different behaviours regarding the T_g of polymer matrices reinforced with clay platelets[38-40]. While an increase in T_g is attributed to the restricted thermal motions of the polymer chains due to improved interactions between the clay platelet surfaces and the polymer chain, [41,42] a decrease in the same property can be associated with the plasticization of the materials by the alkyl chains of the clay modifiers. [43] The theoretical T_gs of the unfilled copolymer materials were calculated using the Fox equation, [44] (see Equation 3.3) and the values were compared with the experimental figures

$$\frac{1}{T_{gPSBA}} = \frac{\frac{mSty}{mSty+mBA}}{T_{g\,Sty}} + \frac{\frac{mBA}{mBA+mSty}}{T_{gBA}} \qquad \textbf{(3.3)}$$

where **mSty** and **mBA** is the mass of styrene and butyl acrylate in grams (g). Figure 3.10 shows the DSC heating profiles for the neat PSBA and the PCNs and Table 3.5 shows the T_g values.

Table 3.5: Thermal properties of the neat PSBA latex films and the PCNs.

PSBA sample	Tg (°C)	PSBA sample	Tg (°C)	PSBA sample	Tg (°C)
-50:50-MMT00%	-1.79	-40:60-MMT00%	-13.95	-30:70-MMT00%	-25.40
-50:50-MMT10%	3.01	-40:60-MMT10%	-13.30	-30:70-MMT10%	-25.89
-50:50-MMt20%	5.81	-40:60-MMT20%	-10.08	-30:70-MMT20%	-24.01
-50:50-MMT30%	11.71	-40:60-MMT30%	-6.39	-30:70-MMT30%	-17.78

According to the DSC measurements, the T_g of the PSBA-50:50 gradually increased with increasing MMT content from -1.8 °C in the unfilled material to 11.7 °C in the PSBA-50:50-MMT30% sample, while the T_g of the PCNs were all higher relative to the neat PSBA-50:50 sample. This is attributed to the restricted copolymer chain mobility by the presence of the

rigid VBDA-MMT clay platelets. The T_g values of the unfilled PSBA-40:60 and PSBA-30:70 samples were higher than their PCNs with VBDA-MMT10%. This can be associated with the competition between plasticization effect of the VBDA alkyl short chains and the restriction of copolymer chain mobility by the rigid MMT platelets. [45]

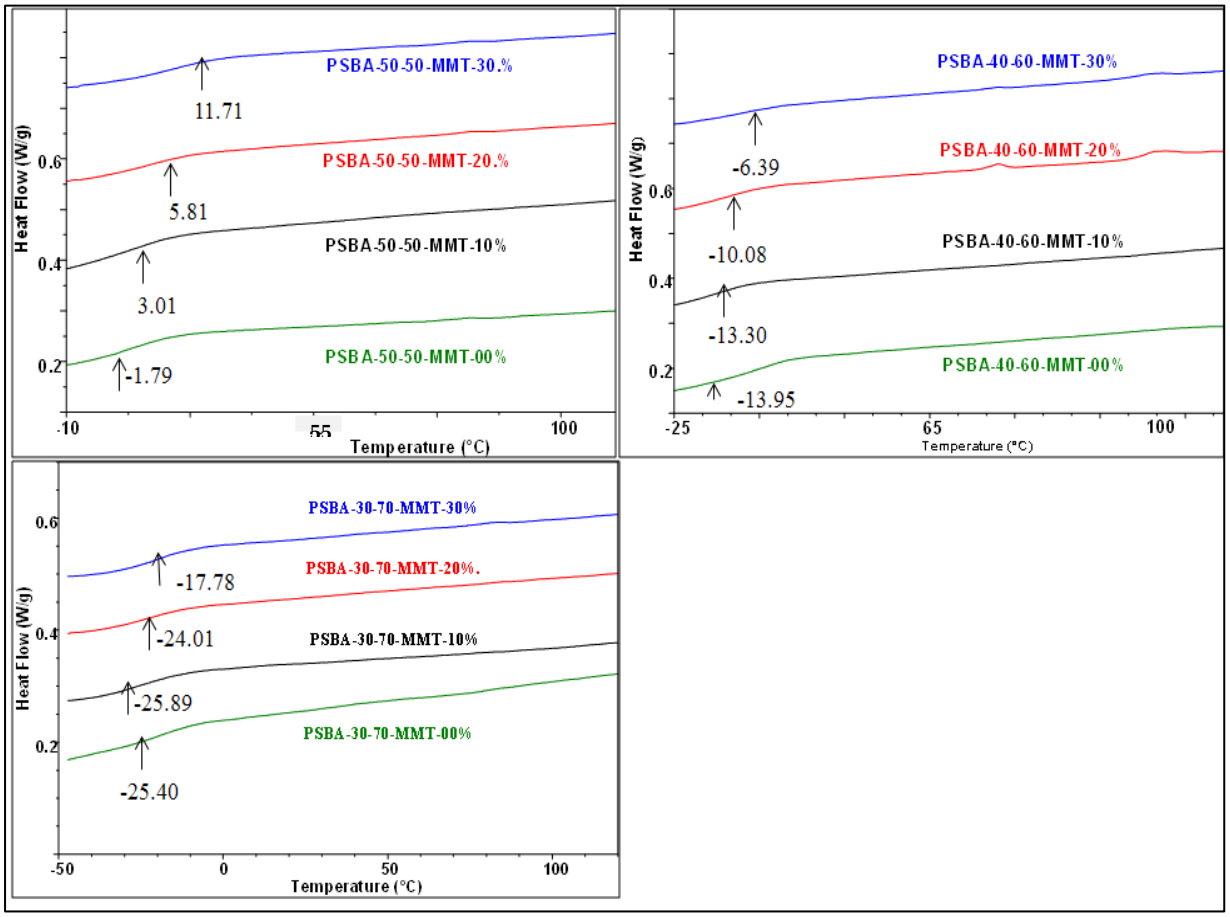

Figure 3.10: Differential scanning calorimetry heating profiles for neat PSBA-50:50, PSBA-40:60, PSBA-30:70 films and the nanocomposites.

The T_g values shifted to lower values from those of the PSBA-50:50, PSBA-40:60 to those of the PSBA-30:70 materials. This was associated with an increase in the low T_g butyl acrylate component of the copolymers.

3.2.6.7.2 DMA

The materials' responses to oscillatory deformation were plotted as storage modulus as a function of a temperature ramp and are displayed in Figure 3.11

The storage modulus values of the neat PSBA materials were all higher than those of the PCNs. This was associated with the ultra-high molecular weights of the neat materials (>10^6 Daltons) relative to the filled counterparts. According to literature, an increase in storage

modulus of polymer matrices reinforced with clay occurs with an increase in clay content. [10,46,47] This is attributed to strong polymer-clay interactions at the interface, hindering the mobility of the polymer chain segments at temperatures below the T_g. [48] In this study, the storage modulus of the materials decreased monotonically with an increase in clay content. Xie et al studied the effect of surfactants on thermomechanical properties of polystyrene-MMT PCNs and attributed such behaviour to the dual role played by organoclay: (a) as nanofiller and reinforcing agent leading to the increase in storage modulus and (b) as a plasticizer leading to a decrease of storage modulus. [49] The plasticizing effect can be explained by different types of polymer-clay interactions. Shi et al, [50] investigated the effects of polymer-clay interactions on the reinforcement properties of PCNs, and verified that the direct interaction of the polymer matrix with the clay basal plane leads to higher increments on the storage modulus than interactions between the polymer matrix and the alkyl chains from the modifier tethered to the clay basal planes.

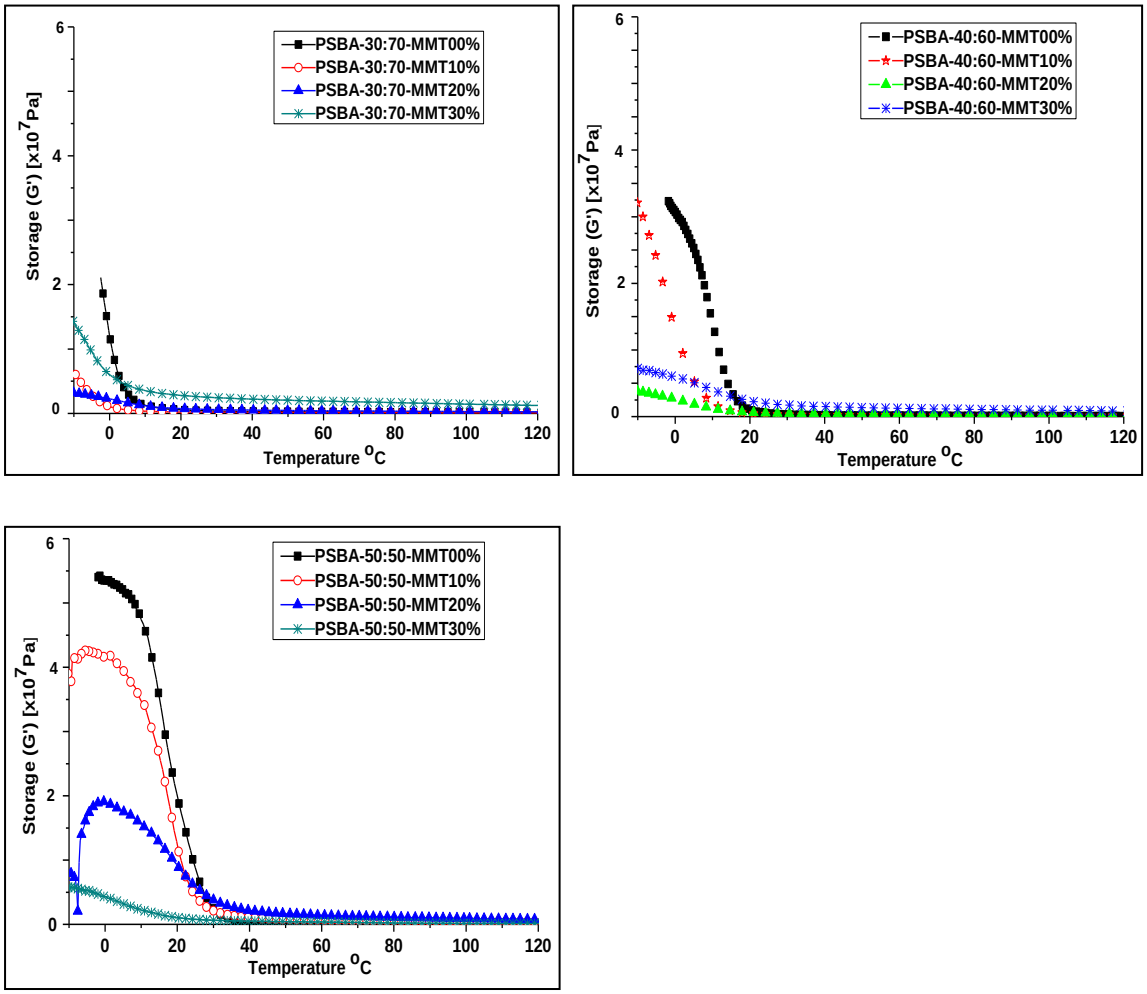

Figure 3.11: Dynamic mechanical analysis showing curves of the neat PSBA-50:50, PSBA-40:60, PSBA-30:70 films and their nanocomposites' elastic behaviour to oscillatory deformation (storage modulus, G′).

It was also observed that an increase in the content of butyl acrylate in the materials leads to a monotonic decrease in the storage modulus. This can be associated with the ability of the poly (n-butyl acrylate) component of the copolymer to initiate rotational movements at lower temperatures, with a consequent decrease in the storage modulus. [51]

Figure 3.12 shows the temperature dependency of tan δ (damping factor). The temperature at the maximum value for the damping factor peak was ~3 °C for PSBA-30:70, ~20 °C for PSBA-40:60 and ~25 °C for PSBA-50:50. This peak is associated with the transition from glassy to rubbery state of the neat PSBA films.

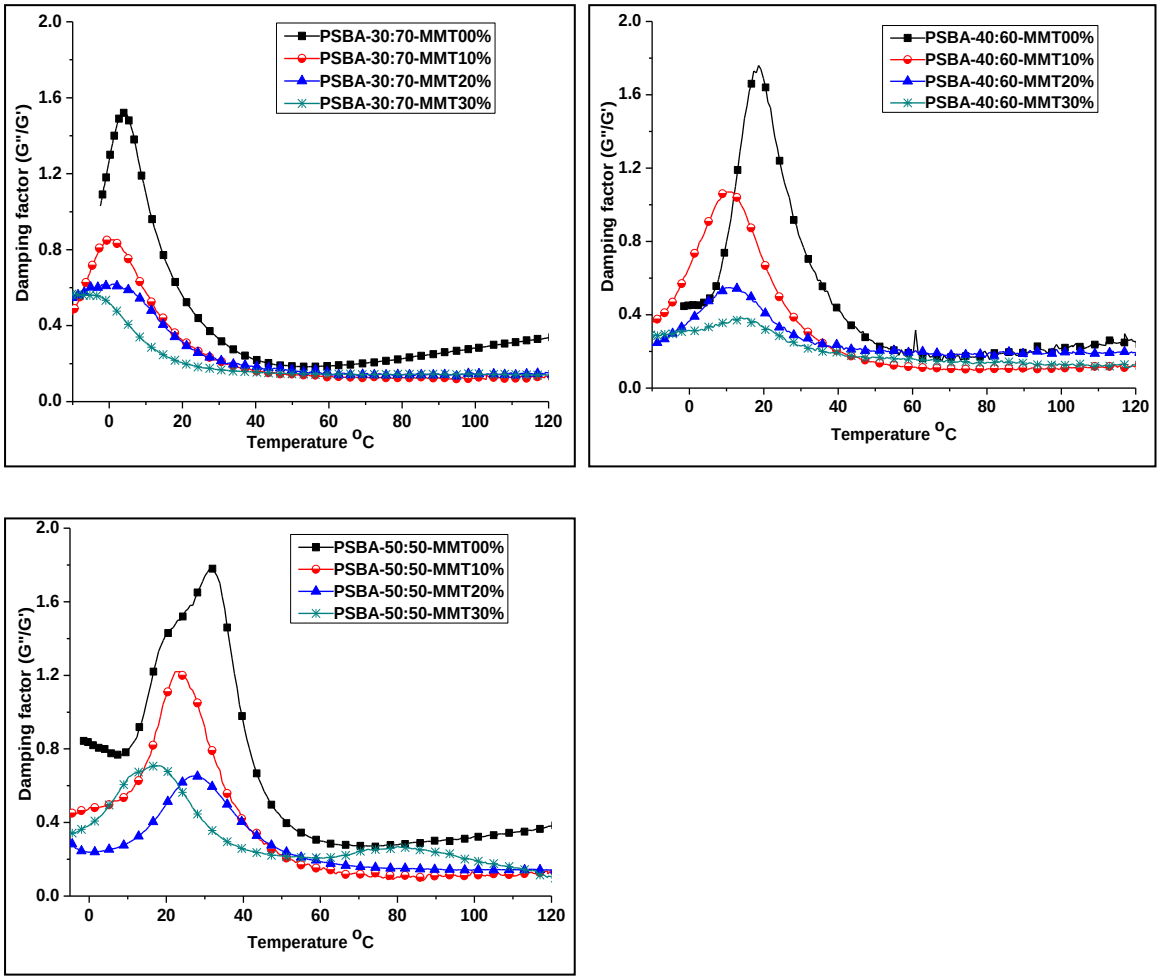

Figure 3.12: Dynamic mechanical analysis showing curves of neat PSBA-50:50, PSBA-40:60, PSBA-30:70 films and the nanocomposites' damping factor (ratio of loss to storage modulus, tan δ).

From the plots shown in Figure 3.12, the intensity of the tan δ peak decreased with increasing MMT clay content, becoming broader in the process. This is associated with the arrest of the segmental motion at the polymer/clay interface. However, the decrease in the damping factor intensity could not be linearly correlated with the clay loading. This trend could be due to broad molecular weight distributions of the copolymer matrix, as a polymer with a broad

molecular weight distribution and high dispersity index may contain a low molecular weight portion which lowers the glass transition temperature of the material in the same manner as plasticizers. [18]

3.3 Conclusions

The use of miniemulsion polymerization was found to be an effective method to incorporate MMT clay platelets into a PSBA matrix. As proposed in other previous studies in the group, the key to the miniemulsification method was in using a wet clay paste rather than the dried powder so as to facilitate the clay dispersion in the polymer matrix. [5] The neat PSBA latexes exhibited high molecular weights (>10^6 g/mol) compared to the PCNs, suggesting the MMT clay platelets had a significant effect on the molecular weight distribution of the hybrid materials. Efforts to separate the clay grafted to the polymer were not successful.

Even though there was ineffective encapsulation of clay platelets into individual copolymer particles, the MMT particles were predominantly adhered onto the surface of the copolymer particles. According to TEM studies, the presence of MMT clay particles stabilized the copolymer latex particles. Significant changes in the latex particles were observed, particularly in the low T_g PSBA-40:60 and PSBA-30:70 materials, in which the irregular shape of the unfilled particles changed from oval-to-dumbbell-shaped particles as seen in the TEM images. This was attributed to the faceting effect of the rigid MMT clay platelets as they attach onto the copolymer particle surface. However, most of the copolymer particles in the PCNs assembled together rather than being isolated as seen in the TEM images of the unfilled latexes, a reason for a possible sharing of a clay platelet amongst a group of copolymer particles.

The films of the PCNs obtained from the latexes were found to be optically clear relative to the unfilled materials especially at clay loadings ≤20 wt.%. In addition, the PSBA-30:70 matrix had better optical clarity properties than PSBA-40:60 and PSBA-50:50, respectively. This was attributed to an increase in the low UV-absorbing butyl acrylate component of the copolymer, which at the same time has a low T_g that suggestively facilitated dispersion of the rigid MMT platelets in the matrix.

The thermal stability of the PCNs correlated with the clay content and dispersion, and not the copolymer composition. However, the thermal properties for PSBA-40:60-MMT10% and PSBA-30:70-MMT10% were lower than the unfilled counterparts as determined by DSC.

The response to oscillatory deformation of the PCNs was not significantly improved as measured by DMA. The deviation in the lower storage modulus of the PCNs compared to the unfilled materials was associated with broad molecular weight distributions observed in the unfilled materials. This behaviour was also associated with plasticization of the PCNs by (a) the presence of short chains in the $VBDA^+$ molecules, with increasing VBDA-MMT content and (b) the ability of the poly(n-butyl acrylate) component of the copolymer to initiate rotational movements at lower temperatures, with increasing butyl acrylate content.

3.4 References

[1] Arora, A.; Padua, G. W. *J. Food Sci.* **2010**, *75*, 43.

[2] Hawker, C. J.; Elce, E.; Dao, J.; Volksen, W.; Russell, T. P.; Barclay, G. G. *Macromolecules* **1996**, *29*, 2686.

[3] Zengeni, E.; Hartmann, P. C.; Pasch, H. *Macromol. Chem. Phys.* **2013**, *214*, 62.

[4] Olad, A.; Hayasi, M. *Adv. Polym. Tech.* **2011**, *50*, 1487.

[5] Zengeni, E.; Hartmann, P. C.; Pasch, H. *ACS Appl. Mater. Interfaces* **2012**, *4*, 6957.

[6] Fu, X.; Qutubuddin, S. *Langmuir : ACS Appl. Mater. Interfaces* **2002**, *18*, 5058.

[7] Ahmadian-Alam, L.; Haddadi-Asl, V.; Roghani-Mamaqani, H.; Hatami, L.; Salami-Kalajahi, M. *J. Polym. Res.* **2011**, *19*.

[8] Xidas, P. I.; Triantafyllidis, K. S. *Eur. Polym. J.* **2010**, *46*, 404.

[9] Moraes, R. P.; Valera, T. S.; Pereira, A. M. C.; Demarquette, N. R.; Santos, A. M. *J. Appl. Polym. Sci.* **2011**, *119*, 3658.

[10] Fu, X.; Qutubuddin, S. *Polym. J.* **2001**, *42*, 807.

[11] Chirowodza, H. PhD, Stellenbosch University, **2012**.

[12] Fukuda, T.; Terauchi, T.; Goto, A.; Tsujii, Y.; Miyamoto, T.; Shimizu, Y. *Macromolecules* **1996**, *29*, 3050.

[13] Georges, M. K.; Veregin, R. P. N.; Kazmaier, P. M.; Hamer, G. K. *Macromolecules* **1993**, *26*, 2987.

[14] Muratoglu, O. K.; Bragdon, C. R.; O'Connor, D. O.; Jasty, M.; Harris, W. H. *J. Polym. Res.* **2001**, *16*, 149.

[15] Zhong, Y.; Zhu, Z.; Wang, S. Q. *Polym. J.* **2005**, *46*, 3006.

[16] Samakande, A. PhD, University of Stellenbosch, **2005**.

[17] Choi, Y. S. C., M. H.; Wang, K. H. *Macromolecules* **2001**, *34*, 8.

[18] Greesh, N.; Sinha Ray, S.; Bandyopadhyay, J. *Ind. Eng. Chem. Res.* **2013**, *52*, 16220.

[19] Greesh, N.; Sanderson, R. D.; Hartmann, P. C. *Polym. J.* **2012**, *53*, 708.

[20] Ziaee, F.; Nekoomanesh, M. *Polym. J.* **1998**, *39*, 203.

[21] Greesh, N.; Hartmann, P. C.; Cloete, V.; Sanderson, R. D. *J. Polym. Sci., Part B: Polym. Phys.* **2008**, *46*, 3619.

[22] Ramirez, L. P.; Landfester, K. *Macromol. Chem. Phys.* **2003**, *204*, 10.

[23] Steiert, N.; Landfester, K. *Macromol. Mater. Eng.* **2007**, *292*, 1111.

[24] Klapyta, Z.; Fujita, T.; Iyi, N. *Appl. Clay Sci.* **2001**, *19*, 5.

[25] Zhang, W. A.; Chen, D. Z.; Xu, H. Y.; Shen, X. F.; Fang, Y. E. *Eur. Polym. J.* **2003**, *39*, 2323.

[26] Krishnamoorti, R.; Giannelis, E. P. *Macromolecules* **1997**, *30*, 4097.

[27] Ahmadi, S. J.; Huang, Y. D.; Li, W. *J. Membr. Sci.* **2004**, *39*, 1919.

[28] Krikorian, V.; Pochan, D. J. *Chem. Mater.* **2003**, *15*, 4317.

[29] Koo, C. M.; Ham, H. T.; Choi, M. H.; Kim, S. O.; Chung, I. J. *Polym. J.* **2003**, *44*, 681.

[30] Powell, C.; Beall, G. *Curr. Opin. Solid State Mater. Sci.* **2006**, *10*, 73.

[31] Cho, J. W.; Paul, D. R. *Polym. J.* **2001**, *42*, 1083.

[32] Pavlidou, S.; Papaspyrides, C. D. *Prog. Polym. Sci.* **2008**, *33*, 1119.

[33] Golubeva, O. Y.; Gusarov, V. V. *Glass Phys. Chem* **2007**, *33*, 237.

[34] Valandro, S. R.; Lombardo, P. C.; Poli, A. L.; Horn Jr, M. A.; Neumann, M. G.; Cavalheiro, C. C. S. *Materials Research* **2014**, *17*, 265.

[35] Li, H.; Kim, H. *Desalination* **2008**, *234*, 9.

[36] Bourbigot, S.; Gilman, J. W.; Wilkie, C. A. *Polym. Degrad. Stab.* **2004**, *84*, 483.

[37] Alexandre, M.; Dubois, P. *Mater. Sci. Eng., R.* **2000**, *28*, 1.

[38] Lavorgna, M.; Piscitelli, F.; Mangiacapra, P.; Buonocore, G. G. *Carbohydr. Polym.* **2010**, *82*, 291.

[39] Fu, X.; Qutubuddin, S. *Materials Letters* **2000**, *42*, 12.

[40] Fischer, H. *Mater. Sci. Eng., C.* **2003**, *23*, 763.

[41] Arora, A.; Choudhary, V.; Sharma, D. K. *J. Polym. Res.* **2011**, *18*, 843.

[42] Zaman, I.; Le, Q.; Kuan, H.; Kawashima, N.; Luong, L.; Gerson, A.; Ma, J. *Polym. J.*

2011, *52*, 497.

[43] Abdelwahab, M.; Agag, T.; Akelah, A.; Takeichi, T. *J. Macromol. Sci., Polym. Rev.* **2012**, *6*, 20.

[44] Calleja, G.; Jourdan, A.; Ameduri, B.; Habas, J. *Eur. Polym. J.* **2013**, *49*, 2214.

[45] Sharma, B.; Mahajan, S.; Chhibber, R.; Mehta, R. *Procedia Chem.* **2012**, *4*, 39.

[46] Liu, X.; Wu, Q. *Polym. J.*

2001, *42*, 10013.

[47] Meneghetti, P.; Qutubuddin, S. *Thermochim. Acta* **2006**, *442*, 74.

[48] Luo, J.; Daniel, I. M. *Compos. Sci. Technol.* **2003**, *63*, 1607.

[49] Xie, W.; Hwu, J. M.; Jiang, G. J.; Buthelezi, T. M.; Pan, W. *Polym. Eng. Sci.* **2003**, *43*, 214.

[50] Shi, H.; Lan, T.; Pinnavaia, T. J. *Chem. Mater.* **1996**, *8*, 1584.

[51] Barata, I.; Fonseca, A. C.; Costa, C. S. M. F.; Ferreira, L.; Júlio, E.; Coelho, J. F. J. *Prog. Org. Coat.* **2014**, *77*, 790.

Chapter 4

4 Correlation of the water vapour sorption behaviour of PSBA-MMT films with molecular properties

The main aim of this study was to investigate the effect of (a) high clay loadings (10, 20 and 30 wt.%) and (b) copolymer composition variation on the water vapour sorption behaviour of the neat PSBA and the PSBA/MMT films, then correlate the impact of the aforementioned parameters with molecular properties of the films. The objective was to use the Intelligent Gravimetric Analyser (IGA-002) to determine the diffusion coefficients for the sorption of water vapour through neat PSBA and PSBA-MMT films. The IGA-002 has been used to study water and hydrocarbon vapour sorption through a wide range of materials that include pharmaceuticals, carbons, catalysts, clays and polymers.

4.1 Introduction

The IGA system uses a gravimetric technique to accurately measure the magnitude and dynamics of gas and/or liquid sorption through materials. [1] This instrument integrates precise computer-control and measurement of the material's weight change, partial pressure, temperature, gas flow and composition. Each point of the isotherm is generated at a specific temperature and partial pressure. The equilibrium point of each isotherm is determined by the operating software.

The system can automatically and reproducibly determine sorption and/or desorption isotherms/isobars under diverse operating conditions. Figure 4.1 shows a general schematic illustration of the IGA gas/vapour system.

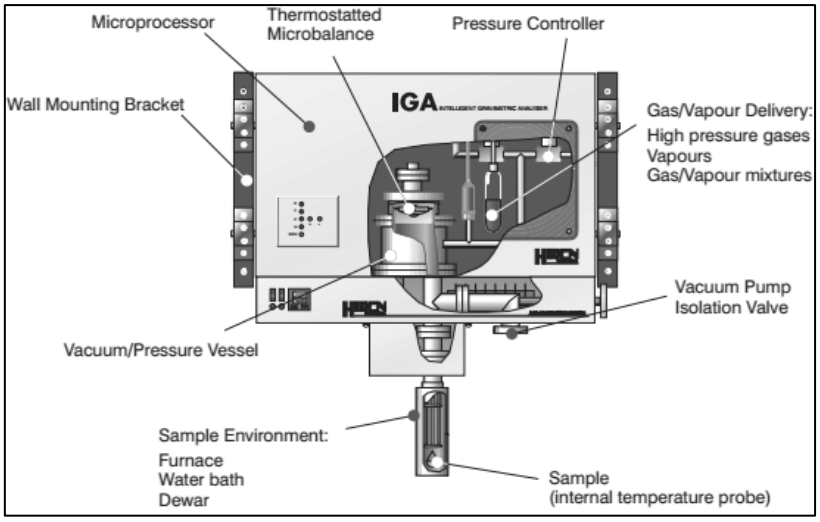

Figure 4.1: Schematic illustration of the IGA gas/vapour system (http://www.zpph.com/userfiles/file/iga_series_brochure.pdf - May 2014)

The unique IGA method exploits the relaxation behaviour of the polymer-penetrant interaction process after composition/temperature or pressure/gas changes to simultaneously evaluate kinetic parameters and the asymptotic uptake. [1,2] By varying the copolymer composition and related molecular properties, changes in properties such as T_g/free volume are perceived to affect the permeability of small molecules through polymeric systems. [3] However, incorporation of nanofillers such as clay platelets changes the structure and morphology of the polymeric film. [4] Platelet-like clay layers are impermeable, hence may act as barriers to the diffusion of gas or vapour molecules through polymer-clay films by providing an alternative tortuous pathway. [5]

4.2 Experimental

4.2.1 Materials

The measurements were performed using a Hiden Isochema gravimetric mass sorption analyser (IGA model 002). This equipment accurately measures the uptake of a gas or vapour by a polymeric film with a resolution of 0.1 µg under accurately controlled conditions of temperature and partial pressure. Water vapour was used as the penetrant for all samples, and the water vapour partial pressure was increased in identical increments, from P/P_o=0.1−0.9, at a constant temperature of 20 °C regulated by a water bath.

4.2.2 Sample preparation and experimental set-up

The films were cast from the latexes using a method described in detail in section 3.2.4.4. It is worth mentioning that this conventional method of film preparation does not guarantee

duplication of results. This is because the film formation process is not entirely reproducible and thus it impacts on the properties of the film obtained making it difficult to get consistent results.

In this study, samples with dimensions measuring 1.5cm × 1.5cm were used for the analysis. The thickness of the specimens was ~250µm as measured by a micrometer screw gauge. All the analyses were performed in the sorption mode, using real time analysis mode F1. Samples were dried prior to starting the isotherm runs using a manual outgas program until a stable mass was obtained.

Since the sorption experiments were time consuming, this study was structured in such a way as to analyse both the effect of varying *MMT clay content* and *copolymer composition* on the water vapour sorption behaviour of the films. Samples derived from the PSBA-30:70 and PSBA40:60 latex compositions were used to investigate the impact of MMT clay content; while samples derived from the PSBA-30:70-MMT20%, PSBA-40:60-MMT20% and PSBA-50:50-MMT20% latexes were used to assess the impact of copolymer composition. The neat samples were employed as the standards in each investigation and specimens were selected as highlighted in Tables 4.1−4.2.

Table 4.1: PSBA samples selected to investigate the impact of MMT clay content on the water vapour sorption behaviour of the films.

PSBA-30:70-MMT00%	PSBA-40:60-MMT00%
PSBA-30:70-MMT10%	PSBA-40:60-MMT10%
PSBA-30:70-MMT20%	PSBA-40:60-MMT20%
PSBA-30:70-MMT30%	PSBA-40:60-MMT30%

Table 4.2: PSBA samples selected to investigate the effect of copolymer composition on the water vapour sorption behaviour of the films.

PSBA-30:70-MMT00%	PSBA-40:60-MMT00%	PSBA-50:50-MMT00%
PSBA-30:70-MMT20%	PSBA-40:60-MMT20%	PSBA-50:50-MMT20%

4.2.3 Results and discussion

4.2.3.1 Equilibrium sorption behaviour

The water vapour sorption behaviour of the PSBA films was monitored over the partial pressure range P/P_o=0.1−0.9 as shown in Figure 4.2−3. The equilibrium concentration of

water vapour was expressed as [wt.%/cm^3] and plotted as a function of partial pressure. The variation in the amount of water vapour sorbed at each partial pressure point was much lower in the neat PSBA compared to that in all PSBA/MMT films. This could be due to the presence of clay platelets which provided micro voids that were occupied by the water vapour molecules. [6] This behaviour was also associated with the higher hydrophilicity of MMT clay relative to the neat PSBA matrix. [7]

The type of sorption curve can be explained by the dual sorption model (see Chapter 2, Figure 2.8). The curves displayed a general trend, showing no major differences in shape despite the variation in the copolymer composition. This suggests that the impact of MMT clay was dominant relative to copolymer composition. Sigmoidal-shaped sorption isotherms such as the ones presented in Figure 4.2 and 4.3 are typical of water vapour sorption in polar hydrophobic polymers, when the solute concentration becomes high enough that Henry's law is no longer adequate for modelling sorption in the equilibrium structure of the polymer. [8] The dual sorption mode represents a combination of interactions of the Langmuir sorption type (isotherm curve concave to the partial pressure activity axis), and Flory-Huggins sorption type (isotherm curve convex to the partial pressure activity axis). At low partial pressures $0.1 \geq P/P_o \leq 0.5$, the sorption behaviour of all the PSBA hybrid films followed a Langmuir sorption mode (polymer-penetrant interactions). This is characteristic of polymers containing micro voids or inorganic fillers, where specific sites within the polymer matrix are occupied by the penetrant. [9] Once all the sites are occupied, a small quantity of molecules may solubilise within the polymer matrix. At high partial pressures $P/Po \geq 0.5$, the sorption behaviour of the PSBA hybrid films followed a Flory-Huggins sorption mode (penetrant-penetrant interactions).

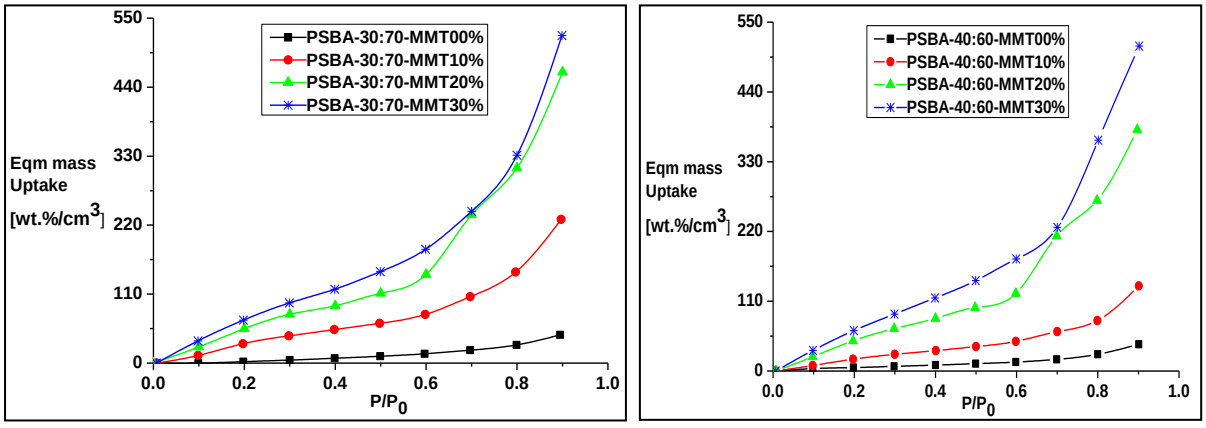

Figure 4.2: Isothermal water vapour sorption curves for neat PSBA-30:70 with its PCNs, and neat PSBA-40:60 with its PCNs.

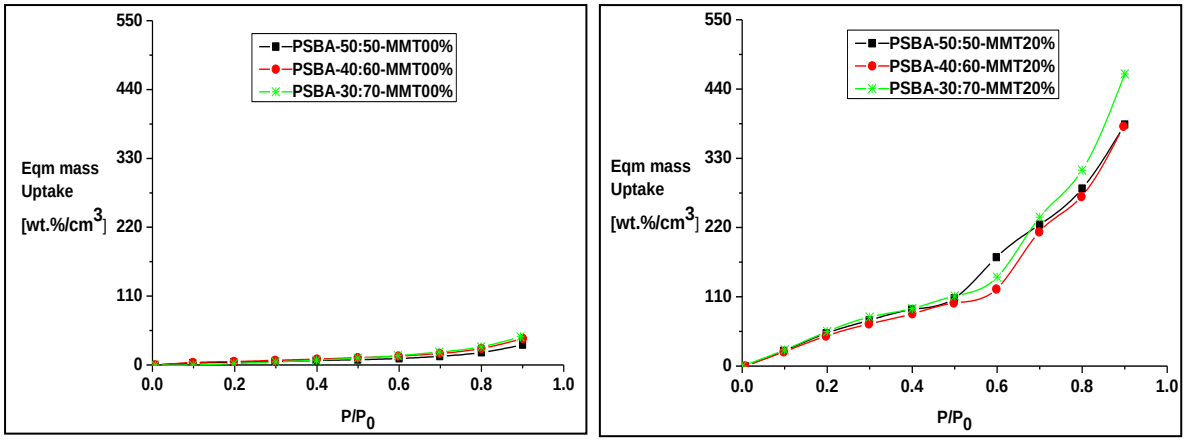

Figure 4.3: Isothermal water vapour sorption curves for neat PSBA and PSBA/MMT films with a fixed 20 wt. % clay content, measured at 20 °C.

These isotherms are evidence of water vapour cluster formation, which becomes progressively more important at higher water vapour activity. [10,11] This sorption behaviour is also characteristic of vapour dissolution within polymers above their glass transition temperatures, where the solubility increases continuously with relative partial pressure. [9,12,13]

4.2.3.2 Water vapour sorption kinetic behaviour

During the sorption experiments, the weight change of each PSBA film sample was measured using the IGA, following a step change in the water vapour partial pressure across the specimen. The weight change curve (M_t/M_{eqm}) was then plotted as a function of the square root of time ($t^{1/2}$ seconds). The diffusivity was accurately calculated from gradient fits using the IGA software and the variations in the diffusion coefficient values for all samples will be described in detail in the next section. If Fick's law holds true for the diffusion, the transport process is called "Fickian". When surface resistance and other external disturbances are neglected the transport process will then have the following characteristics: (1) the initial slope is linear when plotted as a function of the square root of time. [14] (2) Curves for samples of different thicknesses can be superimposed when plotted as a function of time divided by the thickness of the sample as shown in the examples in Figure 4.4−4.6. [15]

For clarity sake, the kinetic responses for the water vapour sorption in the samples for P/P_o = 0.1−0.2 were not included because the partial pressures were probably too low to have an effect on the sorption process which led to lengthy times to reach equilibrium. The rate at which equilibrium was reached decreased upon introduction of clay in the polymer matrixes.

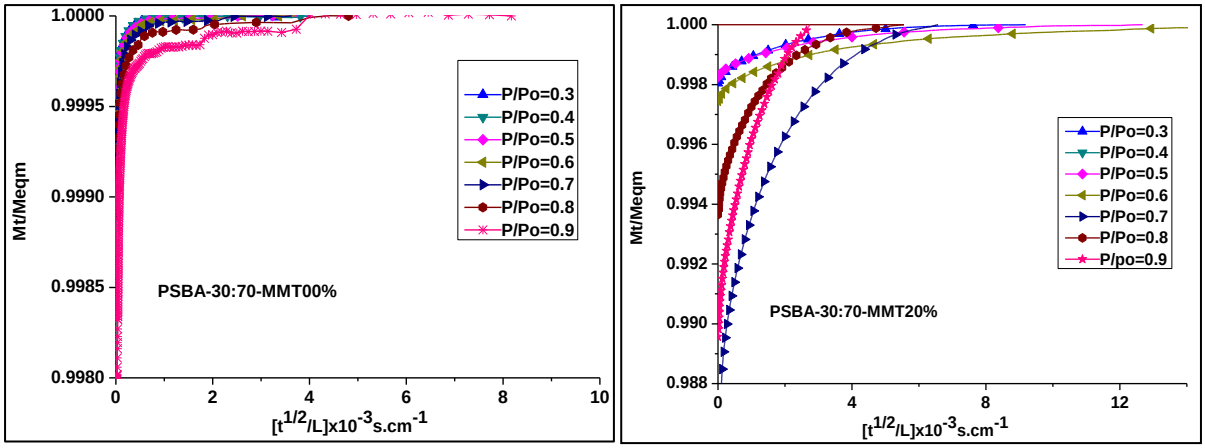

Figure 4.4: Kinetic response for the water vapour sorption through neat PSBA-30:70 film and PSBA-30:70-MMT20% film.

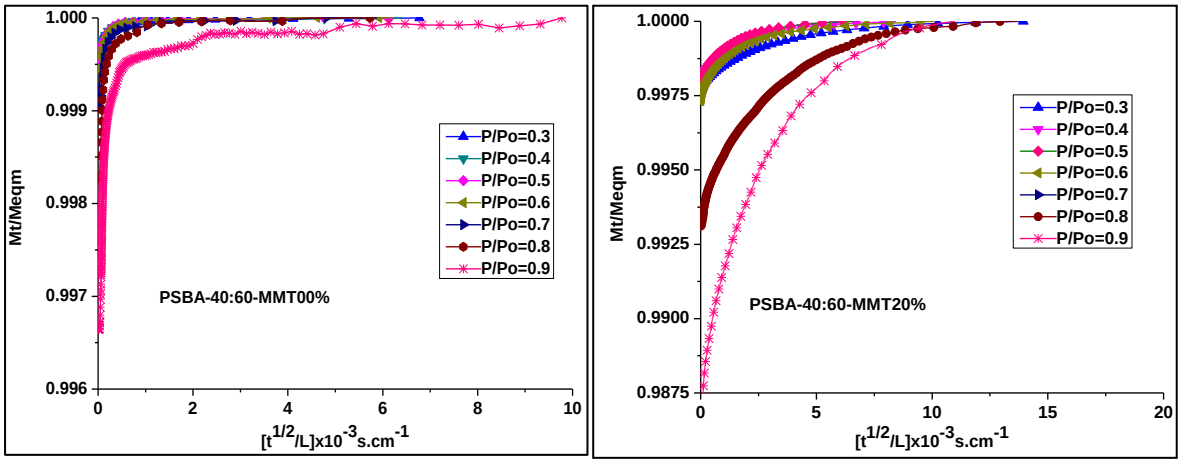

Figure 4.5: Kinetic response for the water vapour sorption through neat PSBA-40:60 film and PSBA-40:60-MMT20% film.

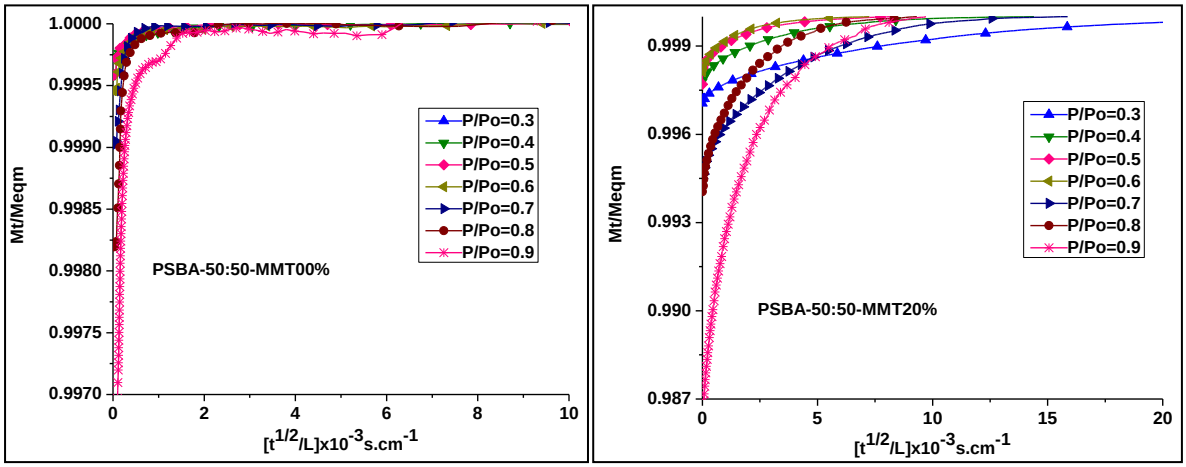

Figure 4.6: Kinetic response for the water vapour sorption through neat PSBA-50:50 film and PSBA-50:50-MMT20% film.

Compared to the neat PSBA films, the kinetic response in the nanocomposites did not correlate linearly with increase in partial pressure. This behaviour was unexpected, as one

would expect to see a decrease in the amount of time taken to reach equilibrium with increasing water vapour concentration.

The time to reach each equilibrium step increased from ~150 min for the unfilled films to ~350 min for the PCNs as shown in the example in Figure 4.7. This was attributed to the presence of the hydrophilic clay platelets in the polymer matrix which obstructed the water vapour molecules as they traversed across the film. [16]

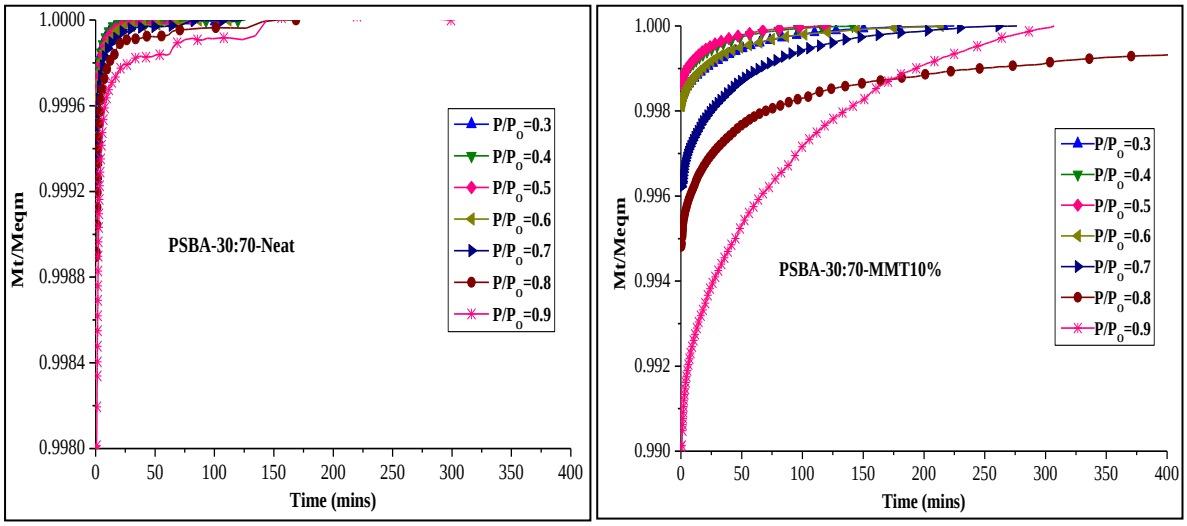

Figure 4.7: Time taken to reach equilibrium for the sorption of water vapour through the neat PSBA-30:70 and the PSBA-30:70-MMT10% films.

4.2.3.3 Impact of MMT content on the sorption behaviour

4.2.3.3.1 Effect of MMT on solubility coefficients

The solubility coefficients were calculated using the mathematical modelling described in Chapter 2 (see Equation 2.7). An example of the parameters used to calculate solubility coefficients for equilibrium water vapour sorption through the neat PSBA-30:70 films are given in Table 4.3.

Table 4.3: Parameters used to calculate the solubility coefficient values for the water vapour sorption through the neat PSBA-30:70 film sample.

P/P_o step	P ($x10^2$ Pa)	M_o ($x10^{-3}$ g)	M_{eqm} ($x10^{-3}$ g)	V_p (cm^3)	M_{H2O} ($g.mol^{-1}$)	V_m ($cm^3.mol^{-1}$)
0.1	2.345	77.1819	77.3008	0.05963	18.0152	22414
0.2	4.695	77.1908	77.2134	0.05963	18.0152	22414
0.3	7.045	77.2134	77.2407	0.05963	18.0152	22414
0.4	9.395	77.2407	77.2689	0.05963	18.0152	22414
0.5	11.745	77.2689	77.3019	0.05963	18.0152	22414
0.6	14.077	77.3019	77.3416	0.05963	18.0152	22414
0.7	16.627	77.3416	77.4001	0.05963	18.0152	22414
0.8	18.765	77.4001	77.4856	0.05963	18.0152	22414
0.9	21.127	77.4856	77.6416	0.05963	18.0152	22414

The plots for the solubility coefficients against varying partial pressures for PSBA-30:70-MMT films are presented in Figure 4.8. The solubility coefficients across the water vapour partial pressure range $0.1 \geq P/P_o \leq 0.5$ for the PSBA-30:70-MMT00%, PSBA-30:70-MMT10%, PSBA-30:70-MMT30% decreased monotonically with increasing partial pressure. This was attributed to the formation of water vapour clusters which slows the sorption process at low partial pressures. [17] At higher water vapour activity $P/P_o > 0.5$, the solubility coefficients gradually increased for PSBA-30:70-MMT00%, PSBA-30:70-MMT10% and PSBA-30:70-MMT20%. This could be probably due to plasticization of the copolymer matrix at high water vapour activities. [18] However, the solubility coefficient for a PSBA-30:70-MMT30% film sample decreased for $P/P_o > 0.5$. This deviation could be due to the high clay content which provided more reactive sites for water vapour molecules to occupy.

The solubility coefficients for PSBA-40:60-MMT films are also displayed in Figure 4.8. The solubility coefficients decreased with increasing water vapour activity for $0.1 \geq P/P_o \leq 0.5$, and then increased for $P/P_o \geq 0.5$. This was attributed to water vapour clustering at low partial pressures and plasticization of the matrix at higher water vapour activity. The solubility coefficients in both PSBA-30:70 and PSBA-40:60 sample sets increased monotonically with increasing MMT clay content. Choudalakis et al, [4,9] ascribed this behaviour to the effect of clay fillers. They suggested that fillers may act in different ways depending on their volume fraction, shape and possible physiochemical interactions with the matrix, which in one case

may increase the free volume, hence the solubility coefficient; and in another case decrease the free volume fraction, hence the solubility coefficient. Cloete et al, [5] attributed the sharp increase in the solubility coefficient at high partial pressures to the Flory-Huggins isotherm type that characterizes the equilibrium water vapour sorption behaviour of a PSBA/MMT nanocomposite.

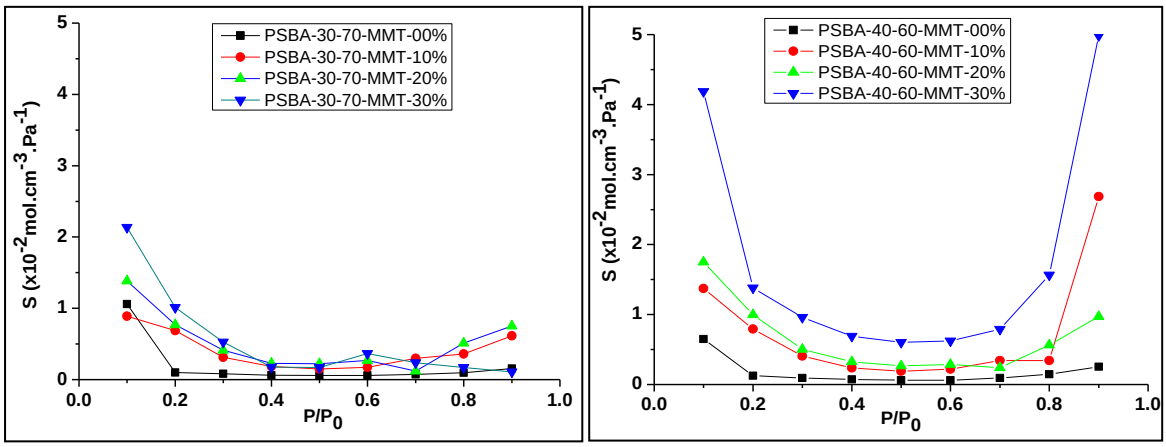

Figure 4.8: Solubility coefficients for PSBA-30:70 and PSBA-40:60 film specimens with increasing MMT contents of 10, 20 and 30 wt. %.

The solubility coefficient values for the PSBA-30:70 film samples were more uniform across the partial pressure range P/P_o = 0.1−0.9 compared to those for PSBA-40:60 film samples. This was attributed to the differing morphological organization of the clay platelets throughout the polymer matrix as suggested by TEM micrographs presented in section 3.3.4. [18-20]

4.2.3.3.2 Effect of MMT on diffusion coefficients

Plots of the diffusion coefficients versus changing partial pressure for PSBA30:70-MMT film specimens are shown in Figure 4.9. The diffusion coefficients for PSBA-30:70-MMT00% increased with increase in the water vapour in the range $0.3 \geq P/P_o \leq 0.9$. This is associated with the lowering of the matrix T_g as more water vapour molecules are absorbed, increasing copolymer chain mobility and hence the rate of diffusion. [21] The diffusivity at P/P_o = 0.1 could not be computed to a best fit since the kinetic response for the water vapour sorption did not reach equilibrium. The deviation at P/P_o = 0.2−0.3 was attributed to the low water vapour concentration values. [5] The diffusion coefficients for PSBA-30:70-MMT10%, PSBA-30:70-MMT20% and PSBA-30:70-MMT30% films increased with increasing water vapour activity over the range $0.1 \leq P/P_o \leq 0.5$, and were lower than the diffusion coefficient values of the neat PSBA-30:70 film across the entire partial pressure range P/P_o = 0.2−0.9. This can be

attributed to the effective tortuous pathway induced by the presence of MMT clay platelets in the film matrix. [7,22,23] The diffusion coefficient values for the PSBA-30:70 PCNs showed no major changes in the range P/P_o=0.6−0.9, remaining almost uniform. Chen et al, [24] attributed such behaviour to clustering of water vapour molecules at high activities. He suggested that if the polymer is hydrophobic or weakly hydrophilic, polar species such as water interact preferentially rather than with the polymer. In this case, the clusters are not in mobile monomeric form but clusters of multiple water vapour molecules, held together by hydrogen bonding, slowing down their migration through the matrix.

The diffusivities of the PSBA-30:70 PCNs decreased with increasing clay content across the entire water vapour activity. This can be associated with an increase in the tortuosity as the clay content increases. [25]

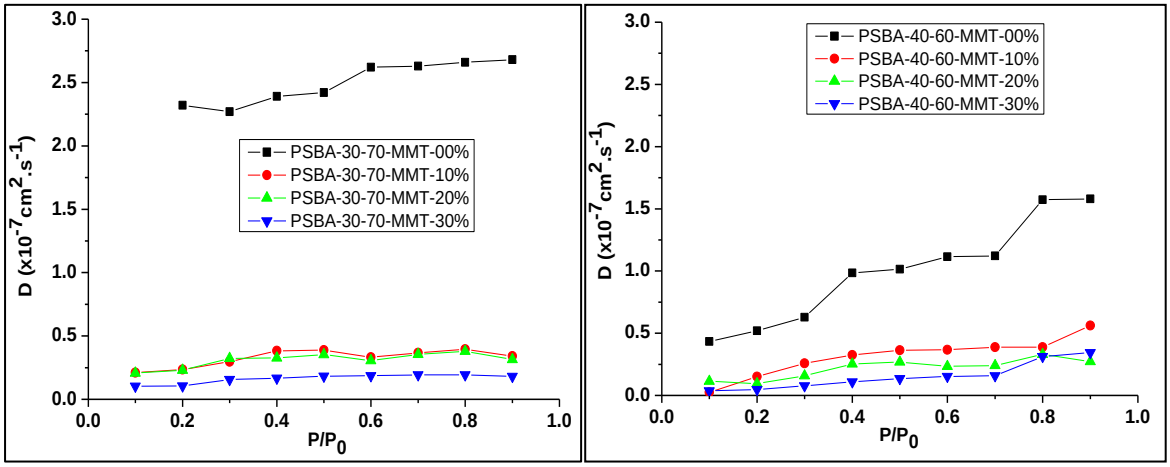

Figure 4.9: Diffusion coefficients for PSBA-30:70 and PSBA-40:60 film specimens with increasing MMT contents of 10, 20 and 30 wt. %.

The plots of diffusion coefficients versus increasing partial pressures for of PSBA40:60-MMT film specimens are displayed in Figure 4.9. The diffusion coefficients for PSBA-40:60-MMT00% increased with increase in the water vapour activity in the range $0.1 \geq P/P_o \leq 0.8$. This was attributed to the change in free volume caused by swelling effects brought about by the water vapour molecules, leading to lowering of the matrix T_g. As such, this led to increased matrix chain mobility and diffusivity as the water vapour concentration increased. [17,26,27] However, saturation was reached and the diffusion coefficient did not change from P/P_o=0.8−0.9. The variation in the diffusion coefficients for PSBA-40:60-MMT10%, PSBA-40:60-MMT20% and PSBA-40:60-MMT30% films increased with increasing water vapour activity in the range $0.1 \geq P/P_o \leq 0.5$, and were lower than the diffusion coefficient values of the neat PSBA-40:60 film across the entire partial pressure range P/Po=0.1−0.9. This was

associated with the longer diffusion pathway induced by the presence of MMT clay platelets in the film matrix. [28] The diffusivities of the PSBA-40:60 PCNs decreased with increasing clay content and water vapour activity for P/P_o=0.1−0.8. This can be associated with an increase in the tortuosity as the clay content increases. The anomaly in the diffusion coefficient variation of PSBA-40:60-MMT20% and PSBA-40:60-MMT30% for P/P_o=0.8−0.9 was attributed to the water vapour clustering phenomena which lead to constant or reduced diffusion coefficients at higher water vapour activity and solute concentration. [24,29]

4.2.3.3.3 Effect of MMT on the permeability coefficients

Permeability (P) was mathematically expressed as the product of the solubility coefficient (S) [$mol.Pa^{-1}.cm^{-3}$] and the diffusion coefficient (D) [$cm^2.s^{-1}$] (refer to Chapter 2, Equation 2.4). Table 4.4 displays an example of parameters used to calculate the permeability coefficients for neat PSBA-30:70. Figure 4.10 shows the permeability coefficients of PSBA-30:70-MMT films across the water vapour partial pressure activity range 0.1-0.9. The permeability coefficients for the neat PSBA-30:70 decreased with increasing water vapour activity over the range $0.2 \leq P/P_o \leq 0.6$. This was associated with the formation of water vapour clusters with increasing vapour concentration gradient which led to reduced permeation rates. [30,31] The permeability coefficients in the neat PSBA-30:70 films increased at higher water vapour activity $P/P_o \geq 0.6$. This was attributed to lowering of the matrix T_g which increased the mobility of the polymer chains leading to higher diffusivities. [32]

The permeability coefficients for the PSBA-30:70-MMT PCNs decreased with increasing water vapour activity for $0.1 \geq P/P_o \leq 0.5$, and was lower than that of the neat PSBA-30-70 film. This was attributed to the longer diffusion route brought about by introduction of MMT clay. The permeability coefficients of PSBA-30:70-MMT10% and PSBA-30:70-MMT20% films increased at higher water vapour activity $P/P_o \geq 0.6$. This was attributed to the change in free volume caused by the swelling effect of clay leading to increased permeation rates. [33]

Table 4.4: Parameters used to calculate the permeability coefficients for the neat PSBA-30:70 films.

P/Po step mbar.mbar^{-1}	D(×10^{-7}) cm^2.s^{-1}	S(×10^{-2}) mol.cm^{-3}.Pa^{-1}	S×D=P(×10^{-9}) mol.cm^2.cm^{-3}.Pa^{-1}.s^{-1}
0.1	no eqm	1.057	----
0.2	2.320	0.100	0.234
0.3	2.265	0.081	0.175
0.4	2.389	0.063	0.137
0.5	2.420	0.058	0.112
0.6	2.620	0.059	0.107
0.7	2.630	0.074	0.171
0.8	2.664	0.095	0.176
0.9	2.684	0.154	0.366

At low water vapour activities, the permeability coefficients decreased with increase in clay content from 10 wt.% to 30 wt.% and was associated with the increase in tortuous pathways. At high water vapour activity, the film loses its structure due to the swelling effect of water molecules and increases the permeation rates.

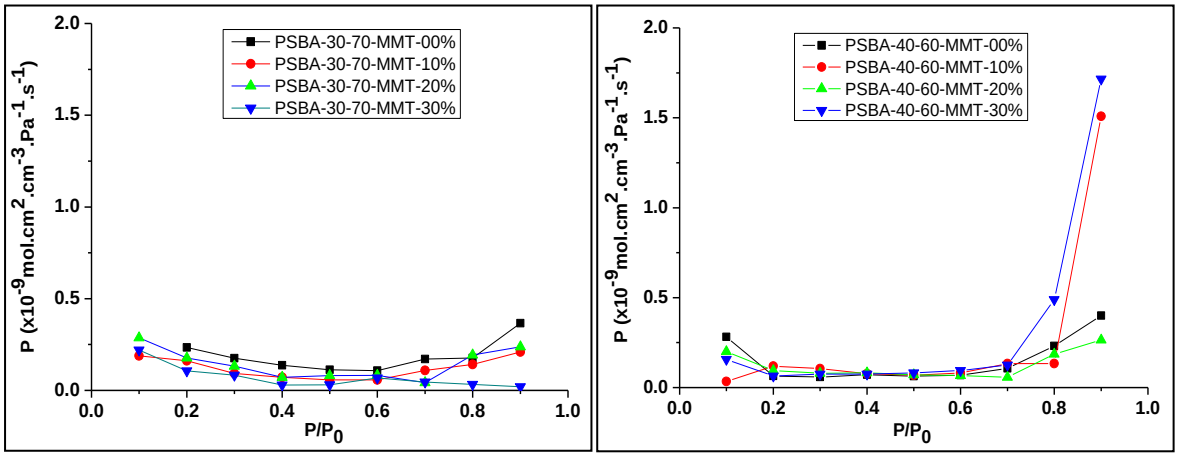

Figure 4.10: Permeability coefficients for PSBA-30:70 and PSBA-40:60 film specimens with increasing MMT contents of 10, 20 and 30 wt. %.

The permeability coefficients for PSBA-40:60-MMT films are also presented in Figure 4.10. The permeability coefficients of the neat PSBA-40:60 and the PCNs with increasing clay content from 10 wt.% to 30 wt.% show a general trend for P/P_o=0.2−0.6 characterized by a steady decrease. This was attributed to the synergistic effect of the diffusion and solubility coefficients as described in section 4.2.3.4.3. However the permeability coefficients in the

PSBA-40:60-MMT10% and PSBA-40:60-MMT30% surged up at higher water vapour activity P/P_o=0.7−0.9. This behaviour was unexpected and based on the findings in this study no correlations could be made. It is generally assumed that sorption of high concentrations of vapours results in linear or even exponential increases in the diffusion coefficient. [10,34] A principle explanation of this behaviour is that at high concentrations, the vapour molecules contribute holes or free volume re-distribution in the polymer matrix, increasing the polymer chain mobility and rates of permeation. [35] However, in PCNs where tortuosity of the clay platelets dominates, there is a significant reduction in gas permeability coefficient. [36,37]

4.2.3.4 Impact of copolymer composition on the sorption behaviour

4.2.3.4.1 Effect of PSBA matrix on the solubility coefficients

The solubility coefficients for neat PSBA latex films with varying copolymer composition are shown in Figure 4.11. The solubility coefficients decreased sharply with increasing water vapour activity from P/P_o=0.1−0.2, then steadily from partial pressure range P/P_o=0.2−0.6. The steady decrease was attributed to contradictory effects of high diffusivity coupled with very low solubility of water vapour molecules in the copolymer matrix. The high diffusion coefficients were associated with the lowering of the matrix T_g, increasing the copolymer chain mobility and thus the diffusion rates. On the contrary, the lower solubility coefficients were attributed to weak attractions formed between the water vapour molecules and the slightly polar carbonyl groups of the butyl acrylate component of the copolymers.

At high water vapour activities $P/P_o \geq 0.6$, the in the solubility coefficients of the neat copolymer films gradually increased. This was associated to the rate of plasticization of the matrix. However, the variation in the copolymer composition had insignificant impact on the solubility coefficients of both the neat copolymer films and the PCNs counterparts with a fixed clay content of 20 wt.%.

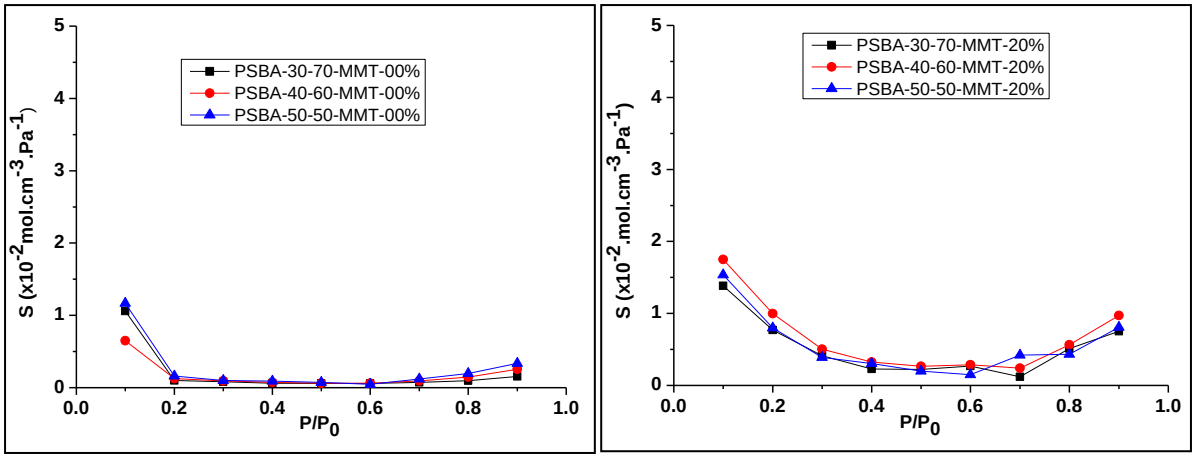

Figure 4.11: Solubility coefficients for neat (PSBA-30:70, PSBA-40:60and PSBA-40:60) film specimens and the PCNs with MMT20 wt. %.

The solubility coefficients of the PSBA copolymers with a fixed clay content of 20 wt.% are also presented in Figure 4.11.The solubility coefficients values across the water vapor partial pressure activity P/P_o=0.1−0.9 show a general trend similar to the neat PSBA counterparts. However, the higher solubility coefficients in the PCNs were attributed to the presence of MMT clay in the PSBA matrix. The clay particles may provide micro voids which favors cluster formation coupled with possible physiochemical interactions between water vapour molecules and the polar groups of the matrix. [3,38,39]

4.2.3.4.2 Effect of copolymer composition on diffusion coefficients

The diffusion coefficients of the virgin PSBA films increased with increased water vapour concentration across the partial pressure range P/P_o=0.1−0.9. This was associated with the swelling effect of the water vapour molecules as their concentration increases, creating more spaces or free holes and enhancing the diffusivity. According to the Vrentas-Duda free volume theory, diffusion in polymers occurs as small molecules traverse through spaces or holes between polymer chains and consequently the diffusion of molecules is enhanced as their local concentration or activity increases. [40] The diffusion coefficients of the neat PSBA with varying copolymer compositions are shown in Figure 4.12.

The diffusion coefficients decreased with decreasing n-butyl acrylate content of the copolymers across the entire partial pressure range for PSBA-30:70 and PSBA-40:60 specimens, and across P/P_o=0.1−0.6 for PSBA-50:50. However the large “jump” in the PSBA-50:50 specimens at higher water vapour activity was associated with an increase in the plasticization factor.

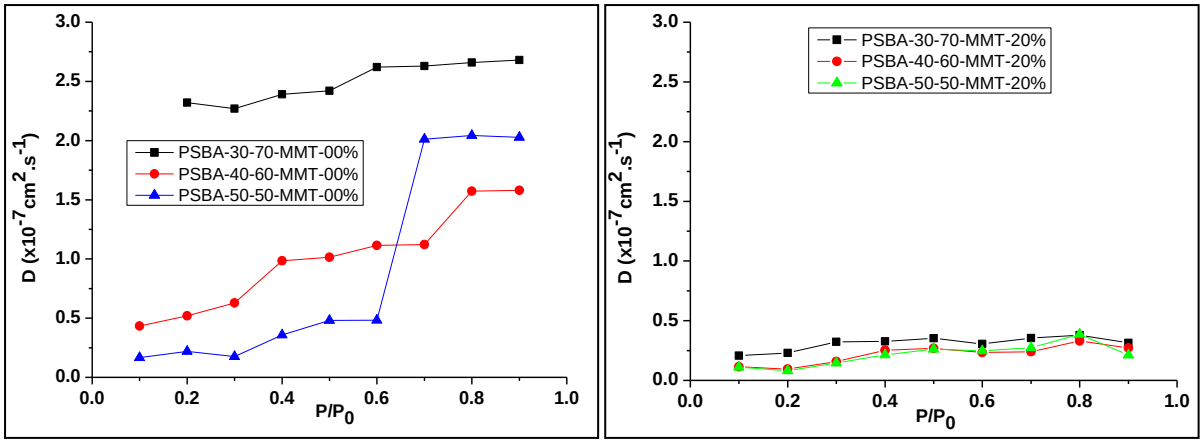

Figure 4.12: Diffusion coefficients for neat (PSBA-30:70, PSBA-40:60and PSBA-40:60) film specimens and the PCNs with MMT20 wt. %.

The absence of such large jumps in the PSBA-30:70 specimen can be explained by either the absence of water clustering because of sufficient polar groups from the BuA moieties, or by a judicious cancellation of a negative (due to water clustering) and a positive (due to free volume increase) effect. [41] The diffusion coefficients of the PSBA-30:70-MMT20%, PSBA-40:60-MMT20% and PSBA-50:50-MMT20% increased steadily with increase in water vapour concentration. The diffusion coefficients for the three specimens were lower compared to their unfilled counterparts across the entire partial pressure range. This was attributed to the longer diffusion pathways brought about by the presence of clay platelets. As such, this suggests the tortuosity was the dominant factor compared to the free volume factor. The effect of varying the copolymer compositions on the diffusivity in specimens with fixed clay content was rather insignificant.

4.2.3.4.3 Effect of copolymer composition on permeability coefficients

The permeability coefficients for neat PSBA latex films with varying copolymer composition are shown in Figure 4.13. The permeability coefficients for neat PSBA-30:70, PSBA-40:60 and PSBA-50:50 latex films decreased with increasing water vapour activity across the range P/P_o=0.1−0.6. This was attributed to the permeation rates being a factor of large diffusion coefficients and small solubility coefficients.

It is generally understood that the barrier properties represent a material's overall resistance to diffusion and sorption of substances and can be interpreted by considering two major contributing factors: (a) The chemical structure (such as chemical affinity to water/vapour) and (b) overall film morphology (such as molecular packing order). [42] The permeability

coefficients increased at high water vapour activities (P/P_o>0.6) and this behaviour was associated with the matrix swelling effect of high concentrations of water molecules.

The permeability coefficients for the PSBA-30:70-MMT20%, PSBA-40:60-MMT20% and PSBA-50:50-MMT20% film samples are also shown in Figure 4.13. The permeability coefficients of the PCNs decreased with increasing water vapour activity in the same fashion as their unfilled counterparts. Choudalakis et al,[9] associated the different kinds of permeability behaviour with the existence of interfacial regions between the matrix and the inorganic particles, which are caused by the surfactant used for the modification of clay particles.

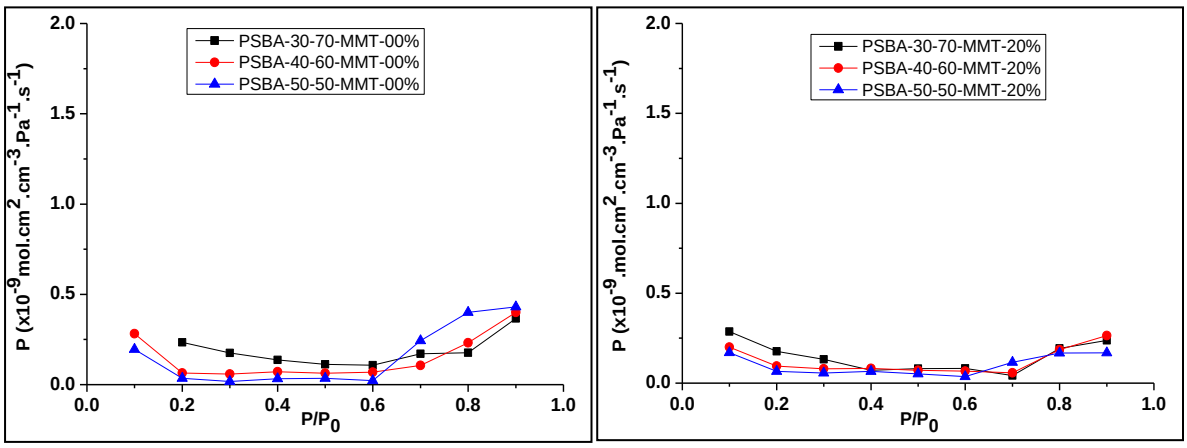

Figure 4.13: Permeability coefficients for neat (PSBA-30:70, PSBA-40:60and PSBA-40:60) film specimens and the PCNs with MMT20 wt. %.

Sorrentino et al, [28,43] suggested that the interfacial regions will mainly affect the solubility coefficient, but may also enhance the diffusion coefficients due to formation of voids between different phases. The variation in copolymer composition had an insignificant effect on the overall permeation rates.

4.3 Conclusions

The presence of MMT clay platelets in PSBA matrixes was found to have the most significant effect on the transport properties relative to the copolymer composition variation. From the kinetic response for the water vapour sorption through PSBA films, it can be concluded that the neat specimens took less time to reach equilibrium relative to the filled counterparts. This was because of the low diffusion rates in the filled specimens where clay platelets provided longer diffusion pathways for the water vapour molecules. The overall transport properties were affected by the presence of interfacial regions. At low water vapour

activity, the polymer-particle interactions were less dominant than the tortuous effect of the clay platelets. Although the glass transition temperature of the PSBA films in their dry state was not enhanced to a greater extent by presence of the MMT particles, this phenomenon had less impact on the water sorption behaviour of the films. This was because the sorption experiments were carried out at temperatures largely above the glass transition temperature of the dry copolymer films. On the contrary, the water clustering in the unfilled copolymer films may be a relatively slow process, but it may influence the overall permeation kinetics. Because the copolymer films were in the rubbery state in our experiments, the segment mobility was high enough to be affected by small amounts of water in the unfilled samples. Therefore, the free volume effect would dominate which led to higher diffusion coefficients. From the transport coefficients gathered in this study, the PCNs derived from PSBA-30:70 compositions were regarded best candidates as barrier structures to the water vapour sorption. These materials were more stable compared to the PSBA40:60 and PSBA-50:50 counterparts, hence less plasticized at higher water vapour activities.

4.4 References

[1] Garg, P.; Singh, R. P.; Choudhary, V. *Sep. Purif. Technol.* **2011**, *80*, 435.

[2] Etxeberria, A.; Garcia, A.; Iriarte, M.; Iruin, J. J.; Uriarte, C. *J. Appl. Polym. Sci.* **2006**, *102*, 2034.

[3] Zengeni, E. MSc, University of Stellenbosch, **2009**.

[4] Choudalakis, G.; Gotsis, A. D. *Eur. Polym. J.* **2009**, *45*, 967.

[5] Cloete, V. PhD, Stellenbosch University, **2011**.

[6] Olabarrieta, I.; Gällstedt, M.; Ispizua, I.; Sarasua, J.; Hedenqvist, M. S. *J. Agric. Food. Chem.* **2006**, *54*, 1283.

[7] Gorrasi, G.; Tortora, M.; Vittoria, V.; Pollet, E.; Lepoittevin, B.; Alexandre, M.; Dubois, P. *Polym. J.* **2003**, *44*, 2271.

[8] Okamoto, K.; Tanihara, N.; Watanabe, H.; Tanaka, K.; Kita, H.; Nakamura, A.; Kusuki, Y.; Nakagawa, K. *J. Polym. Sci., Part B: Polym. Phys.* **1992**, *30*, 1223.

[9] Choudalakis, G.; Gotsis, A. D. In *Handbook of Polymernanocomposites. Processing, Performance and Application*; Springer: **2014**, p 415.

[10] Arce, A.; Fornasiero, F.; Rodríguez, O.; Radke, C. J.; Prausnitz, J. M. *Physical Chem.* **2004**, *6*, 103.

[11] Marais, S.; Metayer, M.; Nguyen, T. Q.; Labbé, M.; Perrin, L.; Saiter, J. M. *Polym. J.* **2000**, *41*, 2667.

[12] Oksanen, C. A.; Zografi, G. *Pharm. Res.* **1990**, *7*, 654.

[13] Hancock, B. C.; Zografi, G. *Pharm. Res.* **1994**, *11*, 471.

[14] Krüger, K.; Sadowski, G. *Macromolecules* **2005**, *38*, 8408.

[15] Sanopoulou, M.; Petropoulos, J. H. *Macromolecules* **2001**, *34*, 1400.

[16] Sengwa, R. J.; Choudhary, S. *J. Appl. Polym. Sci.* **2014**, *131*.

[17] Masclaux, C.; Gouanve, F.; Espuche, E. *J. Membr. Sci.* **2010**, *363*, 221.

[18] Picard, E.; Gérard, J. F.; Espuche, E. *J. Membr. Sci.* **2008**, *313*, 284.

[19] Okamoto, M.; Nam, P.; Maiti, P.; Kotaka, T.; Hasegawa, N.; Usuki, A. *Nano Lett.* **2001**, *1*, 295.

[20] Gain, O.; Espuche, E.; Pollet, E.; Alexandre, M.; Dubois, P. *J. Polym. Sci., Part B: Polym. Phys.* **2005**, *43*, 205.

[21] Gontard, N.; Guilbert, S.; Cuq, J. *J. Food Sci.* **1993**, *58*, 206.

[22] Herrera-Alonso.; Jose, M.; Marand, E.; Little, J. C.; Cox, S. S. *J. Membr. Sci.* **2009**, *337*, 208.

[23] Schmidt, G.; Malwitz, M. M. *Curr. Opin. Colloid Interface Sci.* **2003**, *8*, 103.

[24] Chen, G. Q.; Scholes, C. A.; Doherty, C. M.; Hill, A. J.; Qiao, G. G.; Kentish, S. E. *J. Membr. Sci.* **2012**, *409*, 96.

[25] Chang, K.; Lai, M.; Peng, C.; Chen, Y.; Yeh, J.; Lin, C. S.; Yang, J. *Electrochim. Acta* **2006**, *51*, 5645.

[26] Ito, S.; Hashimoto, M.; Wadgaonkar, B.; Svizero, N.; Carvalho, R. M.; Yiu, C.; Rueggeberg, F. A.; Foulger, S.; Saito, T.; Nishitani, Y. *Biomaterials* **2005**, *26*, 6449.

[27] Levine, H.; Slade, L. *Water Sci.* **1988**, *3*, 79.

[28] Sorrentino, A.; Tortora, M.; Vittoria, V. *J. Polym. Sci., Part B: Polym. Phys.* **2006**, *44*, 265.

[29] Low, H. Y.; Liu, T. X.; Loh, W. W. *Polymer Int.* **2004**, *53*, 1973.

[30] Merinska, D.; Kalendova, A.; Tesarikova, A. *AIP Conference Proceedings* **2014**, *1599*, 186.

[31] Mandai, T.; Mandai, B. M. *Synth. Met.* **1996**, *80*, 83.

[32] Choudalakis, G. A.; Kalo, H.; Breu, J.; Gotsis, A. D. *J. Appl. Polym. Sci.* **2014**.

[33] Felder, R. M.; Huvard, G. S. *Curr. Appl Phys.* **1980**, *16*, 315.

[34] Alexandre, B.; Langevin, D.; Médéric, P.; Aubry, T.; Couderc, H.; Nguyen, Q. T.; Saiter, A.; Marais, S. *J. Membr. Sci.* **2009**, *328*, 186.

[35] Alexandre, M.; Dubois, P. *Mater. Sci. Eng., R.* **2000**, *28*, 1.

[36] Zhou, Q.; Xanthos, M. *Polym. Degrad. Stab.* **2008**, *93*, 1450.

[37] Vlasveld, D. P. N.; Groenewold, J.; Bersee, H. E. N.; Picken, S. J. *Polym. J.* **2005**, *46*, 12567.

[38] Osman, M. A.; Mittal, V.; Lusti, H. R. *Macromol. Rapid Commun.* **2004**, *25*, 1145.

[39] Bo, X.; Zheng, Q.; Song, Y.; Shangguan, Y. *Polym. J.* **2006**, *47*, 2904.

[40] Vrentas, J. S.; Vrentas, C. M. *J. Polym. Sci., Part B: Polym. Phys.* **2003**, *41*, 501.

[41] Marais, S.; Nguyen, Q. T.; Devallencourt, C.; Metayer, M.; Nguyen, T. U.; Schaetzel, P. *J. Polym. Sci., Part B: Polym. Phys.* **2000**, *38*, 1998.

[42] Sapalidis, A. A.; Katsaros, F. K.; Steriotis, T. A.; Kanellopoulos, N. K. *J. Appl. Polym. Sci.* **2012**, *123*, 1812.

[43] Sorrentino, A.; Gorrasi, G.; Tortora, M.; Vittoria, V. *Polym. Compos.* **2006**, 273.

Chapter 5

5 Conclusions and Recommendations

5.1 Conclusions

The use of the ad-miniemulsion polymerization method was an efficient way to incorporate as much as 30 wt.% MMT clay into PSBA matrixes. The physical and thermo-mechanical properties of the PSBA PCNs were found to be influenced more by the clay than the copolymer composition. The morphological properties were significantly affected by both clay and copolymer composition. On the other hand, the morphology of the low T_g PSBA-40:60 and PSBA-30:70 changed from irregular shaped to dumb-bell shaped particles upon incorporation of 10 wt.% of MMT clay. This was associated with the faceting effect of the rigid clay particles as they adhered to the surface of the copolymer latex particles.

The thermo-mechanical properties were not significantly improved by incorporation of the clay, specifically in the case of PSBA-40:60 and PSBA-30:70 with much lower T_g values. This was attributed to an increase in molecular motions of the unattached copolymer chains and the VBDA alkyl short chains used to modify the clay. This deviation was also associated with the high molecular weights of the unfilled latex films. However, the glass transition values of the PSBA-50:50 materials were significantly affected by the presence of clay. This was attributed to restricted molecular motions of the copolymer chains at or near the interfacial region. A similar behaviour was also notable in the significant decrease in the tan(δ) temperature peak which is also associated with T_g.

Compared to the neat films, the PSBA PCNs had remarkable optical properties. The best optical properties were observed in the case of PSBA-30:70 films in which the light transmittance only decreased from 85% (neat film) to 60% (MMT-30% film) and remained higher than the transmittance for PSBA-40:60 and PSBA-50:50 films (for all MMT clay contents).

The water vapour permeation was greater in the unfilled PSBA latex films relative to the PCNs. This was evident from the kinetic response for the water vapour sorption through the films. This was attributed to the longer diffusion pathways due to presence of clay platelets in the copolymer matrix. The diffusion coefficients decreased with increasing clay content. The solubility coefficients were higher in the PCNs than in the unfilled latex films. Furthermore,

the amounts of water vapour sorbed at equilibrium increased with increase in the clay content. This was associated with the ability of the clay to interact with water vapour molecules due to its hydrophilicity. This behaviour was also associated with the formation of micro voids due to free-volume redistribution upon introduction of clay. From the transport coefficients, the PSBA-30:70 hybrid latex films were the best candidates as barrier structures to mass transport. This was associated with the morphological properties of the matrix which to an extent facilitates the distribution of the rigid clay platelets. The overall transport properties were however much more affected by the clay content and distribution and less affected by the copolymer composition variation. This was attributed to the tortuous effect of the impermeable clay platelets playing a dominant role as compared to the free-volume effect.

5.2 Recommendations for future work

The film formation process is a very important stage during preparation of the PSBA materials as it will affect the overall properties of the film. It is therefore worthwhile to investigate the factors affecting the film formation process. This study would help to optimize the barrier properties of the films and elaborate on the reproducibility of the transport coefficients.

Clay platelets are impermeable and have the ability to improve the barrier properties of polymeric structures by inducing a tortuous pathway. As such the presence of interfacial regions plays a major role in determining the rate of mass transport. It is worthwhile to use techniques such as dielectric spectroscopy to measure interfacial polymer relaxations which are a measure of interaction strength.

It is also interesting to extend this study to the characterization and optimization of PSBA blends to determine which variables control the blend morphology and bulk properties. It is worthwhile to use other techniques such as ATR-FTIR to monitor the *in-situ* sorption and diffusion of water or mineral oil into the PSBA PCNs.

The highly filled PSBA nanocomposites are promising cost-effective materials. According to a polymer source, 1kg of poly(styrene-co-butyl acrylate) random copolymers costs around US$11, while 1kg of sodium montmorillonite clay costs around US$0.80.

Appendices

Appendix 1: ^{1}H NMR spectrum of VBDAC

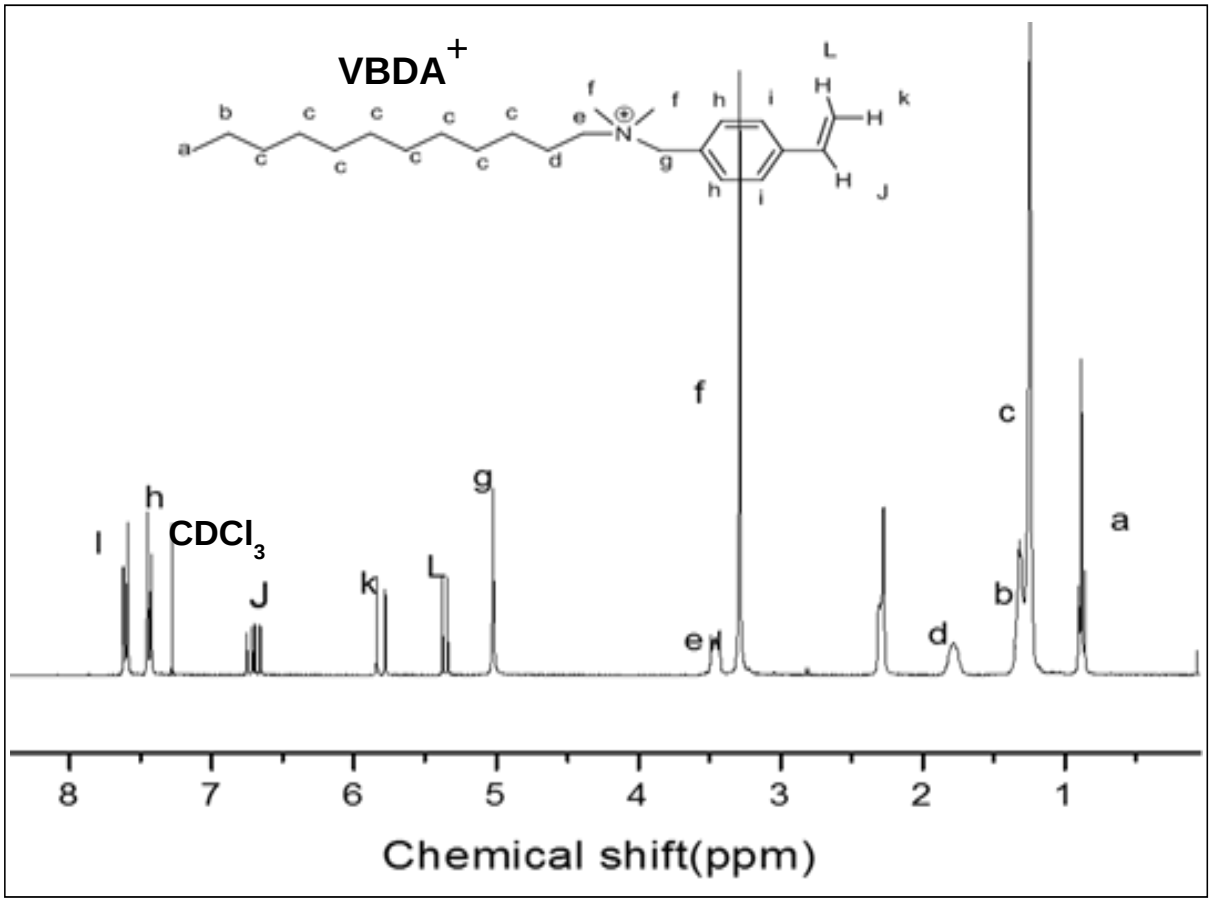

Appendix 2: PSBA and PSBA-MMT miniemulsion formulations

MMT aqueous dispersion				Monomer miniemulsion					
PSBA-MMT% sample	Clay/Paste/Water (g)/(g)/(mL)	SDS (g)	Water (mL)	Sty (g)	BuA (g)	AIBN (g)	HD (mL)	SDS (g)	Water (mL)
PSBA-50:50-MMT00	----/----/-----	----	----	2.24	2.76	0.020	0.26	0.144	50.00
PSBA-50:50-MMT10	0.50/2.04/1.54	0.284	31.25	2.02	2.48	0.018	0.23	0.496	17.21
PSBA-50:50-MMT20	1.00/4.08/3.08	0.297	31.25	1.80	2.20	0.016	0.20	0.452	15.67
PSBA-50:50-MMT30	1.50/6.12/4.62	0.310	31.25	1.60	1.90	0.014	0.18	0.407	14.13
PSBA-40:60-MMT00	----/----/-----	----	----	1.76	3.24	0.020	0.26	0.144	50.00
PSBA-40:60-MMT10	0.50/2.04/1.54	0.284	31.25	1.60	2.90	0.018	0.23	0.496	17.21
PSBA-40:60-MMT20	1.00/4.08/3.08	0.297	31.25	1.40	2.60	0.016	0.20	0.452	15.67
PSBA-40:60-MMT30	1.50/6.12/4.62	0.310	31.25	1.20	2.30	0.014	0.18	0.407	14.13
PSBA-30:70-MMT00	----/----/-----	----	----	1.39	3.71	0.020	0.26	0.144	50.00
PSBA-30:70-MMT10	0.50/2.04/1.54	0.284	31.25	1.20	3.30	0.018	0.23	0.496	17.21
PSBA-30:70-MMT20	1.00/4.08/3.08	0.297	31.25	1.00	3.00	0.016	0.20	0.452	15.67
PSBA-30:70-MMT30	1.50/6.12/4.62	0.310	31.25	0.90	2.60	0.014	0.18	0.407	14.13

Appendix 3: ^{1}H NMR signal integration for the neat PSBA-50:50

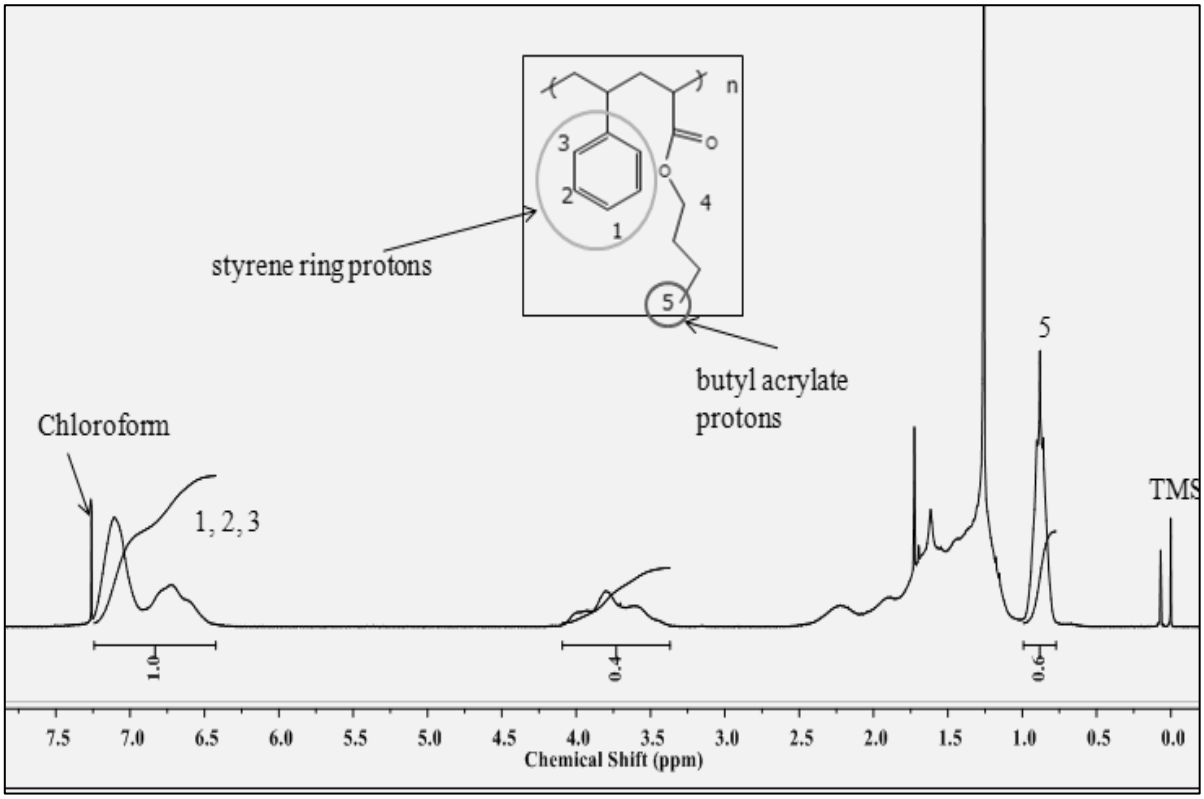

Appendix 4: ^{1}H NMR signal integration for the neat PSBA-40:60

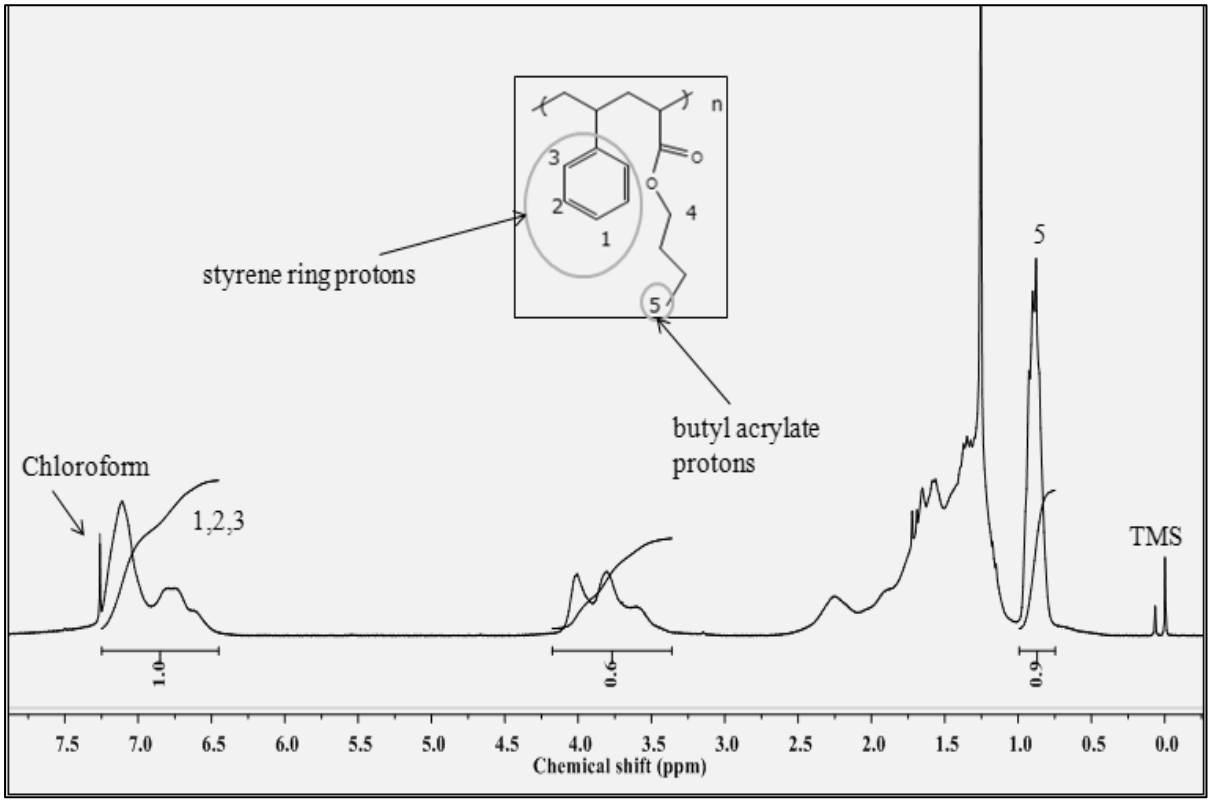

Appendix 5: ^{1}H NMR signal integration for the neat PSBA-30:70